Hege Langjord

Nonlinear observer and control design for electropneumatic clutch actuation

Doctoral thesis
for the degree of philosophiae doctor

Trondheim, March 2011

Norwegian University of Science and Technology
Faculty of Information Technology, Mathematics,
and Electrical Engineering
Department of Engineering Cybernetics

NTNU

Norwegian University of Science and Technology

Doctoral thesis
for the degree of philosophiae doctor

Faculty of Information Technology, Mathematics,
and Electrical Engineering
Department of Engineering Cybernetics

ISBN 978-82-471-2633-2 (printed version)
ISBN 978-82-471-2634-9 (electronic version)
ISSN 1503-8181

ITK Report 2011-2-W

Doctoral theses at NTNU, 2011:54

Electronic version (High resolution images)

Summary

This thesis treats position control of an electropneumatic clutch actuator operated by simple on/off solenoid valves. This clutch actuator is intended for automatic manual transmission systems or clutch-by-wire systems in heavy duty trucks. Pressurized air is already present as a part of the brake system in such vehicles, and pneumatics is therefore the natural choice for actuating the manual transmission in these clutch actuator systems.

Production cost is a crucial factor in all parts of the automobile industry. For the clutch actuator system this influence the choice of number of sensors present in the production system, limiting it to only a position sensor. It also lead to that a set of on/off solenoid valve is chosen for actuation over more commonly used proportional valves, even though it complicates the control task. Production quality sensors are considered in this thesis, and these are sensors which are more influenced by noise than sensors found in test rigs made for research and development. Motor vibration and possible other mechanical influence also have to be taken into consideration when testing in a full-scale truck as done in this thesis.

Motivated by the choice of on/off solenoid valves as the control valves in the clutch actuator system, switched control design is considered. Switched controllers exploit the on/off solenoid valves discrete behavior, switching the valves between fully open and fully closed in a manner such that desired supply or exhaust of air from the actuator chamber is obtained, ensuring the demanded piston position. Based on this line of action, two switched controllers are developed along with a dual-mode switched controller utilizing the best features of the individual controllers. Stability analysis based on standard Lyapunov theory are provided, and the performance of the controllers are tested in a full-scale test truck at Kongsberg Automotive ASA. Both theoretical and practical performance analyses confirm that switch controllers are well suited for actuator piston position control of the clutch actuator system.

Full-state feedback availability is assumed in the design of the switched controllers. Adaptive nonlinear observers are derived to provide estimates of unmeasured states and parameters for the clutch actuator system. These adaptive observers are deterministic with linear output-injection, and have adaptation laws for estimation of clutch load characteristics and friction. A full-order adaptive observer, including filtering of position for suppression of noise, shows best performance. The adaptation of unknown parameters accounts for wear of the clutch and variations in temperature, ensuring a robust design of the clutch actuator model

and improving state estimates. Theoretical analyses of convergence are derived under persistence of excitation condition, and performance of the adaptive observers are validated by experimental data.

The switched controller and the adaptive nonlinear are combined into an observer-based switched controller. Simulation of this is provided, comparing the results with actual truck measurements. These analysis indicate that the pressure sensor can be exchanged with an adaptive nonlinear observer without significant loss of performance for nonlinear state feedback based control designs for the system.

Acknowledgments

This thesis presents the research results of my doctoral studies at the Department of Engineering Cybernetics (ITK) at the Norwegian University of Science and Technology (NTNU) from August 2005 to June 2010, interrupted by parental leaves. The funding have been provided by the Research Council of Norway (NRF) and Kongsberg Automotive ASA (KA).

First of all I would like to thank my supervisor, Professor Tor Arne Johansen at the Department of Engineering Cybernetics, NTNU. He has been a great advisor, always being available for discussion and directions. I am still amazed by how fast he responds all my questions, patiently providing me with new ideas or solution to what I thought to be big problems.

I am also very thankful to my co-supervisor Dr. Glenn-Ole Kaasa. First of all for taking the initiative to the collaboration between ITK and Kongsberg Automotive ASA, making this thesis possible. His knowledge on every aspects of the clutch systems, which he share willingly, still impress me greatly. Sten Roar Snare, Christian Bratli and Håkon H. Solberg at KA also deserves thanks for providing me technical information on the clutch system, and helping me set up the truck for experimental testing. KA even allowed me to do tests after their part of the research project was finished, without these results the thesis would not been complete.

Thanks to Professor Joao P. Hespanha for letting me stay as a visitor at the Center for Control, Dynamical systems, and Computations (CCDC) at the University of California Santa Barbara (UCSB). During the 6 months I stayed there we had some interesting and inspiring meetings, which I highly appreciate.

My mentor Professor Kari Melby, which I met through NTNU Mentorprogram, deserves thanks for helping me regain focus when I mid-way into the studies doubted my work. The same goes to fellow female PhD-student in the program, together we shared an inspiring fellowship.

I would also like to thank Tove, Unni and Eva for help with every administrative task. A stop by your offices often included long chats, mostly about children, providing appreciated breaks from the almost all-male community.

My fellow PhD students deserve thanks for making the time spend working toward this thesis more enjoyable. Especially thanks to my office mate Esten Grøtli for help with a lot of trivial MatLab and Latex problems, and for breaks talking about nothing. Gullik A. Jensen, for always cheering me up either by reminding me that there is a life outside academics or by simply being even more frustrated than me, and having time to listen to my complaints.

I also need to thank my family. My mother and father who alway have supported me and my two sister, and always arranged things such that we could pursue whatever education we liked. Thanks to both my sisters; Hilde, for being my mathematical alibi, and Siv for proofreading. You both undergoing the same type of education as me, have made you supportive conversation partners. My dear friend Kristin Johansson also deserves thanks for helping me with the proofreading.

My husband Trond-Even deserves the biggest gratitude. He have spend hours listening to my worries about my progression, and somehow still believe in me and thinking that I can accomplish anything. At last, I need to mention our two beautiful children, Maren and Sakris. My thesis might been finished a couple of years before without you, but you have provided me with a new prospective in life. Your unconditional love have encouraged me through some tough days the last year.

Kongsberg, February 2011

Hege Langjord

Contents

Chapter 1

Introduction

This thesis considers position control of an electropneumatic clutch system for heavy duty trucks. The main task is to obtain clutch actuator position control, which is accurate enough to provide smooth driving of the vehicle, at the same time as the controller does not introduce unnecessary wear of the clutch or the actuator, and adapts to tear-and-wear and environmental changes. This is achieved by designing controllers and observers suitable for application to the electropneumatic clutch actuator. The intended applications for the clutch actuator are automated manual transmission (AMT) and clutch by wire (CBW) solutions for heavy duty trucks.

1.1 Motivation

Demand on reduction in the fuel consumption and the associated CO_2 emission for vehicles is highly relevant in the discussion on global warming. Large amounts of goods are transported by trucks every day, and due to the high volume even small decreases in the fuel consumption will both improve exhaust emissions and reduce cost considerably. One option for enhancing fuel efficiency is development of better transmission solutions.

Manual Transmission (MT) systems perform better than conventional Automatic Transmission (AT) systems in terms of fuel efficiency, typically a 10 % or better fuel mileage can be expected, Kuroiwa et al. (2004). However, the AT systems provide better driving comfort and simplified vehicle operation, and the drivers prefer these conveniences. This is part of a clear trend in the motor industry, the market share for MT systems is decreasing while the market share for AT systems is increasing. Several semi-automatic systems are developed as a response to this progress. Automated Manuel Transmission (AMT) systems are one of these semi-automatic solutions, combining the best features from MT and AT systems, the high efficiency of MT and the comfort of AT. An AMT system consists of manual transmission with automatic transmission control, and can be used to employ automatic transmission decided by an automatic gear shift control system, or as a clutchless manual transmission exploiting drive-by-wire technology. As the manual

torque transmission is retained, ATMs can easily be added onto existing MT systems. This is an advantage over more conventional AT systems, and it is the main reason for the AMT systems growth in popularity the last decade, especially in the European market. Kongsberg Automotive ASA (KA) delivers AMT systems for heavy duty trucks. AMT systems are especially desired for such trucks, because conventional AT systems for the high torque transfer needed in these vehicles are expensive and have larger loss of power. A great amount of research can be found on AMT systems, as the work by Montanari et al. (2004), Glielmo et al. (2006), Lucente et al. (2007) and Vasca et al. (2010), often considering the task of automatic control of gear shifting as well.

The manual transmission of the AMT systems can be actuated by either hydraulic or pneumatic actuators. Pressurized air is already present in trucks, and pneumatics are therefore chosen over hydraulic actuation which is more common in clutch systems for cars. Pneumatic systems have cost advantages and are easier to maintain than hydraulic systems, and with pneumatics there are no risk for environmental damage in case of leakages. However, the pneumatic actuators are inherently more difficult to control due to nonlinearities mainly caused by the compressibility of air.

Figure 1.1: A heavy duty truck.

Cost is in general a crucial factor in the automotive industry, and this is no different for the heavy duty truck industry. The Scania test truck present at KA has both position and pressure sensors included in the clutch system, but the pressure sensor is unwanted in the finalized production clutch system. The lack of measurement of all desired parameters motivates adaptive observer designs. Cost, combined with space advantages and better robustness properties, have also lead to on/off solenoid valves being chosen as control valves over proportional valves, which is the other common option. The on/off solenoid valves' discrete behavior motivates for switched controller designs.

1.2 Background

The clutch plates transmit torque from the motor to the axle shaft. Smooth engagement of these is crucial, and the clutch is subject to satisfy small friction losses, fast lock-ups and driving comfort, Bemporad et al. (2001), which may be conflicting requirements. To obtain this, position control of the clutch actuator is the most important factor when designing AMT systems, Horn et al. (2003).

Pneumatic actuators are common industry actuators, Smaoui et al. (2005), and are becoming more popular due to recent improvements in valve technology and reduction of component costs, Nguyen et al. (2007). Pneumatic actuators

have advantages as cleanliness, low cost, high ratio of power to weight and easy maintenance, Ali et al. (2009), but they also hold highly nonlinear characteristics due to compressibility of air, stiction and high friction forces which complicate accurate position control. Several papers have been published on the topic of position control of pneumatic actuators, see Ahn and Yokota (2005) and Girin et al. (2009), and references therein.

To control the flow of air to the pneumatic actuator, there are two common choices: servo valves and on/off solenoid valves. Servo valves are the conventional choice, while the much cheaper, but more challenging (from a control point of view) on/off solenoid valves are increasing in popularity. On/off solenoid valves also have advantages as robustness, higher power-to-mass ratio and small size compared to servo valves. The drawbacks are mainly the valve's discrete on/off nature, limitations in response time and a dynamic response which is hard to model accurately. Modeling of on/off solenoid valves are treated in detail only by a few authors. The work by Topcu et al. (2006), Håkansson and Johansson (2007) and Taghizadeh et al. (2009) show that accurate modeling of such solenoid valves is a complex task. In order to get a complete model of the valve, electromagnetics, mechanical movements and fluid flows need to be described in accurate details.

Thus, Pulse Width Modulation (PWM) is usually applied when on/off solenoid valves are used for position control of pneumatic actuators. This approach has been extensively used e.g. Varseveld and Bone (1997), Gentile et al. (2002), Ahn and Yokota (2005) and Messina et al. (2005). Exploiting the PWM technique, only a flow characteristic of the on/off solenoid valve is needed. It also provides the possibility of allowing control laws designed for servo valves to be used for on/off solenoid valves. During the last decades, sliding mode techniques have became a more common approach for designing controllers for pneumatic actuators, especially for systems with on/off solenoid valves since the valves discrete nature can be exploited, e.g. Paul et al. (1994), Shen et al. (2004), Nguyen et al. (2007).

All industrial systems suffer from trade offs between cost of sensors and the need for real-time information. Hence adaptive observers which in addition to estimating the system states also provide online estimation of system parameters, are attractive solutions, and a vast number of papers are published on the subject. One of the earliest publications on adaptive observers for nonlinear systems is Bastin and Gevers (1988) which present an adaptive observer for Single-Input Single-Output observable systems that can be transformed into a certain canonical from, followed by Marino (1990) which extended the results to Multiple-Input Single-Output systems with the same properties. Marino and Tomei (1992) and (1995a) present adaptive observers for nonlinear single-output systems which are linear with respect to an unknown constant parameter vector and transformable through a filtered transformation. Under persistency of excitation (PE) conditions, convergence of the parameters is guaranteed. Adaptive observers for more general classes of nonlinear systems, not needed to be linearizable, are treated in Rajamani and Hedrick (1995), Cho and Rajamani (1997) and Besancon (2000). Their papers treat a class of nonlinear systems which holds Lyapunov functions satisfying particular conditions. An general overview of observer tools for nonlinear systems is given by Besancon (2007). But there exist no general theory on designing adaptive

observers for arbitrary nonlinear systems and observers are most often designed individually for a specific system, exploiting the systems characteristics. This is also the common approach for pneumatic actuator systems.

1.2.1 Other work on electropneumatic clutch actuator systems

A sketch giving an overview of the considered clutch actuator system is shown in Figure 1.2. The valve body contains a set of on/off solenoid valves, and the actuator is connect to clutch plates through a clutch lever. Because of this, the clutch actuator system is called a Pneumatic External Actuated (PEA) clutch system. The thesis by Kaasa (2006), "Nonlinear output-feedback control applied to electropneumatic clutch actuation in heavy-duty trucks", also considers position control of a electropneumatic clutch actuation system and obtaining experimentally extremely high tracking performance in the test rig. This thesis consider a similar clutch actuator with the following main differences in mechanical design and control hardware:

- On/off solenoid valves are used instead of proportional valves, as discussed above.
- The clutch actuator is no longer concentric, which means that the actuator can be exchanged without dismounting the transmission.
- A mechanical alteration of the system is conducted to reduce the dead volume, with the sole purpose of reducing the hysteresis effect in the system.

While Kaasa (2006) in his thesis considers output-feedback control, including nonlinear observers designed for the system, this thesis considers switched control and provides adaptive observers for the system.

Work by Grancharova and Johansen, (Grancharova and Johansen (2009a), (2009b) and (2010)), consider Nonlinear Explicit Model Predictive Control for the clutch actuator system with on/off valves. Good quality reference tracking is obtained using this type of controller combined with PWM. The system has also been considered in master theses at NTNU, Knudsen (2005), Vallevik (2006), Løkken (2006), Gjone (2007) and Helgeland (2008) with various topics within modeling, control and observer design.

There are not much research published on pneumatic clutch actuation systems, other than the work on the KA clutch actuator system. Pneumatic clutch systems have been treated in the work by Tanaka et al.; Shimazu et al. (1986) develop a direct control pneumatic clutch, and Tanaka and Wada (1995) deal with fuzzy control for clutch engagement. Some earlier work by Tanaka also consider pneumatic clutch systems, see references within the latter articles. Xiang and Wikander consider modeling and control of a pneumatic actuated truck clutch system in a Technical report, Xiang and Wikander (1997) included in the PhD thesis Xiang (2001). Recently, Szabo et al. (2010) presented a linearization based observer for an electropneumatic clutch system actuated by on/off solenoid valves.

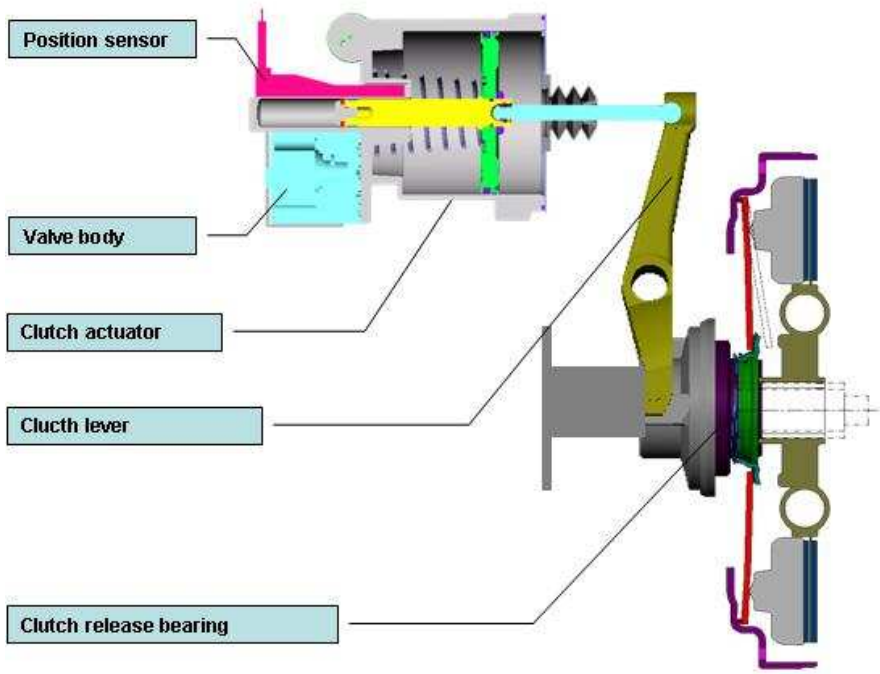

Figure 1.2: An overview of the considered clutch actuator system. Coutersy of Kongsberg Automotive ASA.

KA is currently using a PD-controller, only considering position measurement. Note that some further mechanical improvements of the clutch actuator system have been implemented after our experimental tests.

1.3 Overview of the Thesis

The remaining chapters in this thesis are organized as follows:

- *Chapter 2* - An overview of the electropneumatic clutch actuator is given, outlining its operation and describing the major mechanical parts. Configuration of the system for experimental testing in a test truck is presented, and aspects concerning the experiments are discussed.
- *Chapter 3* - This chapter considers modeling of the electropneumatic clutch actuator, and provides a basis for the models used for control and observer designs, and simulations in the later chapters. Physical phenomena are presented, and assumptions valid for the electropneumatic clutch actuator are discussed.
- *Chapter 4* - This chapter deals with switched control with emphasis on position control. A 3rd order model of the clutch actuator is presented for the purpose of control design. Two switched state feedback controllers are developed and evaluated, along with a combined state feedback dual-mode switched controller, utilizing both these controllers' individual strengths. Stability proofs of the controllers are derived, and experimental results for all three controllers are provided. The two individual controllers are presented in Sande et al. (2007) and Langjord et al. (2008a), respectively, while the combined dual-mode design is presented in Langjord et al. (2009) and Langjord and Johansen (2010).
- *Chapter 5* - Adaptive nonlinear observers for the clutch actuator system are considered, for the purpose of state feedback for the switched controllers developed in Chapter 4. Both a reduced order observer and a full-order observer are presented, the latter for reduction of the noise impact. Persistence of excitation conditions for convergence of the estimated errors and boundness of the adaptated parameters are derived. Performance of the adaptive observers are evaluated compared to experimental results from the test truck. The reduced-order adaptive observer is treated in Langjord et al. (2010) and the full-order observer is presented in Langjord et al. (2011a).
- *Chapter 6* - The dual-mode switched controller from Chapter 4 and the full-order adaptive observer from Chapter 5 are combined for position control of the actuator piston. A simulation model of the system is presented, validated and used to show performance of the resulting adaptive observer-based switched controller. This chapter contains simulation results, indicating that the pressure sensor can be eliminated by an adaptive observer used as a basis for a nonlinear state feedback control design. This work is presented in Langjord et al. (2011b).

- *Chapter 7* - Conclusions on the work presented in the thesis are made, and recommendations for further work are given.

The following is the list of the author's publications related to the work presented in this thesis. The only publication not directly included in the thesis is Langjord et al. (2008b) (included in the Appendix), which treats off-line estimation of the clutch load characteristics. This work is regarded as preparation for on-line estimation treated in Chapter 5, and the publications Langjord et al. (2010) and Langjord et al. (2011a). Note that the author's surname has changed from *Sande* to *Langjord* during the period of the given publications.

- Langjord, H., Kaasa, G. O. and Johansen, T. A., Adaptive nonlinear observer for electropneumatic clutch actuator with position sensor, To appear, as a brief paper, in IEEE Transactions on Control Systems Technology
- Langjord, H., Kaasa, G. O. and Johansen, T. A., Adaptive observer-based switched control for electropneumatic clutch actuator with position sensor, Submitted to: IFAC World Congress 2011
- Langjord, H. and Johansen, T. A., Dual-mode switched control of an electropneumatic clutch actuator, IEEE/ASME Transaction on Mechatronics 15, 969-981
- Langjord, H., Johansen, T. A. and Kaasa G. O., Nonlinear observer and parameter estimation for electropneumatic clutch actuator, *in* Proceedings of the 8th IFAC Symposium on Nonlinear Control Systems, Bologna, Italy, 2010
- Langjord, H., Johansen, T. A. and Bratli, C., Dual-mode switched control of an electropneumatic clutch actuator with input restrictions, *in* Proceedings of the 10th European Control Conference, Budapest, Hungary, 2009
- Langjord, H., Johansen, T. A., Snare, S. R. and Bratli, C., Estimation of electropneumatic clutch actuator load characteristics, *in* Proceedings of the 17th IFAC World Congress, Seoul, South Korea, 2008
- Langjord, H., Johansen, T. A. and Hespanha, J. P., Switched control of an electropneumatic clutch actuator using on/off valves, *in* Proceedings of the 27th American Control Conference, Seattle, USA, 2008
- Sande, H., Johansen, T. A., Kaasa, G. O., Snare, S. R. and Bratli, C., Switched backstepping control of an electropneumatic clutch actuator using on/off valves, *in* Proceedings of the 26th American Control Conference, New York, USA, 2007

1.4 Contributions

The main challenge adressed in this thesis is position control of an electropneumatic clutch actuator system actuated by on/off solenoid valves. As sensors in the

production system should be limited to a position sensor, estimates of other states of the system are needed. Parameter estimation is also needed, as models for accurate description of the system are complex and need to be simplified according to assumption on the system. In addition characteristics of the clutch actuator will change as it is used, due to wear and other external influences such as temperature.

The main contributions of this thesis can be summarized as:

- The development of switched controllers presented in Chapter 4. The on/off solenoid valves discrete behavior is exploited to design simple nonlinear controllers that switches the on/off solenoid valves between fully open and fully closed. Using such switched controllers avoids the modeling task of the on/off solenoid valves, as for operation no knowledge of the dynamics of the on/off solenoid valves are needed for accurate nonlinear control. Controllers based on PWM provide similar control inputs as these switched controllers, but to be able to calculate the PWM control signal, an inverse characteristic of the flow through the valves is needed, hence an accurate flow model is needed also in this case. For analysis of performance of the switched controllers, an expression of maximum flow through the valves is needed and knowledge about response times. The simplicity of the switched controllers also make them easy implementable.

- The development of the adaptive nonlinear observer designs presented in Chapter 5. No other adaptive observer with derived sufficient conditions for convergence of the estimation errors, is found in literature for systems like the considered clutch actuator system. This would be systems that are characterized by strongly uncertainties and time-varying clutch load characteristic, strong dynamic friction and with only position sensor available. This contribution is important for position control of the clutch actuator as the proposed switched controllers require state feedback.

- The experimental evaluations of the switched controllers in a full scale truck using production sensors. Experimental results are also used to validate the performance of the adaptive nonlinear observers. These experimental evaluations are important contributions as they confirm the theoretical analysis, and show that the designs are suitable for implementation in a heavy duty truck.

- The development of the adaptive observer-based switched control considered in Chapter 6. Although this chapter focuses on simulation results, and do not include mathematical stability and experimental performance proofs for the switched controller with feedback from the adaptive observer, it still is considered as a major contribution. Simulation results indicate that the combined design is well suited for position control of the clutch actuator system, and position control is considered as the most important task to solve in this thesis. The simulations also show that the adaptive observer can replace the pressure sensor without any significant loss of performance of the controller.

Chapter 2

Electropneumatic clutch actuator

This chapter gives an overview of the electropneumatic clutch actuator that is considered in this thesis. The main components of the system are described and the operation of the clutch is outlined. Important aspects about the setup for experimental testing in the test truck are discussed.

2.1 System overview

Figure 2.1 presents a schematic which gives an overview of the clutch actuator system. This clutch actuator system consists mainly of an Electronical Control Unit (ECU), a set of on/off solenoid valves, a pneumatic actuator, position and pressure sensors and a piston rod which connects the actuator to the clutch plates. Pneumatics are chosen to drive this system, as pressurized air already is present in heavy duty trucks. The ECU calculates the control signals which are sent to the on/off solenoid valves. Based on these, the on/off solenoid valves control the flow to and from the actuator chamber. The piston position is a result of the acting forces, mainly the friction, the pressure, the actuator spring and the clutch compression springs, and this position determines the state of the clutch plates. The plates can either be engaged, slipping or disengaged. When engaged, the clutch transmits torque from the motor to the axle shaft. The clutch is of pull type, which means that the clutch plates are fully engaged at zero piston position. As the piston moves to the right (air added to the actuator chamber) the clutch plates are pulled apart, first they will be slipping and then fully disengaged. A lip seal is used to avoid leakage between the piston and the cylinder wall, and thereby avoid flow between the two chambers in the actuator.

The clutch load force is the lumped force of the clutch compression spring and the counteracting, much weaker actuator spring. The characteristic of the clutch compression spring changes due to wear, hence the clutch load force also changes. Both the magnitude of the force and the shape of the load characteristic curve

are subject to change. The initial piston position, defined as the piston position corresponding to no actuation and the chamber pressures equal to the ambient pressure, will be influenced. As the clutch gets worn, this initial piston position will move and result in a negative position measurement. To avoid having to deal with negative position as changes in the initial position happen, the measured zero piston position is adjusted such that it always correspond to the actual initial position. In the production clutch actuator system this will be automatically calibrated at start up of the vehicle.

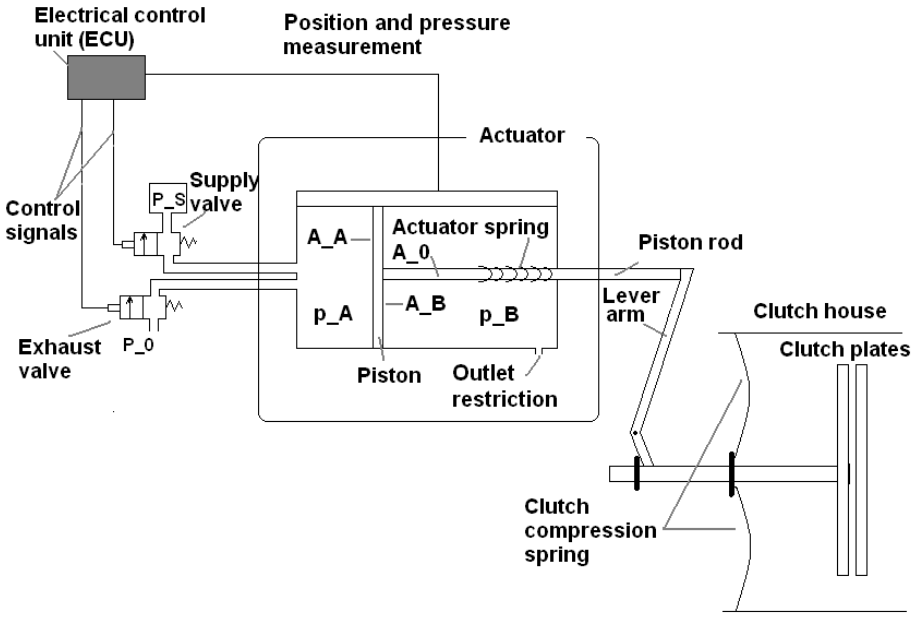

Figure 2.1: Electropneumatic clutch actuator system.

On/off solenoid valves are chosen over proportional valves as control valves, because they are smaller, cheaper and more robust, even though the on/off valves dynamics are harder to model accurately. Figure 2.2 shows cross-section illustrations of the on/off solenoid valves. They consist mainly of an electromagnet (pink), a valveseat (blue), an armature (green) and a spring. The illustration on the left shows a closed on/off solenoid valve, while the right one shows a fully open on/off solenoid. High pressure is indicated in yellow, and low pressure by dark gray. When an electric force is applied to the electromagnet, this sets up a magnetic field which will attract the armature and try to open the valve. The spring and the friction acts as closing forces, in addition to the pressure force over the valve seat which in

magnitude will vary considerably with the valve opening degree.

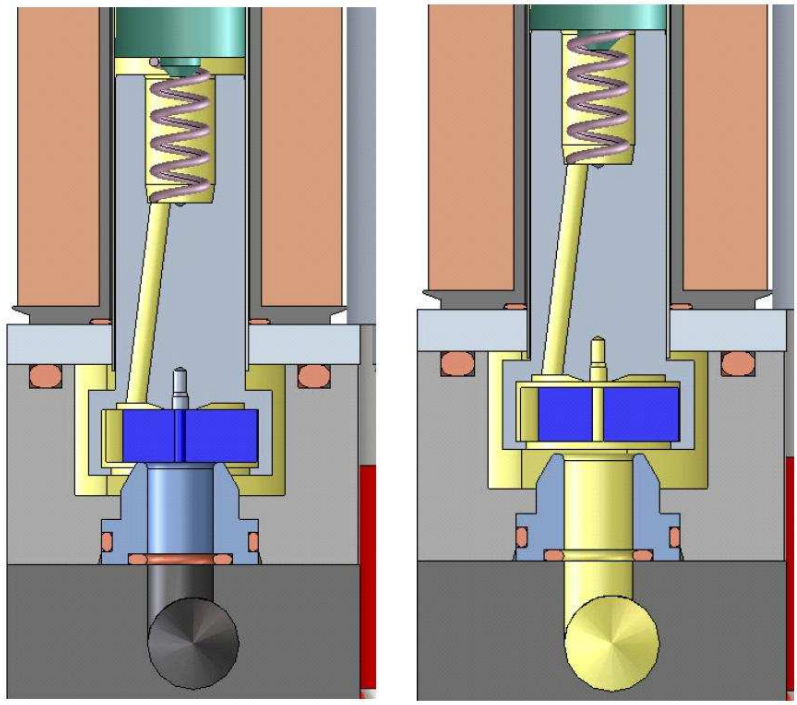

Figure 2.2: Cross-sections of an on/off solenoid valve, the left one illustrating a closed valve and the right illustrating a fully open valve.

2.2 Experimental testing - system configuration

The experimental tests presented in this thesis have been conducted in a Scania test vehicle, Gamal, at Kongsberg Automotive ASA, see Figure 2.3. In this vehicle both position and pressure sensors are present, although only a position sensor will be available in the finalized production system. Position and pressure are measured at a rate of 1 ms. The controller algorithms are designed in a Matlab/Simulink environment and run on a dSpace MABX 1401 unit. The sampling interval, and the controller updating interval, are both set to 1 ms. Figure 2.4 shows how the test system is connected. A virtual instrument control panel was developed in a dSpace Control Desk program. Through this panel parameters can be adjusted, and variables and measurements can be plotted on-line. The reference position for the piston was set manually through this instrument panel in the experimental test. In normal operation, this reference position will either be set by the truck

driver through an electrical signal from the clutch pedal, or by calculations from an automated gear shift control system.

Experiments for testing the switched controller were conducted with different control valves (see section below and Chapter 4), in February 2008 and April 2009, and hence with different degree of wear of the clutch and temperature. After the tests in April 2009, the configuration of the clutch system were altered to an actuator with integrated control unit, and after this further testing was not available. For this reason, experimental data obtained from the test truck in November 2007 has been used for validation of the observer design in Chapter 5.

Figure 2.3: The test truck, "Gamal".

2.2.1 Requirements for system performance

A benchmark clutch sequence for evaluating control system performance is shown in Figure 2.5. It is desired that the controller makes the system reach the reference point within 0.1 s, and with a steady state position error of less than 0.2 mm in the area where the clutch engage/disengage. This area is marked in Figure 2.5. Outside this area, the requirements can be somewhat relaxed. Using a somewhat smoother curve as reference clutch sequence might improve controller performance

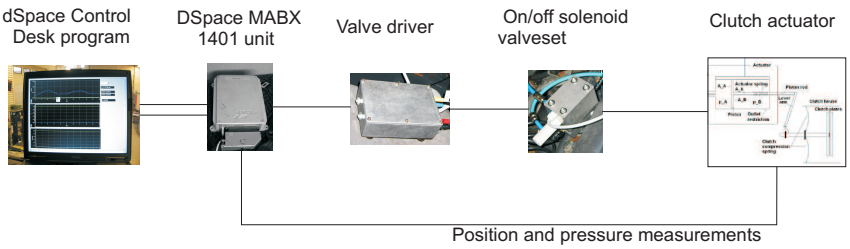

Figure 2.4: System configuration.

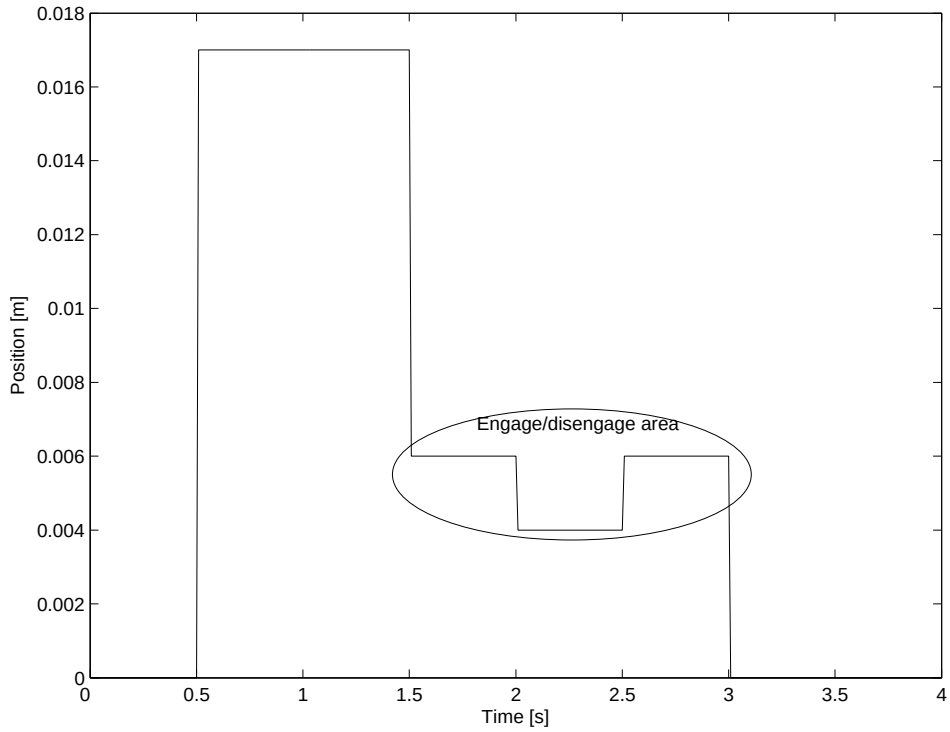

Figure 2.5: Clutch sequence used as position reference in the experiments to test control system performance.

in terms of less overshoot and reduced oscillation. The proposed clutch sequence is still used as it equals typical sequences used for testing of the clutch actuator system by KA.

2.2.2 Control valves

Two sets of on/off solenoid valves have been used in the experimental tests. Both sets are delivered by the Swedish company SO-Elektic, which has specialized in producing valves with short opening and closing times, that also maintain good response times even with large flow areas. A pre-prototype SO-valveset was used in the tests in February 2008 and a prototype SO-valveset was used in the testing in April 2009. Their characteristics have been examined by testing at KA and are given in Table 2.1. The valvesets are quite similar, the main difference is the shape of the valvehead, which were altered for the prototype valveset mainly to reduce acoustic noise. The experimental tests for validation of the adaptive observer are conducted with the pre-prototype valveset present in the truck. Since

Characteristic	*Pre-prototype*	*Prototype*
Opening time	0.5 ms	$0.8 - 1$ ms
Closing time	2.5 ms	$2.2 - 2.4$ ms
Maximum volumetric flow rate, supply	14 l/s	14 l/s
Maximum volumetric flow rate, exhaust	16 l/s	16 l/s

Table 2.1: Valveset characteristics.

both valvesets are prototypes, and suffering from overheated electronics, care had to be taken not to blow fuses or destroy the valveset electronic unit during testing. For the prototype valveset, the somewhat artificial restriction that the valves only could open once in every 20 ms was imposed to be sure to avoid overheating.

All on/off solenoid valves will experience a delay in response, due to current dynamics in the coil of the electromagnet in the solenoid. This delay will appear as a delay between the time the valve command input signals are set to the time when accumulated air starts changing. Due to compressibility of air and friction, a delay from the time accumulated air changes and until the time a change in position is detected will also be experienced in the system. Average values found through experiments for these delays are given in Table 2.2.

Delay	*Pre-prototype*	*Prototype*
Input to accumulated air	0.67 ms	5 ms
Acc. air to change in position	7.2 ms	3.5 ms

Table 2.2: Average delays of the valvesets, values found from experimental data.

2.2.3 Clutch load

The clutch load characteristic changes with wear and temperature, and was different at the two testing times of the switched controller in Chapter 4. Figure

2.6 shows the tuned clutch load characteristic models compared to experimental results. The load obtained from experiments also include dynamic friction, which explains the shown hysteresis. The characteristic from the data obtained in November 2007, is very similar to that of February 2008 and is therefore not shown in the figure.

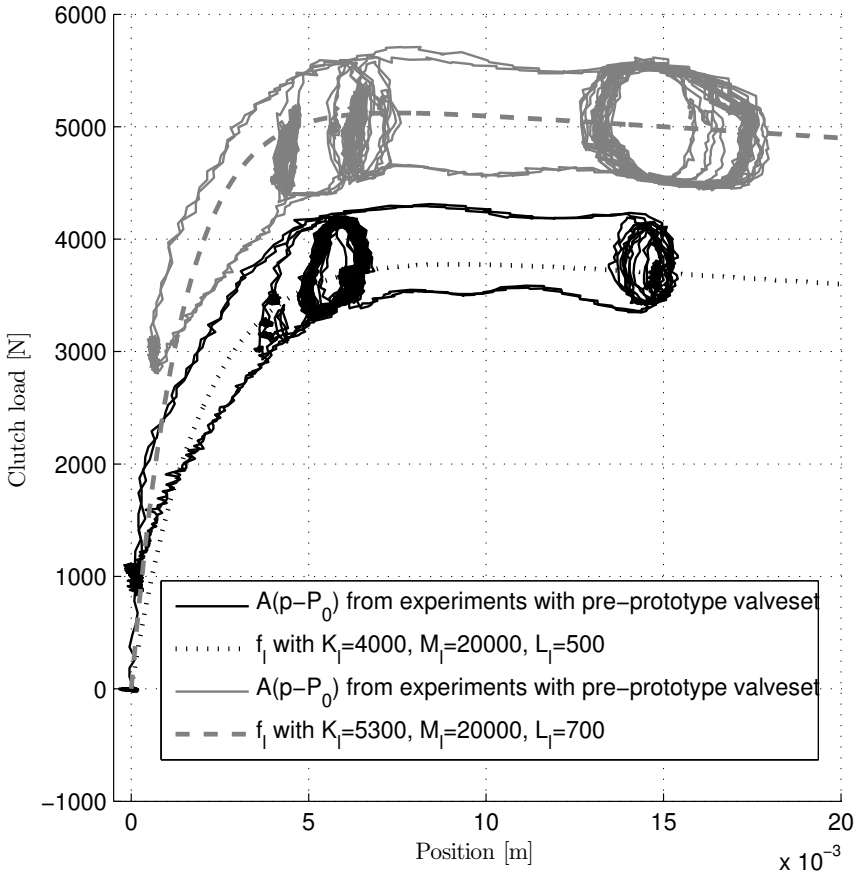

Figure 2.6: Clutch load characteristic for the tests in February 2008 (black) and April 2009 (gray), modeled in dashed and estimated from measurements in solid.

2.2.4 Sensors

The sensors are production quality sensors. These suffer from more noise than more expensive, higher quality sensors used in test rigs made for research and development, as the ones used by Kaasa (2006). Since the tests are performed in the actual truck, the measurements are also influenced by the motor vibrations of the test truck. These vibrations can make the clutch piston move, even with no

actuation of the clutch actuator. Figure 2.7 shows position measurement provided by the position sensor in the test truck with no actuation, that is, no supply and no exhaust of air to/from the actuator chamber and reference position $y = 0$. The noise in these measurements correspond to variance $9.72 \cdot 10^{-3}$ mm^2 and mean -0.0183 mm. Similar position measurement noise is also detected with no actuation for the piston in other position.

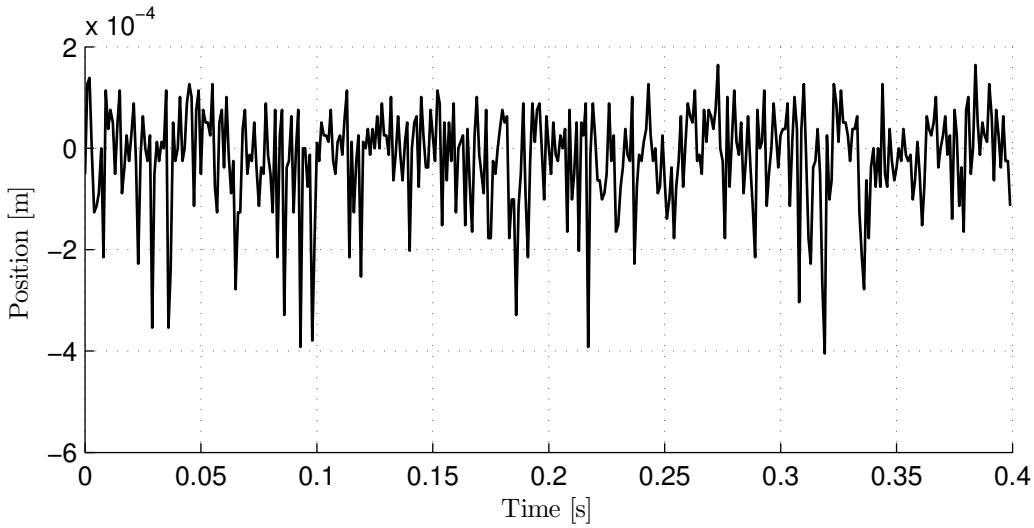

Figure 2.7: Position measurement provided by the position sensor when no input is given, and reference position is $y = 0$, showing the noise caused by motor vibration and signal transmission in the position sensor.

Chapter 3

Modeling

This chapter treats modeling of the clutch actuator system. In principle, the same clutch actuator system was also treated by Kaasa (2006) in his doctoral thesis, and in general we refer to this for more details on modeling of the system. The most significant difference in the system here considered, is the change of control valve from from a proportional valve to a set of on/off solenoid valves.

3.1 Motion dynamics

The motion dynamic of the clutch actuator piston is described by using Newton's second law

$$M\dot{v} = f_p(\cdot) - f_l(y) - f_f(\cdot) \tag{3.1}$$

where M is piston mass, v is piston velocity, f_p describes the pressure force, f_l describes the clutch load characteristic and f_f describes the friction force. Considering the schematic in Figure 2.1, it is clear that the resulting pressure force is given by

$$f_p(p_A, p_B) = A_A p_A - A_B p_B - A_0 P_0 \tag{3.2}$$

where A_A and A_B are the areas of chambers A and B, respectively, p_A and p_B are the pressures in the chambers, $A_0 = A_A - A_B$ is the area of the piston rod and P_0 is the ambient pressure.

3.2 Friction

The friction force is a substantial force in the clutch actuator, and the elasticity of the seal on the piston makes modeling of pre-sliding properties important for an accurate friction model. The friction will increase with increased pressure in the actuator, because the seal is pressed harder against the cylinder wall, causing hysteresis to arise.

Pre-sliding friction forces describes friction without movement of the piston. This is friction due to asperity junctions arising between the actuator piston and the cylinder wall when an external force is applied to the bodies. These junctions behave like springs, and result in an elastic deformation of the asperities, Egeland and Gravdahl (2002). At a certain force the junctions will be broken and the piston will start to move, and this force is called the break-away force. This break-away force will also vary with the pressure in the clutch actuator, depending on how hard the seal is pressed against the cylinder.

The friction force with a moving piston, called sliding friction, is dependent on the piston velocity. The simplest friction model is the viscous friction model

$$f_f = Dv \tag{3.3}$$

where the friction is proportional to velocity, and D is the viscous friction constant. This model is the best description of the friction force in cases where the bodies are separated by a lubricate building a full fluid film between the bodies, but can also be tuned to represent systems as damped rather well for other cases, Andersson et al. (2007). A common model is the Coulomb friction model, in its simplest form given as

$$f_f = F_C sgn(v) \tag{3.4}$$

where the Coulomb friction F_C is given by

$$F_C = \mu N. \tag{3.5}$$

where μ is the friction coefficient and N is the load. The Coulomb friction is derived by assuming no contaminations on the surfaces, and is often referred to as dry friction, but is also used to model friction for boundary and lubricated contacts. The friction decreases with increased velocity for lubricated sliding contacts, until a full fluid film is built between the contacts. Similar behavior is also found for dry contacts, Andersson et al. (2007), and is called the Stribeck effect. A Stribeck friction model is

$$f_f = F_C + (F_S - F_C)e^{-\left|\frac{v}{v_s}\right|^\sigma} \tag{3.6}$$

where F_C is the Coloumb friction, F_S is the break-away force, v_s is called the Stribeck velocity and σ is a parameter which determine the characteristics of the Stribeck curve. Including the Stribeck effect gives a smooth description of the transition from the pre-sliding to the sliding friction regime when combining pre-sliding friction and sliding friction models. The viscous, the Coulomb and the Stribeck friction models are all static models, and to account for the dynamic phenomena as the hysteresis discussed above, a dynamic model will be needed.

The LuGre model was proposed in Canudas de Wit et al. (1995) as a model well suited to describe friction forces for hydraulic and pneumatic control systems. This is a model capturing most friction behaviors discussed above; viscous friction, Coulomb friction, the Stribeck effect, hysteresis and varying break-away forces can

all be included. This model is given as

$$\dot{z} = v - \frac{K_z}{f_d}|v|z \tag{3.7}$$

$$f_f = K_z z + D_{\dot{z}}\dot{z} + Dv \tag{3.8}$$

where f_d is dry friction, K_z is deflection stiffness and $D_{\dot{z}}$ is the deflection damping coefficient. The state z is the friction state, and can here be described as the pre-sliding seal deflection.

3.3 Pressure dynamics

Air flow dynamics are described by both pressure and temperature dynamics. Kaasa (2006) presents a detailed derivation of a full model of the systems air flow dynamics based on elementary thermodynamics using conservation of energy. Here we propose a reduced isothermal model of the pressure dynamics. That is, we consider all temperatures in the system to be equal to the standardized atmospheric temperature (T_0), which is done as the pressure dynamics sensitivity to temperature changes is found to be small for the clutch actuator system, Kaasa (2006).

The reduced model is obtained by taking the following assumptions, based upon the assumptions listed in chapter 4 in Kaasa (2006):

- At the attainable pressure, air behaves like an ideal gas obeying the ideal gas equation of state with negligible error.
- The thermodynamic properties are uniformly distributed (homogeneous) within the control volume, i.e., perfectly mixed. This is reasonable due to the small dimension of the system, and a complex distributed problem formulation is avoided.
- The energy change in the fluid due to elevation is negligible.
- The flow through pipes, valves and restrictions in the system is assumed to be isentropic. That is, frictionless flow is assumed, and the effect of heat transfer on the flow is disregarded (adiabatic flow). This is a common assumption when system dimensions are small, Bobrow and McDonell (1998).
- The kinetic energy within the chambers are neglectable as the chambers can be considered to be reservoirs.
- We assume isothermal conditions, which means that the chamber temperatures are constant. Furthermore, we assume that all temperatures equals the standardized atmospheric reference condition (T_0) given by the ISO standards. This gives constant specific heats c_p and c_v of air.
- We have a constant supply pressure p_S, and assume that the exhaust pressure p_E equals a constant atmospheric pressure.

This gives us the following equations for the pressure dynamics,

$$\dot{p}_A = -\frac{A_A v}{V_A(y)} p_A + \frac{RT_0}{V_A(y)} w_v \tag{3.9}$$

$$\dot{p}_B = \frac{A_B v}{V_B(y)} p_B + \frac{RT_0}{V_B(y)} w_r \tag{3.10}$$

where R is the ideal gas constant of air, $w_v = w_{in,A} - w_{out,A}$ and $w_r = w_{in,B} - w_{out,B}$ are the resulting flows into the chambers A and B through, respectively, the on/off solenoid valves and the outlet restriction. The variables $V_A(y)$ and $V_B(y)$ are the chamber volumes at a given position, $V_A(y) = V_{A,0} + A_A y$ and $V_B(y) = V_{B,0} + A_B y$ where $V_{A,0}$ and $V_{B,0}$ are the chamber volumes at initial position, $y = 0$.

3.4 Valve flow dynamics

Flow through the on/off solenoid valves and the outlet restriction can be modeled as flow through a restriction. In ISO (1989) the standardized orifice flow equation is defined as

$$w = \rho_0 \sqrt{T_0} C \omega(r) \frac{p_h}{\sqrt{T_h}}$$

where C is conductance, ρ_0 is density, $r = \frac{p_l}{p_h}$ is the ratio between the low (p_l) and the high (p_h) pressure at the sides of the orifice and ω is a pressure ratio function which determine how the flow depends on the pressure rate. By assuming the the exhaust pressure to equal to the ambient pressure and all temperatures equal to standardized atmospheric reference condition, T_0 as in previous section, a simplified version of the standardized orifice flow equation (see also chapter 5.3 in Kaasa (2006)) can be used to describe flow through a restriction

$$w = \rho_0 C \omega(r) p_h. \tag{3.11}$$

A general pressure ratio function is given by

$$\omega(r, B) \quad = \quad \Omega_0(r) + B\Omega_1(r, sgn(B)), \quad B \in [-1, 1] \tag{3.12}$$

where

$$\Omega_0(r) = \begin{cases} \sqrt{1 - r^2}, & r \in [0, 1] \\ 0, & r > 1 \end{cases} \tag{3.13}$$

$$\Omega_1(r, +1) = -\Omega_0 + \begin{cases} 1, & r \in [0, B_0] \\ \sqrt{1 - \left(\frac{r - B_0}{1 - B_0}\right)^2}, & r \in \langle B_0, 1] \\ 0, & r > 1 \end{cases} \tag{3.14}$$

$$\Omega_1(r, -1) = \Omega_0 - \begin{cases} 1 - r, & r \in [0, 1] \\ 0, & r > 1 \end{cases} \tag{3.15}$$

and $B_0 = 0.528$ is the isentropic critical pressure ratio for air. The pressure ratio function (3.12) with the expressions in (3.14) and (3.15) can be characterized as approximately isentropic and incompressible laminar flow, respectively. The value of B decides between the two flow types.

Experiments have shown that we can set $B = 0$, that is using the pressure ratio function

$$\omega(r) = \Omega_0(r) = \begin{cases} \sqrt{1-r^2}, & r \in [0,1] \\ 0, & r > 1. \end{cases} \tag{3.16}$$

and get a simplified model that still describes the flow through the on/off solenoid valves and the outlet restriction with sufficient accuracy for control purposes.

3.4.1 Flow of chamber A

Equation (3.11) with the pressure ratio function given in (3.16) is used to describe the maximum flow through the on/off solenoid valves. The resulting air flow to/from chamber A is

$$\begin{aligned} w_v(p_A, u) &= w_{c,s}u_s - w_{c,e}u_e \\ &= \rho_0 C_s \omega\left(\frac{p_A}{P_S}\right) P_S u_s - \rho_0 C_e \omega\left(\frac{P_0}{p_A}\right) p_A u_e \end{aligned} \tag{3.17}$$

where the subscripts "s" and "e" stand for supply and exhaust, respectively, and u_s and u_e are valve command inputs obtained from the input as shown in Table 3.1.

u	u_s	u_e
1	1	0
0	0	0
−1	0	1

Table 3.1: Relations between the input to the system and the valves command input.

Remark 3.4.1. *In Chapter 5, we compare our developed observer to experiments conducted in the test truck by KA. In these experiments PWM are used, and for describing flow through the on/off solenoid valves in this case, (3.17) needs to be rewritten to take the opening degree of the valves into consideration,*

$$\begin{aligned} w_v(p_A, u) &= w_{c,s}y_{u,s} - w_{c,e}y_{u,e} \\ &= \rho_0 C_s \omega\left(\frac{p_A}{P_S}\right) P_S y_{u,s} - \rho_0 C_e \omega\left(\frac{P_0}{p_A}\right) p_A y_{u,e}. \end{aligned} \tag{3.18}$$

where

$$y_{u,s} = sat_{[0,1]}\left(\frac{1}{R_{1,s} - R_{0,s}}(u_s - R_{0,s})\right) \tag{3.19}$$

$$y_{u,e} = sat_{[0,1]}\left(\frac{1}{R_{1,e} - R_{0,e}}(u_e - R_{0,e})\right) \tag{3.20}$$

describes the mean valve opening where u_s and u_e are the command inputs of the valves PMW input. $R_{0,s}$ and $R_{0,e}$ are the command inputs where the valves start to open and $R_{1,s}$ and $R_{1,e}$ are the command inputs for which the valves are fully open. In the rest of the thesis the opening degree of the on/off solenoid valves are considered as fully open or fully closed, corresponding to PWM design with only command inputs 0 and 1, respectively. As the set $\{0,1\}$ is a subset of the input range $u_{s/e} \in [0,1]$, the equation (3.18) is still valid, and can be used in both cases.

3.4.2 Flow of chamber B

The resulting flow to/from chamber B is

$$\begin{aligned} w_r(p_B) &= w_{in} - w_{out} \\ &= \rho_0 C_r \omega\left(\frac{p_B}{P_0}\right) P_0 - \rho_0 C_e \omega\left(\frac{P_0}{p_B}\right) p_B \end{aligned} \tag{3.21}$$

where w_{in} represents the flow through the outlet restriction if $P_0 > p_B$ and w_{out} represents the flow if $p_B > P_0$.

These chamber flow functions satisfy

$$\frac{\partial w_v}{\partial p_A}(p_A, u) \leq 0, \quad \forall p_A \in [P_0, P_S], \forall u \in [-1, 1] \tag{3.22}$$

$$\frac{\partial w_r}{\partial p_B}(p_B) < 0, \quad \forall p_B \in [0, \infty\rangle \tag{3.23}$$

as verified in Figures 3.1(a) and 3.1(b).

3.5 Clutch load characteristic

The clutch load force describes the lumped force of the actuator spring and the clutch compression spring. The actuator spring is linear, while the compression spring is highly nonlinear and of a much higher magnitude than the actuator spring. The clutch load depends mainly on the piston position, and can generally be parameterized in the linear form

$$f_l(y) = \phi^T(y)\,\theta \tag{3.24}$$

where $\phi(y) = (\phi_1(y), \phi_2(y), ...\phi_n(y))^T$ is a vector of basis functions and θ is the corresponding weighting parameter vector. The linear parameterized form is well

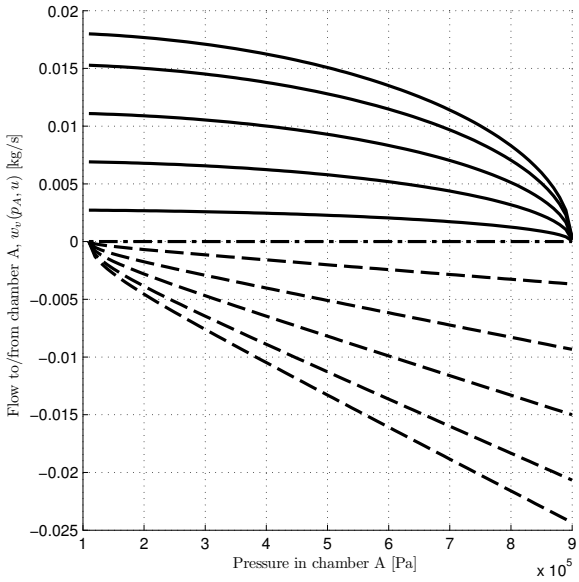

(a) The valve flow $w_v(p_A, u)$. Flow with positive u are shown in solid, where the value of u increases upwards, while flow with negative u, where the value decreases downwards are shown in dashed. The dot dashed curve represents no flow, $u = 0$.

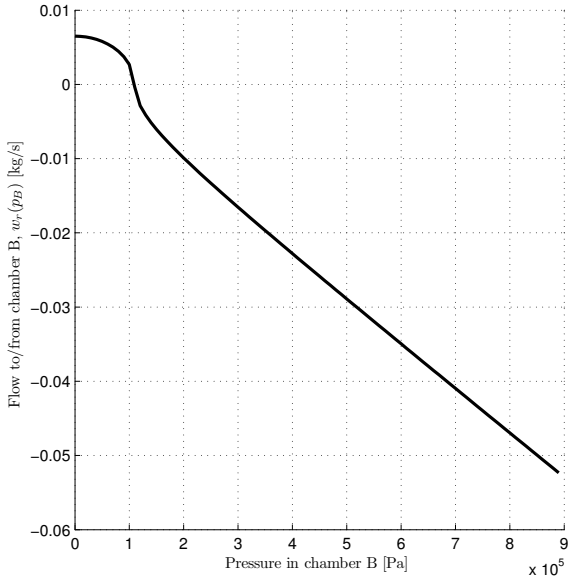

(b) The restriction flow $w_r(p_B)$.

Figure 3.1: The flows $w_v(p_A, u)$ and $w_r(p_B)$ are monotonically decreasing in respectively p_A, p_B, for fixed u.

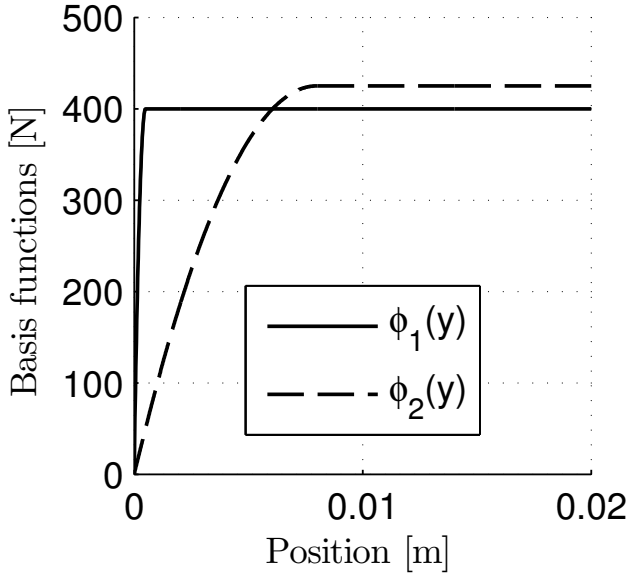

(a) The basis functions used for clutch load modeling.

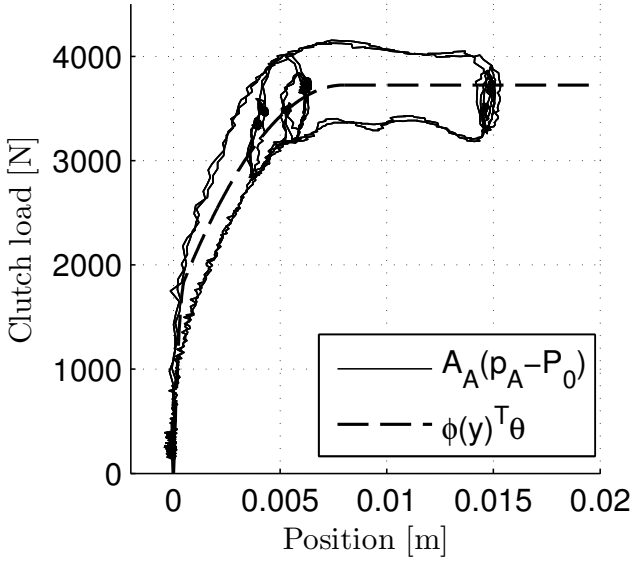

(b) Clutch load, modeled (dashed) and experimental (dashed). The experimental data include not only the clutch load force but also the effect of dynamic friction (hysteresis).

Figure 3.2: Clutch load characteristics model with $n = 2$, i.e. two B-spline basis functions.

suited for estimation, which is needed as the clutch load characteristics change with temperature and wear of the clutch.

A model with $n = 2$ and the following B-splines are proposed. The spline basis functions are built up by polynomials

$$\phi_1(x) = \begin{cases} 0, & x < t_1 \\ a_1x^2 + b_1x, & t_1 \leq x < t_2 \\ a_1t_2^2 + b_1t_2, & x \geq t_2 \end{cases} \tag{3.25}$$

$$\phi_2(x) = \begin{cases} 0, & x < t_1 \\ 10^5(x - t_1), & t_1 \leq x < t_2 \\ a_2x^2 + b_2x + c_2, & t_2 \leq x < t_3 \\ a_2t_3^2 + b_2t_3 + c_2 & x \geq t_3 \end{cases} \tag{3.26}$$

where the knots are set to $t_1 = 0\ mm$, $t_2 = 0.5\ mm$ and $t_3 = 8\ mm$. To be able to find the spline coefficients from the positions of the knots we need some criteria:

- ϕ_1
  - Derivative in t_2 is to be equal to zero
  - The value is to be 400 in t_2
- ϕ_2 :
  - Transition between the linear and the quadratic part is to be smooth
  - Derivative in t_2 is to be equal to one
  - Derivative in t_3 is to be equal to zero

Mathematically written this gives

$$\eta_i = A_i^{-1}B_i \qquad i = 1, 2$$

where

$$A_1 = \begin{bmatrix} t_2^2 & t_2 \\ 2t_2 & 1 \end{bmatrix}$$

$$A_2 = \begin{bmatrix} t_2^2 & t_2 & 1 \\ 2t_2 & 1 & 0 \\ 2t_3 & 1 & 0 \end{bmatrix}$$

$$B_1 = [400, 0]^T$$

$$B_2 = \left[10^5(t_2 - t_1), 10^5, 0\right]^T$$

and

$$\eta_1 = [a_1, b_1]^T$$

$$\eta_2 = [a_2, b_2, c_2]^T$$

As an example, Figure 3.2 show the proposed splines and the resulting clutch load model using $\theta_0 = [4, 5]$ compared with a clutch load characteristic obtained from experimental data. To account for the clutch load curve moving significantly to the left/right due to wear and temperature, a Multiple Model Scheme can be used. Here a supervisory logic choosing the best set of basis functions from multiple models where ϕ_1 deflects at different positions similar to approaches in Bakkeheim and Johansen (2006) and Narendra and George (2002). This is illustrated in Figure 3.3, where a set of ϕ_1's are given along with resulting clutch load models.

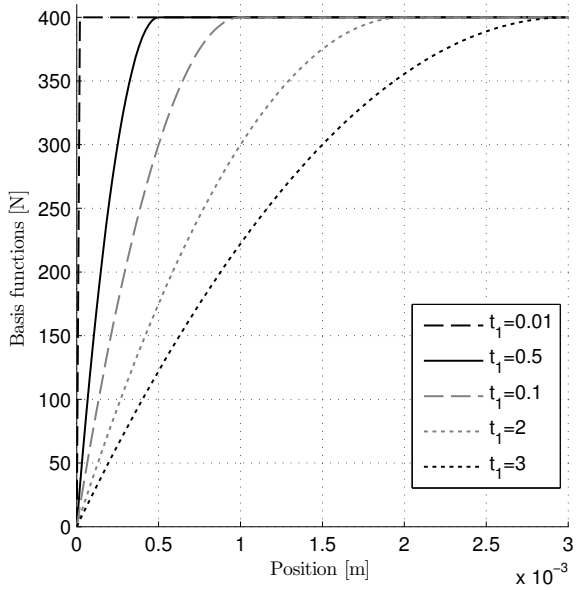

(a) Different configuration of ϕ_1.

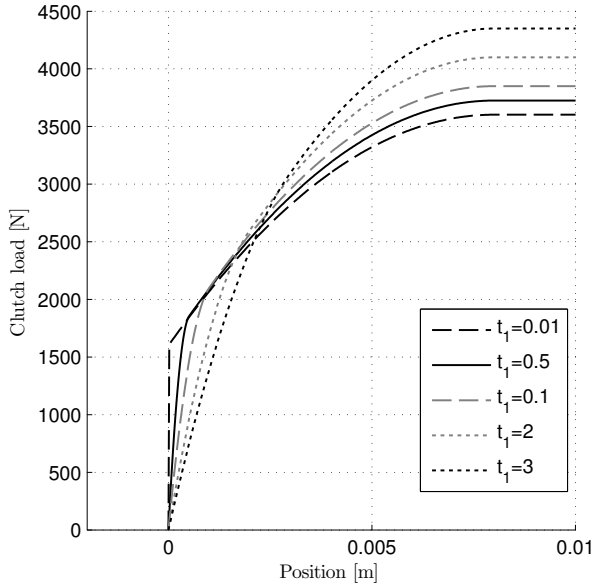

(b) The resulting clutch load models with the ϕ_1's shown in (a).

Figure 3.3: Clutch load characteristics using $\theta = [4, 5]$. These are examples of models that could be used for a Multiple Model Scheme.

Chapter 4

Switched control

This chapter considers nonlinear state-feedback position control of the electropneumatic clutch actuator assuming a given nonlinear model. Two switched controllers are designed along with one dual-mode switched controller combining these. This chapter is mainly based on Sande et al. (2007), Langjord et al. (2008a), Langjord et al. (2009) and Langjord and Johansen (2010). Adaptive observer-based extensions are given in Chapter 5 and 6.

4.1 Introduction

On/off solenoid valves are used to control the airflow to/from the actuator, and accurate position control of the actuator piston depend on good control of these valves. The on/off valve can, in contrast to what the name indicates, also be controlled to take positions in between fully open and fully closed. But as the on/off valves dynamics are highly nonlinear, and thus hard to model accurately, an interesting approach will be to consider the valve as only being able to hold one of the two positions; fully open or closed. This motivates for a switched controller design.

Switched systems have received lots of interest the last decade, with a vast number of publication in fields as control of mechatronic systems and automotive industry. Switched controllers used for continuous systems is one of two cases where switched systems arises, the other case being abrupt changes in the structure and the parameters of dynamic systems. In general, the main motivation for using a switched controller is to achieve better performance. The switched designs in this chapter are in addition motivated by the possibility of exploiting the on/off solenoid valves discrete behavior and thereby simplifying the modeling task for control design.

Dealing with discrete input devices, such as on/off solenoid valves, Pulse Width Modulation (PWM) is often employed. PWM may allow control laws made for proportional valves to be used for solenoid valves. Varseveld and Bone (1997) show how fast, accurate and inexpensive position control for pneumatic actuators can be obtained using on/off solenoid valves and PWM. Carducci et al. (2004) propose

a vision feedback on a robotic arm where the on/off solenoid valves are driven by PWM techniques, while Ahn and Yokota (2005) propose a modified PWM scheme to improve steady-state error often arising when using on/off valves.

During the last decades, sliding mode techniques have also become a common approach to design controllers for pneumatic actuators actuated by on/off solenoid valves. Many of the controllers developed by sliding mode are continuous and implemented by PWM, as in Shen et al. (2004) which create a sliding mode control with equivalent control and the use of PWM to produce the control signal. Some utilize the discrete nature of the on/off solenoid valves and the sliding mode technique. Paul et al. (1994) propose a position control algorithm based on sliding mode control for a pneumatic cylinder with on/off valves, and Nguyen et al. (2007) also use a sliding mode approach to construct a control signal which can be directly applied to solenoid valves.

One of the main advantages by designing controllers that can be applied without employing PWM, is that we do not need to know the on/off valves characteristics. The only knowledge needed are their response times and the maximum flow capacities for design, stability and performance analyses of the controllers. The switched controllers may also achieve faster closed loop response time since the controller is not limited by the PWM duty cycle.

As part of the switched controller designs in this chapter, the backstepping method is considered. Backstepping is in general used to produce stabilizing controllers through a recursively design, while also construct a Control Lyapunov function (CLF) for the system. This technique is not extensively used for pneumatic actuator systems. Rao and Bone (2008) propose a Multiple Input Multiple Output control law for a pneumatic actuator with four low-cost two-way proportional valves, Kimoto and Iti (2003) extend a linear controller by a nonlinear robust compensation obtained through backstepping and Smaoui et al. (2006) present a backstepping approach used to synthesize a controller for pneumatic actuator with two three-way proportional valves. Kaasa (2006) considers output-feedback control for the clutch actuator system with a proportional valve. A model-based nonlinear tracking controller is designed by a recursive observer-based backstepping approach, producing a robust controller design.

4.1.1 Model for control design

For control design a simple model of the electropneumatic clutch actuator is desired. Some assumptions are made, in addition to the aspects discussed in Chapter 3, to obtain a model adequate for control design:

- The pressure dynamics in chamber B are neglected, that is assuming $p_B = P_0$. This reduces the pressure dynamics to

$$\dot{p} = -\frac{Av}{V(y)}p + \frac{RT_0}{V(y)}w. \tag{4.1}$$

  where $p = p_A$, $A = A_A$ and $V(y) = V_A(y)$ for simplicity of notation.

- The clutch load characteristic is modeled by a nonlinear function
$$f_l(y) = K_l(1 - e^{-L_l y}) - M_l y \tag{4.2}$$
where K_l, M_l and L_l are constants that are tuned manually.
- Dynamic friction is neglected, leaving only viscous friction Dv.
- The flow through the on/off solenoid valves are expressed by $w = U_{max}u$, where u is the control input and $U_{max} = \rho_0 C P_S$ is a simplified, constant expression for the maximum flow capacity through these valves.

The supply and exhaust capacities are in general different and are dependent on the pressure difference over the valves and the ambient temperature. The simplifying assumption on the flow capacity can by done by assuming choked flow conditions. In the most important operational region, the engage/disengage area, the pressure drop tends to be significant due to a supply pressure of 9.5 bar and a maximum cylinder pressure of less than 6 bar. The only region where the choked flow assumption is not valid is when the clutch is completely disengaged and the cylinder is being emptied from air. However, this modeling error is disregarded in this chapter as control accuracy is not as important in this region.

To simplify notation, we denote the state variables in this chapter by $x = [x_1, x_2, x_3]$ where

$$\begin{aligned} x_1 &= y \\ x_2 &= v \\ x_3 &= pV(x_1), \end{aligned}$$

that is, x_1 is piston position $[m]$, x_2 is velocity $[m/s]$ and x_3 is accumulated air $[kgm^2/s]$, which is proportional to the amount of air in the actuator chamber, and $V(x_1) = V_0 + Ax_1$ describes the volume in chamber A.

The resulting 3rd order model for control design is

$$\dot{x}_1 = x_2 \tag{4.4a}$$
$$\dot{x}_2 = \frac{1}{M}\left(-f_l(x_1) - Dx_2 + \frac{Ax_3}{V(x_1)} - AP_0\right) \tag{4.4b}$$
$$\dot{x}_3 = RT_0 U_{max} u \tag{4.4c}$$

where u is the valve control input. The state errors are written as $\tilde{x}_i = x_i - x_i^*$, where x_i^* are reference points, $x^* = [x_1^*, 0, x_3^*]^T$. The reference piston position x_1^* is given, and x_3^* is given by the steady-state relation

$$x_3^* = \frac{V(x_1^*)}{A}(K_l(1 - e^{-L_l x_1^*}) - M_l x_1^* + AP_0). \tag{4.5}$$

The theoretical region of operation for the considered clutch actuator is $O = \{x_1 \in [0, 0.025], x_2 \in \mathbb{R}, x_3 \in \langle\, 0, \infty \,]\}$, where the position limits correspond to mechanical end stop. The only available inputs using one supply and one exhaust on/off valve are

$$u \in \{-1, 0, 1\}, \tag{4.6}$$

and Table 4.1 gives the realtion between input and valve positions.

Input	*Supply valve*	*Exhaust valve*
-1	Closed	Open
0	Closed	Closed
1	Open	Closed

Table 4.1: Valve positions corresponding to the inputs.

In this chapter we assume full state feedback. The test truck provides position and pressure measurements, while velocity for the experiments in this chapter is numerically diffetentiated from the position measurement using a second order low pass filter with coincident poles in -40 rad/s. Parametric values are given in Table 4.2.

Parameter	*Notation*	*Value*	*Unit*
Mass	M	10	kg
Actuator area	A	$12.3 \cdot 10^{-3}$	m
Ambient pressure	P_0	$1 \cdot 10^5$	Pa
supply pressure	P_S	$9.5 \cdot 10^5$	Pa
Temperature	T_0	293	K
Gas constant of air	R	288	J/kgK
Volume at $y = 0$	V_0	$0.148 \cdot 10^{-3}$	m^3
Viscous damping	D	2000	Ns/m
Conductance	C	$26.7 \cdot 10^{-9}$	m^4s/kg
Density	ρ_0	1.185	kg/m^3

Table 4.2: Parameters for the clutch actuator model.

4.1.2 Control strategy

Li et al. (2001) establish two major tasks that should be accomplished as a switched controller is designed. These are the design of basic controllers, and the definition of the switching law of the basic controllers. The input restrictions, limiting our controller choices to $u \in \{-1, 0, 1\}$, reduce the piston position control problem to finding a switching law that can govern switching between these available inputs, in a way that stabilizes the system. We pose the following control strategy

Control strategy: *At each sampling instant, choose the available input which gives the most negative definite Lyapunov function time derivative with a well chosen control Lyapunov function (CLF).*

Utilizing this strategy, a new task has to be solved, that is the design of appropriate CLFs. In this chapter we consider two different methods for this:

- Using backstepping
- Based on knowledge of the system

By performing a full backstepping controller design, a Lyapunov function for the clutch actuator system is designed. Second we choose a Lyapunov function based on knowledge of the system. This is done by extending a Lyapunov function used to show stability of the second order reduced open loop system ($u = 0$, $x_3 = x_3^*$), to yield for the 3rd order system.

4.2 Controller 1 - "Local controller"

Backstepping is a well known technique to design a state feedback control input and a Lyapunov function proving its stability in the same operation, see Kristic et al. (1995). If we assume no restrictions on the input, backstepping can be used to find a suitable control Lyapunov function for the system.

4.2.1 Backstepping

Step 1
First we define

$$\xi_1 = x_1 - x_1^* \tag{4.7}$$

which gives

$$\dot{\xi}_1 = x_2. \tag{4.8}$$

We choose the virtual control $x_2 = \phi_1(\xi_1) = -k\xi_1$, where k is a positive constant. From the Lyapunov-like function

$$U_1(\xi_1) = \frac{\alpha_1}{2}\xi_1^2 \tag{4.9}$$

it is easy to show that this virtual control gives

$$\dot{U}_1 = -\alpha_1 k \xi_1^2.$$

Step 2
The change of variables

$$\xi_2 = x_2 - \phi_1(\xi_1) = x_2 + k\xi_1 \tag{4.10}$$

transforms the system into

$$\dot{\xi}_1 = \xi_2 - k\xi_1 \tag{4.11a}$$

$$\dot{\xi}_2 = \frac{1}{M}\left(-K_l(1 - e^{-L_l x_1}) - D(\xi_2 - k\xi_1) + M_l x_1 + A\frac{x_3}{V(x_1)} - AP_0\right) + k\xi_2 - k^2\xi_1. \tag{4.11b}$$

We now choose x_3 as the virtual control $\phi_2(x_1, \xi_1, \xi_2)$ and

$$U_2(\xi_1, \xi_2) = U_1(\xi_1) + \frac{\beta_1}{2}\xi_2^2. \tag{4.12}$$

From

$$\begin{aligned}\dot{U}_2 =&\alpha_1\xi_2\xi_1 - \alpha_1 k\xi_1^2 + \frac{\beta_1}{M}\xi_2\Big(- K_l(1-e^{-L_l x_1}) + M_l x_1 \\ &- D(\xi_2 - k\xi_1) + A\frac{\phi_2(x_1,\xi_1,\xi_2)}{V(x_1)} - AP_0\Big) + \beta_1 k\xi_2^2 - \beta_1 k^2\xi_1\xi_2\end{aligned}$$

and by setting

$$\alpha_1 = \beta_1 k^2$$

we get

$$\begin{aligned}\dot{U}_2 =& - \alpha_1 k\xi_1^2 + \frac{\beta_1}{M}\xi_2\Big(- K_l(1-e^{-L_l x_1}) + M_l x_1 - D(\xi_2 - k\xi_1) \\ &+ A\frac{\phi_2(x_1,\xi_1,\xi_2)}{V(x_1)} - AP_0\Big) + \beta_1 k\xi_2^2.\end{aligned}$$

We choose the virtual control as

$$\phi_2(x_1,\xi_1,\xi_2) = \frac{V(x_1)}{A}(K_l(1-e^{-L_l x_1}) - M_l x_1 - Dk\xi_1 + AP_0 - Mk\xi_2) \tag{4.13}$$

to get

$$\dot{U}_2 = -\alpha_1 k\xi_1^2 - \beta_1\frac{D}{M}\xi_2^2.$$

Step 3
The change of variables

$$\begin{aligned}\xi_3 =&x_3 - \phi_2(x_1,\xi_1,\xi_2) \\ =&x_3 - \frac{V(x_1)}{A}(K_l(1-e^{-L_l x_1}) - M_l x_1 - Dk\xi_1 + AP_0 - Mk\xi_2)\end{aligned} \tag{4.14}$$

transforms the system into

$$\dot{\xi}_1 =\xi_2 - k\xi_1 \tag{4.15a}$$

$$\dot{\xi}_2 =\frac{A\xi_3}{MV(x_1)} - k^2\xi_1 - \frac{D}{M}\xi_2 \tag{4.15b}$$

$$\begin{aligned}\dot{\xi}_3 =&RT_0U_{max}u - (\xi_2 - k\xi_1)(K_l(1-e^{-L_l x_1}) - M_l x_1 - Dk\xi_1 \\ &+ AP_0 - Mk\xi_2) - \frac{V(x_1)}{A}\Big((\xi_2 - k\xi_1)K_l L_l e^{-L_l x_1} \\ &- M_l(\xi_2 - k\xi_1) + Dk^2\xi_1 - Mk\Big(\frac{A\xi_3}{MV(x_1)} - k^2\xi_1\Big)\Big)\end{aligned} \tag{4.15c}$$

A new Lyapunov function is chosen

$$V_1(\xi) = U_2(\xi_1,\xi_2) + \frac{\lambda_1}{2}\xi_3^2 \tag{4.16}$$

and this leads to

$$\begin{aligned}\dot{V}_1 =& -\alpha_1 k\xi_1^2 - \beta_1\frac{D}{M}\xi_2^2 + \frac{\beta_1 A\xi_2\xi_3}{M(V_0+Ax_1)} + \lambda_1\xi_3((RT_0U_{max}u \\ &- (\xi_2 - k\xi_1)(K_l(1-e^{-L_l x_1}) - M_l x_1 - Dk\xi_1 + AP_0 - Mk\xi_2) \\ &- \frac{V(x_1)}{A}\Big((\xi_2 - k\xi_1)K_l L_l e^{-L_l x_1} - M_l(\xi_2 - k\xi_1) + Dk^2\xi_1 \\ &- Mk\Big(\frac{A\xi_3}{MV(x_1)} - k^2\xi_1\Big)\Big)\end{aligned} \tag{4.17}$$

By choosing the input as

$$\begin{aligned}u =& \frac{1}{RT_0U_{max}}\Big(-\frac{\beta_1 A\xi_2}{M\lambda_1(V_0+Ax_1)} + (\xi_2 - k\xi_1)(K_l(1-e^{-L_l x_1}) \\ &- M_l x_1 + Dkx_1 + AP_0 - Mk\xi_2) - \frac{V(x_1)}{A}\Big((\xi_2 - k\xi_1)K_l L_l e^{-L_l x_1} \\ &- M_l(\xi_2 - k\xi_1) + Dk^2\xi_1 - Mk\Big(\frac{A\xi_3}{MV(x_1)} - k^2\xi_1\Big)\Big) - b\xi_3\Big)\end{aligned} \tag{4.18}$$

where b is a positive constant, we get

$$\dot{V}_1 = -\alpha_1 k\xi_1^2 - \beta_1\frac{D}{M}\xi_2^2 - \lambda_1 b\xi_3^2.$$

This shows exponential stability of the system reference equilibrium with the backstepping controller, when there are no restrictions on the control input u.

4.2.2 Controller

The imposed input restrictions on the system make the input (4.18) not applicable. But the designed Lyapunov function

$$V_1(\xi) = \frac{\alpha_1}{2}\xi_1^2 + \frac{\beta_1}{2}\xi_2^2 + \frac{\lambda_1}{2}\xi_3^2$$

can still be used as a CLF. Recall the Lyapunov function time derivative along the trajectories of (4.15) given by (4.17), and notice that the only term dependent on the input is

$$\lambda_1\xi_3 RT_0U_{max}u$$

such that minimizing $\dot{V}_1$ is achieved by minimizing $\lambda_1\xi_3 RT_0U_{max}u$. Since R, T_0, U_{max} and λ_1 are constants, choosing the input which satisfies

$$sgn(u) = -sgn(\xi_3)$$

will render the smallest $\dot{V}_1$. The control input can then be written as

$$u_1 = \begin{cases} sgn(\xi_3) & \text{if} \quad \xi_3 \neq 0 \\ 0 & \text{if} \quad \xi_3 = 0 \end{cases} \tag{4.19}$$

Every switch between $u_1 = -1$ and $u_1 = 1$ will be done when

$$\begin{aligned}\xi_3 = 0 =& x_3 - \frac{V(x_1)}{A}\Big(K_l(1 - e^{-L_l x_1}) \\ &- M_l x_1 - Dk\tilde{x}_1 + AP_0 - Mk(x_2 + k(x_1 - x_1^*))\Big)\end{aligned}$$

which can be interpreted as the nonlinear switching surface.

Remark 4.2.1. *Nonlinear switching surfaces are also treated in several papers where sliding mode controllers are designed, as in Lee et al. (1991) and Lyshevski (2000). While we design a control Lyapunov function first and the switching surface is found from this, the sliding mode case define the surface first, and uses this to design a controller that proves stability of the system.*

Proposition 4.2.2. *The equilibrium x^* of the system (4.4) with the switched control input given by (4.19) is locally exponentially stable.*

Proof. First we prove existence, uniqueness and continuity of the solution using Filippov solution theories as in Sekhavat et al. (2005). The discontinuity surface can be described by

$$S := \{\xi : \xi_3 = 0\}$$

and this divides the solution domain Ω into two regions: $\Omega^- := \{\xi : \xi_3 < 0\}$ and $\Omega^+ := \{\xi : \xi_3 > 0\}$. As the right hand side of (4.15) is defined everywhere in Ω and is measurable and bounded for bounded states, the system (4.15) satisfies condition B of Filippov's solution theory, Filippov (1960). According to Theorems 4 and 5 in the same reference, we then have local existence and continuity of a solution. Further, since the right hand of (4.15) is continuous before and after the discontinuity surface, S, and this surface is smooth and independent of time, conditions A, B, C of Filippov's solution, Filippov (1979), are satisfied. Following the procedure introduced in Filippov (1960) the vector functions f^- and f^+ are defined as the limiting values of the right-hand sides of the state space equations in Ω^- and Ω^+ :

$$f^- = \begin{bmatrix} \xi_2 - k\xi_1 \\ \frac{A\xi_3}{MV(x_1)} - k^2\xi_1 - \frac{D}{M}\xi_2 \\ RT_0U_{\max} - \dot{\phi}(x_1, \xi_1, \xi_2) \end{bmatrix}$$

$$f^+ = \begin{bmatrix} \xi_2 - k\xi_1 \\ \frac{A\xi_3}{MV(x_1)} - k^2\xi_1 - \frac{D}{M}\xi_2 \\ -RT_0U_{\max} - \dot{\phi}(x_1, \xi_1, \xi_2) \end{bmatrix}$$

where

$$\begin{aligned}\dot{\phi}(x_1, \xi_1, \xi_2) =& (\xi_2 - k\xi_1)(K_l(1 - e^{-L_l x_1}) - M_l x_1 - Dk\xi_1 \\ &+ AP_0 - Mk\xi_2) - \frac{V(x_1)}{A}\Big((\xi_2 - k\xi_1)K_l L_l e^{-L_l x_1} \\ &- M_l(\xi_2 - k\xi_1) + Dk^2\xi_1 - Mk\Big(\frac{A\xi_3}{MV(x_1)} - k^2\xi_1\Big)\Big).\end{aligned}$$

For all points on the discontinuity surface vector $\mathbf{h}$ is defined as

$$\mathbf{h} = f^+ - f^- = \begin{bmatrix} 0 \\ 0 \\ -2RT_0U_{\max} \end{bmatrix}$$

which is along the normal of the discontinuity surface, $\mathbf{N_s} = (0, 0, 1)^T$. The scalar, h_N, defined as the projection of $\mathbf{h}$ on $\mathbf{N}_s$ is

$$h_N = \mathbf{N}_s\mathbf{h} = -2RT_0U_{\max} < 0$$

and will always be negative. According to Lemma 7 in Filippov (1979), uniqueness of the Filippov solution is then guaranteed.

Second we consider stability of the solution. The Lyapunov function time derivative along the trajectories of (4.15) given in (4.17) can be rewritten as

$$\dot{V}_1 \leq -\sigma V_1 - \lambda_1(RT_0U_{\max}|\xi_3| + \xi_3 a(\xi))$$

where

$$\begin{aligned} a(\xi) = &- b\xi_3 - \frac{\beta_1 A\xi_2}{\lambda_1 MV(x_1)} + (\xi_2 - k\xi_1)(K_l(1 - e^{-L_l x_1}) - M_l x_1 - Dk\xi_1 \\ &+ AP_0 - Mk\xi_2) + \frac{V(x_1)}{A}\Big((\xi_2 - k\xi_1)(K_l L_l e^{-L_l x_1} - M_l(\xi_2 - k\xi_1) \\ &+ Dk^2\xi_1) - Mk\Big(\frac{A\xi_3}{MV(x_1)} - k^2\xi_1\Big)\Big) \end{aligned}$$

and

$$\sigma = 2\min(k, \frac{D}{M}, b).$$

Since $a(0) = 0$ and $a(\xi)$ is continuous there must exist an $\delta > 0$ such that for $|\xi| \leq \delta$ we have $|a(\xi)| \leq RT_0U_{\max}$. It follows that for $|\xi| \leq \delta$ we get

$$\dot{V}_1 \leq -\sigma V_1$$

and the equilibrium point x^* is locally exponentially stable. □

The region of attraction contains the invariant set

$$\bar{\Omega}_1 = \{\xi | V_1(\xi) \leq \epsilon\}, \tag{4.20}$$

where ϵ is the largest value such that $\bar{\Omega}_1 \subseteq \Omega_1$ and

$$\Omega_1 = \{\xi \,||a(\xi)| \leq RT_0U_{\max}\}. \tag{4.21}$$

Remark 4.2.3. *As the size of ϵ be will be decided from the area where the input u from (4.18) fulfills*

$$|u| < RT_0U_{\max},$$

the region of attraction will be large in the context of local stability. ϵ depends on parameter values and tuning variables and are respectively $9.7 \cdot 10^{-7}$ and $4.5 \cdot 10^{-7}$ for the pre-prototype and the prototype valvesets considering the parameters given in Table 4.2 and the tuning variables given in Table 4.3.

4.3 Controller 2 - "Global controller"

The lack of a stability proof in the whole operation region for Controller 1 motivates the design of another switched controller. We choose a Lyapunov function based on knowledge of the system. The proposed CLF is based upon a Lyapunov function which can be used to prove stability of the reduced order system defined by $\tilde{x}_3 = 0$ and $u = 0$. First, we study this reduced order system.

4.3.1 Open loop stability of reduced order system

Consider the input $u = 0$ and assume $x_3 = x_3^*$. We can rewrite the system as a second order system

$$\dot{x}_1 = x_2 \tag{4.22a}$$

$$\dot{x}_2 = \frac{1}{M}\left(-K_l(1 - e^{-L_l x_1}) + M_l x_1 + \frac{A x_3^*}{V(x_1)} - AP_0 - Dx_2\right) \tag{4.22b}$$

which also can be expressed as

$$\ddot{\tilde{x}}_1 + \frac{D}{M}\dot{\tilde{x}}_1 + f(x_1, x_3^*) = 0$$

where $\tilde{x}_1 = x_1 - x_1^*$ and

$$f(x_1, x_3^*) = \frac{1}{M}\left(K_l(1 - e^{-L_l x_1}) - M_l x_1 - \frac{A x_3^*}{V(x_1)} + AP_0\right). \tag{4.23}$$

For this system we state the following result:

Proposition 4.3.1. *The function*

$$U_3(\tilde{x}_1, \tilde{x}_2) = \frac{1}{2}\tilde{x}_2^2 + \int_0^{\tilde{x}_1} f(y + x_1^*, x_3^*)dy \tag{4.24}$$

which is the sum of potential and kinetic energy (except for a factor M) can be used as a Lyapunov function to show asymptotic stability of the equilibrium $(x_1^*, 0)$ of the system (4.22) in O', the largest invariant set in O, under the condition

$$M_l < \frac{A(K_l(1 - e^{-L_l x_{max}}) + AP_0) + V(x_{\max})K_l L_l e^{-L_l x_{\max}})}{A x_{\max} + V(x_{\max})}\,[1]$$

on the clutch load model parameters.

Proof. The proposed Lyapunov function candidate is positive definite if for $\tilde{x}_1 \neq 0$

$$\int_0^{\tilde{x}_1} f(y + x_1^*, x_3^*)dy > 0.$$

[1] This limit on M_l will in practice be fulfilled for real clutch load characteristics, and (4.27) are assumed to be true in the rest of this chapter.

For $\tilde{x}_1 > 0$ this is the true if

$$f(y + x_1^*, x_3^*) > 0 \text{ for all } y \in [0, \tilde{x}_1]$$

and for $\tilde{x}_1 < 0$ if

$$f(y + x_1^*, x_3^*) < 0 \text{ for all } y \in [\tilde{x_1}, 0]$$

as $\int_a^b f(x)dx > 0$ if $f(x) > 0$ for all $a < x < b$. This can be summarized in the following condition for positive definiteness of (4.24),

$$f(x_1, x_3^*)\tilde{x}_1 > 0 \tag{4.25}$$

for all $x_1 \in [0, 0.025]$ such that $\tilde{x}_1 = x_1 - x_1^* \neq 0$ and x_3^* as function of $x_1^* \in [0, 0.025]$ as described in (4.5).

We have that

$$\begin{aligned} f(x_1, x_3^*) &= \frac{1}{M}\left(K_l(1 - e^{-L_l x_1}) - M_l x_1 - \frac{A x_3^*}{V(x_1)} + AP_0\right) \\ &= \frac{1}{M}\Big(K_l(1 - e^{-L x_1}) - M_l x_1 \\ &- \frac{A\frac{V(x_1^*)}{A}(K_l(1 - e^{-L_l x_1^*}) - M_l x_1^* + AP_0)}{V(x_1)} + AP_0\Big) \\ &= \frac{1}{M}\left(g(x_1) - \frac{V(x_1^*)}{V(x_1)} g(x_1^*)\right) \\ &= \frac{1}{MV(x_1)}\left(P(x_1) - P(x_1^*)\right) \end{aligned} \tag{4.26}$$

where $V(x) = Ax + V_0$ is a positive strictly increasing function in x for $x \in [0, 0.025]$, and $g(x) = K_l(1 - e^{-L_l x}) - M_l x + AP_0$ and $P(x) = V(x)g(x)$. Furthermore, $P(x)$ is a positive strictly increasing function in x for $x \in [0, 0.025]$, if $\frac{dP(x)}{dx} > 0$ which leads to the condition

$$M_l < \frac{A(K_l(1 - e^{-L_l x_{max}}) + AP_0) + V(x_{\max})K_l L_l e^{-L_l x_{\max}})}{Ax_{\max} + V(x_{\max})} \tag{4.27}$$

Since (4.27) holds, for $\tilde{x}_1 > 0$ we have

$$\tilde{x}_1 > 0 \Leftrightarrow x_1 > x_1^* \Leftrightarrow P(x_1) > P(x_1^*) \Leftrightarrow f(x_1, x_3^*) > 0$$

which gives

$$f(x_1, x_3^*)\tilde{x}_1 > 0.$$

For $\tilde{x}_1 < 0$ we have

$$\tilde{x}_1 < 0 \Leftrightarrow x_1 < x_1^* \Leftrightarrow P(x_1) < P(x_1^*) \Leftrightarrow f(x_1, x_3^*) < 0$$

which gives

$$f(x_1, x_3^*)\tilde{x}_1 > 0.$$

Hence, the condition given in (4.25) is satisfied, and this establishes that the function (4.24) is a CLF. The Lyapunov function candidate time derivative along trajectories of (4.22) is

$$\begin{aligned}\dot{U_3} =& \tilde{x}_2\dot{\tilde{x}}_2 + f(x_1, x_3^*)\dot{\tilde{x}}_1 \\ =& -\frac{D}{M}\tilde{x}_2^2 - f(x_1, x_3^*)\tilde{x}_2 + f(x_1, x_3^*)\tilde{x}_2 \\ =& -\frac{D}{M}\tilde{x}_2^2 \leq 0.\end{aligned}$$

Consider $S = \left\{x \in O^{'} | \dot{U}_3(\tilde{x}) = 0\right\}$. The only solution that can stay identically in S is the equilibrium point $(\tilde{x}_1, \tilde{x}_2) = 0$ as

$$\tilde{x}_2 \equiv 0 \Longrightarrow \dot{\tilde{x}}_2 \equiv 0 \Longrightarrow f(x_1, x_3^*) \equiv 0 \Longrightarrow \tilde{x}_1 \equiv 0.$$

Then by the LaSalle-Krasovski's theorem, Khalil (2000), the origin is proved asymptotically stable in $O^{'}$. □

4.3.2 Lyapunov function

We extend the Lyapunov function for the reduced open loop system and for the 3rd order closed loop system we propose the control Lyapunov function

$$V_2(\tilde{x}) = \alpha_2 \int_0^{\tilde{x}_1} f(y + x_1^*, x_3^* + \tilde{x}_3)dy + \frac{\alpha_2}{2}\tilde{x}_2^2 + \frac{\lambda_2}{2}\tilde{x}_3^2 \tag{4.28}$$

where α_2 and λ_2 are positive constants. First we show that the proposed control Lyapunov function is positive definite under a condition on the ratio $\frac{\alpha_2}{\lambda_2}$.

Positive definiteness of the Lyapunov function $V_2(\tilde{x})$

Consider

$$f(x_1, x_3) = f(x_1, x_3^*) - \frac{A\tilde{x}_3}{MV(x_1)} \tag{4.29}$$

and the Lyapunov function (4.28) can be rewritten as

$$V_2(\tilde{x}) = \alpha_2 \int_0^{\tilde{x}_1} f(y + x_1^*, x_3^*)dy + \frac{\alpha_2}{2}\tilde{x}_2^2 + \frac{\lambda_2}{2}\tilde{x}_3^2 - \frac{\alpha_2}{M}\int_0^{\tilde{x}_1} \frac{A\tilde{x}_3}{V(x_1^* + y)}dy \tag{4.30}$$

where we know that $\int_0^{\tilde{x}_1} f(y + x_1^*, x_3^*)dy$ is positive from the calculations above. If the last term is dominated by $\frac{\lambda_2}{2}\tilde{x}_3^2$, i.e.

$$\frac{\alpha_2}{M}\int_0^{\tilde{x}_1} -\frac{A\tilde{x}_3}{V(x_1^* + y)}dy + \frac{\lambda_2}{2}\tilde{x}_3^2 = \tilde{x}_3\left(-\frac{\alpha_2}{M}\ln\left(\frac{V(x_1)}{V(x_1^*)}\right) + \frac{\lambda_2}{2}\tilde{x}_3\right) > 0$$

we have $V_2(\tilde{x}) > 0$ for all $\tilde{x} \neq 0$, as the other terms of (4.30) are positive. This condition is satisfied if

$$\frac{\lambda_2}{2}\left|\tilde{x}_3\right| > \frac{\alpha_2}{M}\left|\ln\left(\frac{V(x_1)}{V(x_1^*)}\right)\right|,$$

hence positive definiteness of (4.28) is established for $|\tilde{x}_3| > \frac{2\alpha_2}{\lambda_2 M}\left|\ln\left(\frac{V(x_1)}{V(x_1^*)}\right)\right|$. For $|\tilde{x}_3| \leq \frac{2\alpha_2}{\lambda_2 M}\left|\ln\left(\frac{V(x_1)}{V(x_1^*)}\right)\right|$, positive definiteness can be shown if the first term of (4.28) is shown to be positive. This is true if

$$f(x_1, x_3)\tilde{x}_1 > 0 \tag{4.31}$$

for all $x_1, x_1^* \in [0, 0.025]$ such that $\tilde{x}_1 = x_1 - x_1^* \neq 0$ and $x_3 \in (0, \infty]$ such that $|\tilde{x}_3| = |x_3 - x_3^*| \leq \frac{2\alpha_2}{\lambda_2 M}\left|\ln\left(\frac{V(x_1)}{V(x_1^*)}\right)\right|$. By considering (4.29), the condition (4.31) can be rewritten as

$$f(x_1, x_3)\tilde{x}_1 = f(x_1, x_3^*)\tilde{x}_1 - \frac{A\tilde{x}_3}{MV(x_1)}\tilde{x}_1.$$

From the analysis in the proof of Proposition 4.3.1 we have that $f(x_1, x_3^*)\tilde{x}_1 > 0$ for $\tilde{x}_1 \neq 0$, and if $f(x_1, x_3^*)$ dominates the term $\frac{A\tilde{x}_3}{MV(x_1)}$ the condition (4.31) is fulfilled. Recall that

$$f(x_1, x_3^*) = \frac{P(x_1) - P(x_1^*)}{MV(x_1)}$$

and (4.31) is true if the condition

$$|P(x_1) - P(x_1^*)| > |A\tilde{x}_3|$$

holds for $\tilde{x}_1 \neq 0$. Considering $|\tilde{x}_3| \leq \frac{2\alpha_2}{\lambda_2 M}\left|\ln\left(\frac{V(x_1)}{V(x_1^*)}\right)\right|$, this condition can be rewritten as

$$|P(x_1) - P(x_1^*)| > \frac{2\alpha_2 A}{\lambda_2 M}\left|\ln\left(\frac{V(x_1)}{V(x_1^*)}\right)\right|$$

giving

$$\frac{\alpha_2}{\lambda_2} < \frac{M}{2A}\left|\frac{P(x_1) - P(x_1^*)}{\ln\left(\frac{V(x_1)}{V(x_1^*)}\right)}\right|. \tag{4.32}$$

Figure 4.1 shows the value of the right-hand side of (4.32) as a function of x_1 with constant x_1^*'s for the parameters of the actuator clutch model. From this it is clear that a lower bound, dependent on the values of K_l, M_l and L_l, for the condition (4.32) can be found giving an upper bound on $\frac{\alpha_2}{\lambda_2}$.

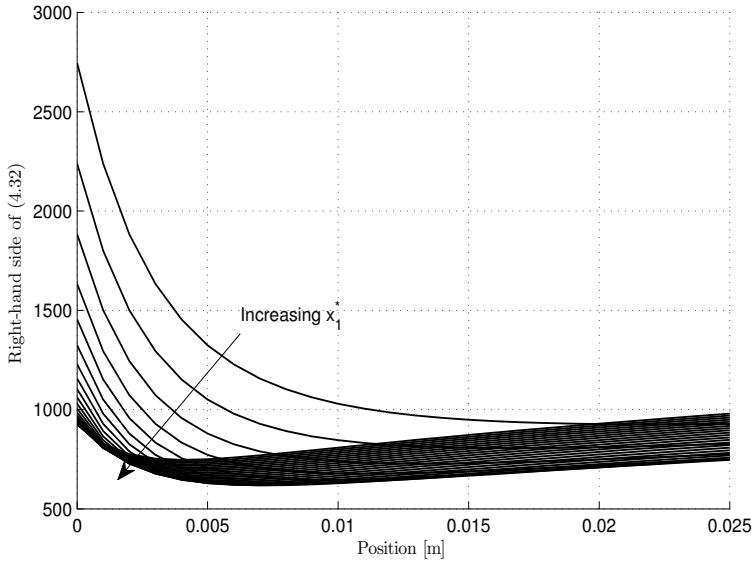

Figure 4.1: Curves showing the value of the right-hand side of (4.32) as function of x_1 for constant $x_1^* \in [0, 0.025]$.

Remark 4.3.2. *The value of the right-hand side of (4.32) is not defined for* $x_1 = x_1^*$ *as*

$$\lim_{x_1 \to x_1^*} \frac{P(x_1) - P(x_1^*)}{\ln\left(\frac{V(x_1)}{V(x_1^*)}\right)} = \frac{0}{0}.$$

But from L'Hospital's Rule we have that $\lim \frac{f_1(x)}{f_2(x)} = \lim \frac{\frac{df_1(x)}{dx}}{\frac{df_2(x)}{dx}}$ *if* $\frac{\frac{df_1(x)}{dx}}{\frac{df_2(x)}{dx}}$ *has a finite value or if the limit is* $\pm\infty$*. We have*

$$\frac{\frac{d(P(x_1)-P(x_1^*))}{dx}}{\frac{d(\ln\left(\frac{V(x_1)}{V(x_1^*)}\right)}{dx}} = \frac{V(x_1)(Ag(x) + V(x_1)(K_l L_l e^{-L_l x_1}))}{A}$$

which gives

$$\lim_{x_1 \to x_1^*} \frac{P(x_1) - P(x_1^*)}{\ln\left(\frac{V(x_1)}{V(x_1^*)}\right)} = \frac{V(x_1^*)(Ag(x_1^*) + V(x_1^*)(K_l L_l e^{-L_l x_1^*}))}{A}.$$

Hence it is shown that the Lyapunov function given by (4.28) is positive definite in O, given that the condition (4.32) on the ratio $\frac{\alpha_2}{\lambda_2}$ is fulfilled. Summarized, we have the CLF

$$V_2(\tilde{x}) = \alpha_2 \int_0^{\tilde{x}_1} f(y + x_1^*, x_3^* + \tilde{x}_3)dy + \frac{\beta_2}{2}\tilde{x}_2^2 + \frac{\lambda_2}{2}\tilde{x}_3^2 \tag{4.33}$$

for the 3rd order system

$$\dot{\tilde{x}}_1 = \tilde{x}_2 \tag{4.34a}$$

$$\dot{\tilde{x}}_2 = -f(x_1, x_3) - \frac{D}{M}\tilde{x}_2 \tag{4.34b}$$

$$\dot{\tilde{x}}_3 = RT_0U_{max}u. \tag{4.34c}$$

The Lyapunov function time derivative along the trajectories of (4.34) is

$$\begin{aligned}\dot{V}_2 =& \alpha_2 f(x_1, x_3)\tilde{x}_2 - \frac{\alpha_2}{M}\ln\left(\frac{V(x_1)}{V(x_1^*)}\right) RT_0U_{max}u \\ & - \alpha_2\tilde{x}_2\left(f(x_1, x_3) + \frac{D}{M}\tilde{x}_2\right) + \lambda_2\tilde{x}_3 RT_0U_{max}u \\ =& -\frac{\beta_2 D}{M}\tilde{x}_2^2 + \left(\lambda_2\tilde{x}_3 - \frac{\alpha_2}{M}\ln\left(\frac{V(x_1)}{V(x_1^*)}\right)\right) RT_0U_{max}u \\ =& -\frac{\beta_2 D}{M}\tilde{x}_2^2 + s(\tilde{x}_1, \tilde{x}_3)RT_0U_{max}u\end{aligned} \tag{4.35}$$

where

$$s(\tilde{x}_1, \tilde{x}_3) = \lambda_2\tilde{x}_3 - \frac{\alpha_2}{M}\ln\left(\frac{V(x_1^* + \tilde{x}_1)}{V(x_1^*)}\right). \tag{4.36}$$

4.3.3 Controller

The input dependent term of the Lyapunov function time derivative given by (4.35) is

$$s(\tilde{x}_1, \tilde{x}_3)RT_0U_{\max}u$$

and minimizing $\dot{V}_2$ is achieved by minimizing this term. R, T_0 and $U_{\max}$ are constants, such that choosing the input u which satisfies

$$sgn(u) = -sgn(s(\tilde{x}_1, \tilde{x}_3))$$

will render the smallest $\dot{V}_2$ and ensure that $\dot{V}_2$ is non-positive. The switched control law can be written as

$$u_2 = \begin{cases} -sgn(s(\tilde{x}_1, \tilde{x}_3)) & \text{if} \quad s(\tilde{x}_1, \tilde{x}_3) \neq 0 \\ 0 & \text{if} \quad s(\tilde{x}_1, \tilde{x}_3) = 0 \end{cases} \tag{4.37}$$

and we get a negative semidefinite Lyapunov function time derivative,

$$\dot{V}_2 = -\frac{\beta_2 D}{M}\tilde{x}_2^2 - \left|\lambda\tilde{x}_3 - \frac{\alpha_2}{M}\ln\left(\frac{V(x_1^* + \tilde{x_1})}{V(x_1^*)}\right)\right| RT_0U_{\max} \leq 0$$

where the variables α_2 and λ_2 can be tuned to weight the parts of $s(\tilde{x}_1, \tilde{x}_3)$.

Every switch between $u_1 = -1$ and $u_1 = 1$ will be done when

$$s(\tilde{x}_1, \tilde{x}_3) = 0 = \lambda_2\tilde{x}_3 - \frac{\alpha_2}{M}\ln\left(\frac{V(x_1^* + \tilde{x_1})}{V(x_1^*)}\right)$$

which can be interpreted as the nonlinear switching surface.

Proposition 4.3.3. *The equilibrium point x^* of the system (4.4) with the switched controller given in (4.37) is asymptotical stable in the largest invariant region in the region of operation O if the condition (4.32) on $\frac{\alpha_2}{\lambda_2}$ is satisfied.*

Proof. First we prove existence, uniqueness and continuity of the solution using Filippov solution as in Sekhavat et al. (2005). The discontinuity surface is described by

$$S := \{\mathbf{x} : s(\tilde{x}_1, \tilde{x}_3) = 0\}$$

which divides the solution domain Ω into two regions

$$\Omega^- := \{\mathbf{x} : s(\tilde{x}_1, \tilde{x}_3) < 0\}$$
$$\Omega^+ := \{\mathbf{x} : s(\tilde{x}_1, \tilde{x}_3) > 0\}.$$

The right hand side of (4.4) is defined everywhere in Ω and is measurable and bounded. This means that the system (4.4) satisfies condition B of Filippov's solution theory, Filippov (1960), and according to Theorems 4 and 5 in the same reference, we then have local existence and continuity of a solution. The right hand side of (4.4) is also continuous before and after the discontinuity surface, S, and this surface is smooth and independent of time. Hence, the conditions A, B and C of Filippov's solution, Filippov (1979), are satisfied. By following the procedure introduced in Filippov (1960) the vector functions f^- and f^+ can be defined as the limiting values of the right-hand sides of the state equations in Ω^- and Ω^+

$$f^- = \begin{bmatrix} x_2 \\ -f(x_1, x_3) - \frac{D}{M}x_2 \\ RT_0U_{max} \end{bmatrix}$$
$$f^+ = \begin{bmatrix} x_2 \\ -f(x_1, x_3) - \frac{D}{M}x_2 \\ -RT_0U_{max} \end{bmatrix}.$$

The vector $\mathbf{h}$, which is along the normal of the discontinuity surface,

$$\mathbf{N_s} = \left(-\frac{\alpha_2 A}{\lambda_2 V(x_1^* + \tilde{x}_1)}, 0, \lambda_2\right)^T$$

is defined as

$$\mathbf{h} = f^+ - f^- = \begin{bmatrix} 0 \\ 0 \\ -2RT_0U_{max} \end{bmatrix}$$

for all points on the discontinuity surface. The scalar, h_N, defined as the projection of $\mathbf{h}$ on $\mathbf{N_s}$ is

$$h_N = \mathbf{N_s}\mathbf{h} = -\lambda_2 2RT_0U_{max} < 0$$

and will always be negative. According to Lemma 7 in Filippov (1979), the uniqueness of the Filippov solution is then guaranteed.

Next we consider the stability properties of the solution. From (4.3.3) we have that $\dot{V}_2 \leq 0$, and we use LaSalle's invariance principle, Khalil (2000), to prove asymptotical stability. From $\dot{V}_2 = 0$ we get

$$\tilde{x}_2 = 0 \quad \& \quad |s(\tilde{x}_1, \tilde{x}_3)| = 0.$$

From this it follows that $\tilde{x}_2 = 0 \Rightarrow \dot{\tilde{x}}_1 = 0 \Rightarrow \tilde{x}_1 = c_1$, $\tilde{x}_2 = 0 \Rightarrow \dot{\tilde{x}}_2 = 0 \Rightarrow f(x_1, x_3) = 0$ and $|s(\tilde{x}_1, \tilde{x}_3)| = 0 \quad \& \quad \tilde{x}_1 = c_1 \Rightarrow \tilde{x}_3 = c_2$. This gives the solution $(\tilde{x}_1, \tilde{x}_2, \tilde{x}_3) = (c_1, 0, c_2)$. It then remains to show that $c_1 = c_2 = 0$ is the only possible solution. The equation

$$|s(\tilde{x}_1, \tilde{x}_3)| = 0$$

is true if

$$\tilde{x}_3 = 0 \quad \& \quad \frac{\alpha_2}{M} \ln\left(\frac{V(x_1)}{V(x_1^*)}\right) = 0 \Rightarrow \tilde{x}_1 = 0$$

or

$$\tilde{x}_3 = \frac{\alpha_2}{\lambda_2 M} \ln\left(\frac{V(x_1)}{V(x_1^*)}\right). \tag{4.38}$$

The equation

$$f(x_1, x_3) = f(x_1, x_3^*) - \frac{A\tilde{x}_3}{MV(x_1)} = 0$$

where $f(x_1, x_3^*) = \frac{P(x_1) - P(x_1^*)}{MV(x_1)} = 0$ if $\tilde{x_1} = 0$, is true if

$$f(x_1, x_3^*) = 0 \quad \& \quad \frac{A\tilde{x}_3}{MV(x_1)} = 0$$
$$\tilde{x}_1 = 0 \quad \& \quad \tilde{x}_3 = 0$$

or

$$\begin{aligned} f(x_1, x_3^*) &= \frac{A\tilde{x}_3}{MV(x_1)} \\ \tilde{x}_3 &= \frac{MV(x_1)}{A} f(x_1, x_3^*). \end{aligned} \tag{4.39}$$

By combining (4.38) and (4.39)

$$\frac{\alpha_2}{\lambda_2 M} \ln\left(\frac{V(x_1)}{V(x_1^*)}\right) = \frac{V(x_1)}{A}\left(\frac{1}{V(x_1)}(P(x_1) - P(x_1^*)\right)$$

and rearranging we get

$$P(x_1) - P(x_1^*) = \frac{\alpha_2 A}{\lambda_2 M} \ln\left(\frac{V(x_1)}{V(x_1^*)}\right). \tag{4.40}$$

From the analysis of positive definiteness of the Lyapunov function we know that

$$|P(x_1) - P(x_1^*)| > \frac{2A\alpha_2}{M\lambda_2} \left|\ln\left(\frac{V(x_1)}{V(x_1^*)}\right)\right|$$

has to be fulfilled. From this it follows that the only solution of (4.40) is $\tilde{x}_1 = 0$, hence the only solution which can stay identically in the set $S = \left\{ x \in O^{'} | \dot{V}_2(x) = 0 \right\}$, where $O^{'}$ is the largest invariant set contained in O, is the equilibrium point $(\tilde{x}_1, \tilde{x}_2, \tilde{x}_3) = 0$. By the LaSalle-Krasovski's theorem, Khalil (2000), asymptotical stability of the equilibrium point x^* is proved under the condition (4.32) on $\frac{\alpha_2}{\lambda_2}$, in the region $O^{'}$.

□

Remark 4.3.4. *It is possible to characterize the largest invariant set in O, but we have chosen not to do so since the practical experiments show there are no practical limit. For this reason, we refer to this controller as the "global" controller.*

4.4 Controller 3 - "Dual-mode controller"

We design a third controller by combining the two former switched controllers into one that makes use of the individual controller's best qualities. The global controller is stable in the operation region of the clutch system, and can be used to bring the system close to the equilibrium point, and the local controller, whose control action depend more strongly on the position error and has better robustness properties, is suitable for use close to the equilibrium point. Notice that $\tilde{x} = 0$ if and only if $\xi = 0$ such that we get a consistent formulation of a combined controller

$$u_c = \begin{cases} u_2, & \xi \in \Omega_2 \\ u_1, & \xi \in \bar{\Omega}_1 \end{cases} \tag{4.41}$$

where $\Omega_2 = O \backslash \bar{\Omega}_1$ and $\bar{\Omega}_1$ is defined by (4.20).

Proposition 4.4.1. *The equilibrium point x^* of the system (4.4) with the combined controller given in (4.41) is asymptotically stable in the largest invariant region in O.*

Proof. In the region $\bar{\Omega}_1$, $u_c = u_1$ guarantees local exponential stability of the system's equilibrium point. The equilibrium point lies inside $\bar{\Omega}_1$, and if the system at the initial time t_0 is in the region $\bar{\Omega}_1$ the exponential stability of the local controller and invariance of $\bar{\Omega}_1$, will ensure that the region is not left and that the equilibrium point is asymptotically stable. If the system at t_0 is outside the region $\bar{\Omega}_1$, but in $O^{'}$, the asymptotic stability of the global controller ensures that the system will reach the region $\bar{\Omega}_1$ after some finite time, and the switch to the local controller will bring the system to the equilibrium point. Hence the equilibrium point x^* is asymptotically stable in the region $O^{'}$. □

Remark 4.4.2. *Experimental results indicate that the guaranteed region of attraction, $\bar{\Omega}_1$ is rather conservatively estimated due to the sufficiency of the Lyapunov function conditions, and that the local controller is stable also outside of this region. For this reason, the value of ϵ defining the the region of attraction for the local controller, and thereby also influencing the choice of switched controller, may be somewhat relaxed in the experimental testing.*

4.5 Experimental results

The performance of the proposed controllers has been tested in the KA test truck, with the two on/off solenoid valvesets as described in Chapter 2. The clutch load characteristic was determined manually before any experiments with the controllers were carried out. These tuned parameters are given in Table 4.3 along with the control parameters used in the experiments.

Variable	*Pre-prototype*	*Prototype*	*Unit*	*Description*
K_l	4000	5300	$\frac{\mathrm{N}}{\mathrm{m}}$	Load characteristic term
L_l	500	700	-	Load characteristic term
M_l	20000	20000	$\frac{\mathrm{N}}{\mathrm{m}}$	Load characteristic term
α_1	400	400	-	Tuning parameters
β_1	0.03	4	-	Tuning parameters
λ_1	0.01	0.00001	-	Tuning parameters
α_2	3.839	2.726	-	Tuning parameters
λ_2	1	1	-	Tuning parameters
k	382	10	-	Tuning parameters
b	10	10	-	Tuning parameters

Table 4.3: Load characteristics and control parameters.

4.5.1 Performance under nominal conditions

Figures 4.2, 4.3 and 4.4 show experimental results of the local, the global and the dual-mode controller under nominal conditions, respectively. The response times are given in Table 4.4, displaying both the average time it takes before the piston position first reaches the acceptable position error area, and the time elapsed before the piston position has settled within this area. The table also lists the number of switches between the available inputs conducted for the respective controllers. This is a important performance factor as excessive use of the on/off solenoids valves leads to more rapid wear of the mechanical parts and should be avoided.

The local controller suffer from some chattering and oscillations. The position requirements are not met in the presence of oscillations, but for the cases not suffering from oscillations the requirements are fulfilled, see Figure 4.2. Although the theoretical analysis only managed to ensure local stability, the experimental results indicate that stability of the whole operation range is actually obtained. The high number of input switched for the local controller originate from the chattering. The requirements are almost fulfilled using the global controller with some excess input switching. The restriction on $\frac{\alpha_2}{\lambda_2}$, defined by (4.32), limits the performance of the controller as it does not allow us to weight the position error as highly as desired. The error in accumulated air which is directly related to the pressure error, will be the main driving error of the controller, which leads to poor robustness properties of this controller since the calculation of x_3^* is subject to model error. The desired behavior of the dual-mode controller is shown, the local controller is active close to the equilibrium point, while the global controller is active elsewhere.

The exception is when the position reference is zero (clutch fully engaged), here the global controller is active as the restriction on position error is relaxed. The chattering experienced using the local controller alone is no longer present when the local controller is the active controller of the dual-mode controller. This is presumably because the local controller is used only close to the equilibrium point, where stability of the controller can be guaranteed. The improvement using the dual-mode compared to the local and the global controller alone is evident. Better accuracy, less oscillations and fewer switches between inputs are achieved.

Controller	*Reach time*	*Settle time*[2]	*Number of switches of input*
Local	44.7 ms	-	255
Global	41.6 ms	102.8 ms	131
Dual-mode	40.8 ms	85.0 ms	91

Table 4.4: Response times for the controllers under nominal conditions, average time to reach reference and time to settle within acceptable area, and number of switches of inputs.

4.5.2 Robustness considerations

Experiments where errors in the parameters of the clutch load characteristic model in the controller model are introduced, have been conducted. One lower and one higher clutch load characteristic is used to test robustness of the controller designs, obtained by setting $K_l = 3500$ and $K_l = 6500$, respectively, see Figure 4.5.

The effect in terms of position error by including these errors in the modeled clutch load characteristic is shown in Figure 4.6 and Table 4.5. The dual-mode controller fails in terms of position error whenever the global controller is active, while the performance is much better whenever the local controller is active. The local controller is, as expected, more robust to model errors. This is due to the fact that the switching surface depend on the errors of all three states, and that the parameters α_1 and λ_1 can be tuned without restrictions. The global controller, on the other hand, relies only on position and accumulated air errors, and in addition the condition on $\frac{\alpha_2}{\lambda_2}$ results in higher gain on the accumulated air error than the position error. Under nominal conditions a small accumulated air error correlates to a small position error, while with model errors introduced, the relation between x_1^* and x_3^* described by (4.5) is no longer valid, and this realtionship between these errors are not longer guaranteed.

4.5.3 Performance considering different valvesets

Figures 4.7 and 4.8 show the performance of the dual-mode controller under nominal conditions with the two different SO valvesets. In the region of engagement we see that the position error requirement is only partly fulfilled. This is mainly

[2]There are oscillations in some cases, such that the response has not always settled, and an average settle time cannot be calculated.

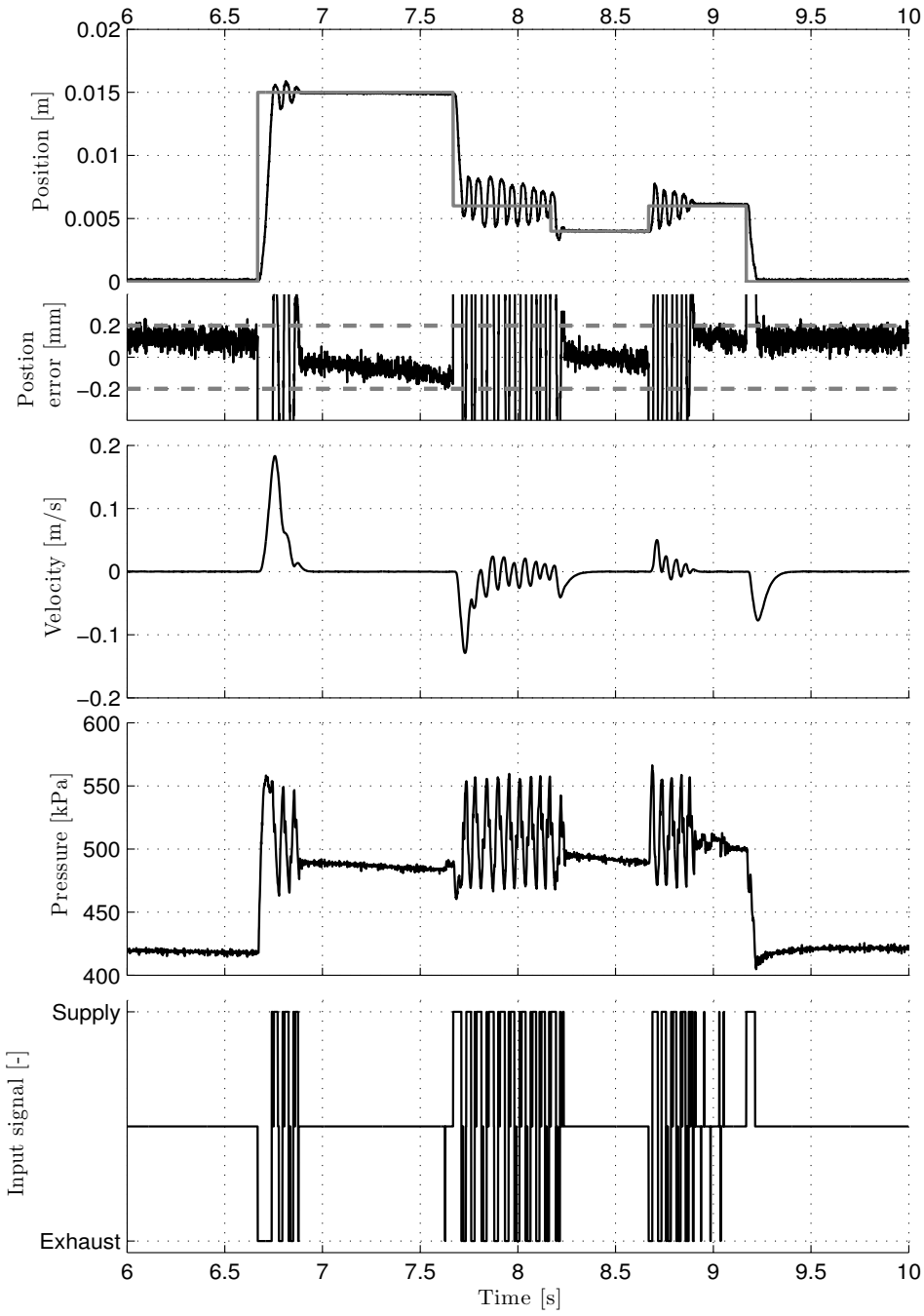

Figure 4.2: Result from experimental testing showing the performance of local controller under nominal conditions. The gray curve for position is the reference position, while the dashed gray lines for position error are the requirement limits.

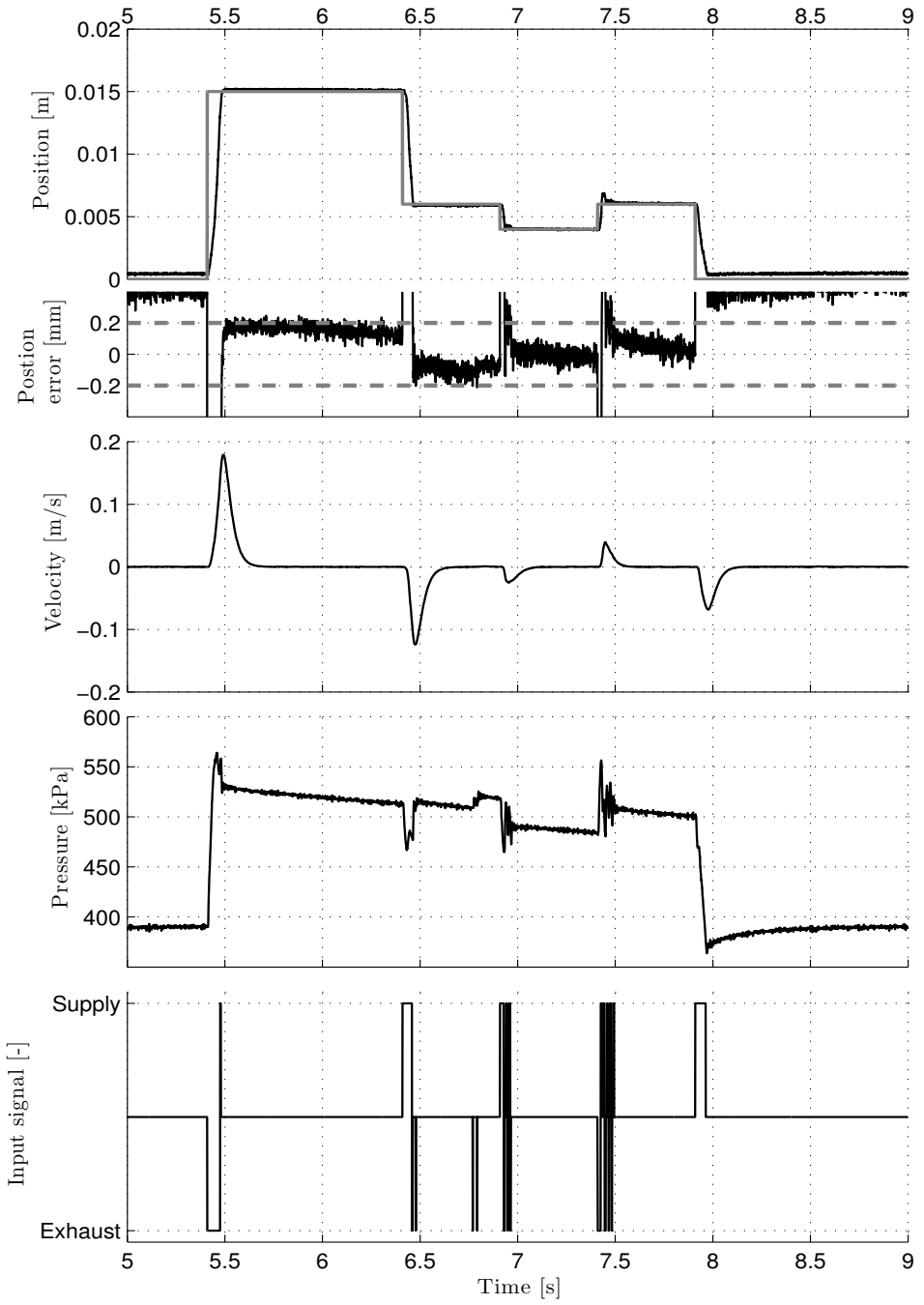

Figure 4.3: Result from experimental testing showing the performance of global controller under nominal conditions. The gray curve for position is the reference position, while the dashed gray lines for position error are the requirement limits.

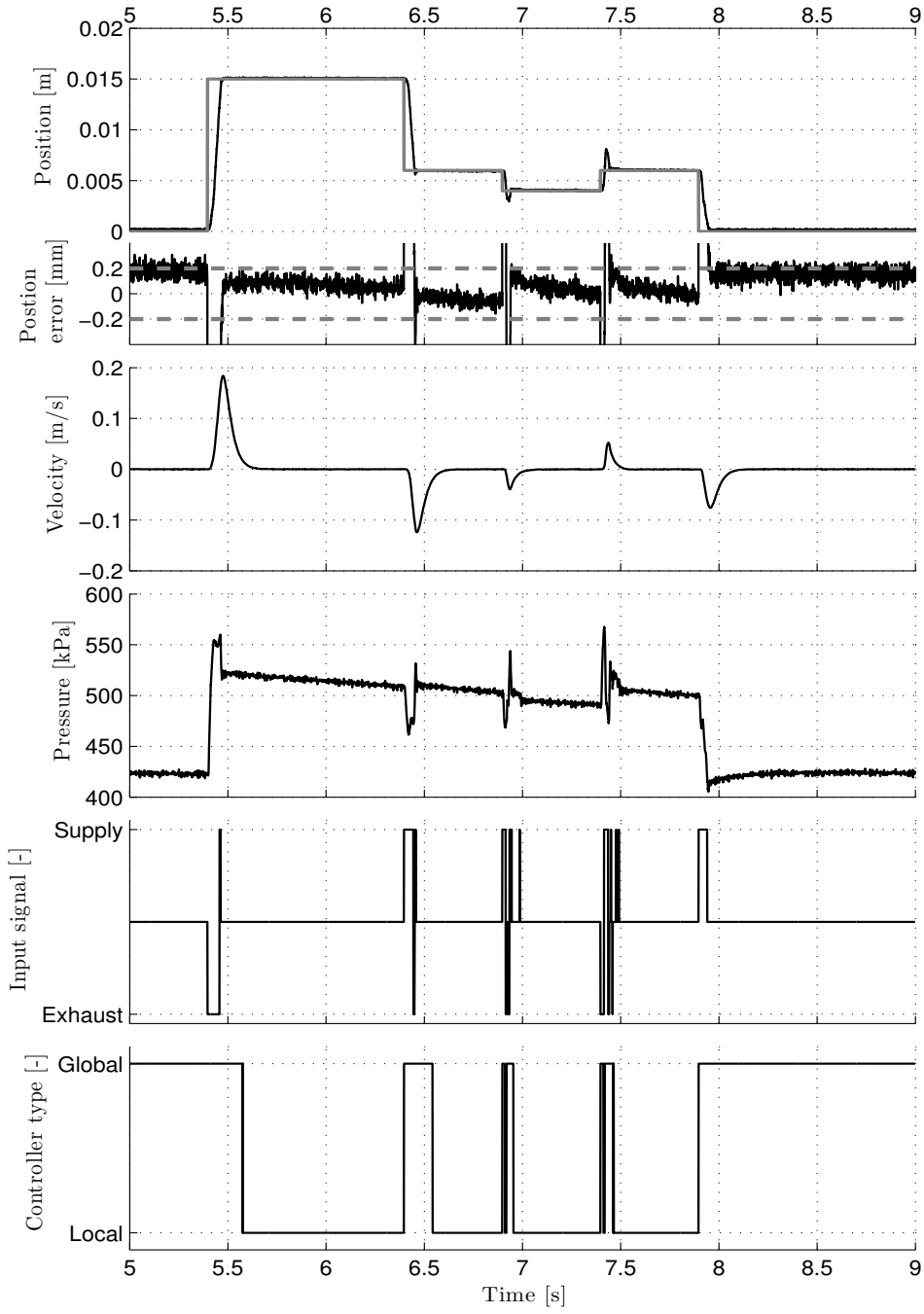

Figure 4.4: Result from experimental testing showing the performance of dual-mode controller under nominal conditions. The gray curve for position is the reference position, while the dashed gray lines for position error are the requirement limits.

Controller	*Lower clutch load*	*Higher clutch load*
Local	0.8 mm	1.1 mm
Global	4.7 mm	4.4 mm
Combined	3.9 mm	3.6 mm

Table 4.5: Average absolute position errors with errors in the modeled clutch load characteristic.

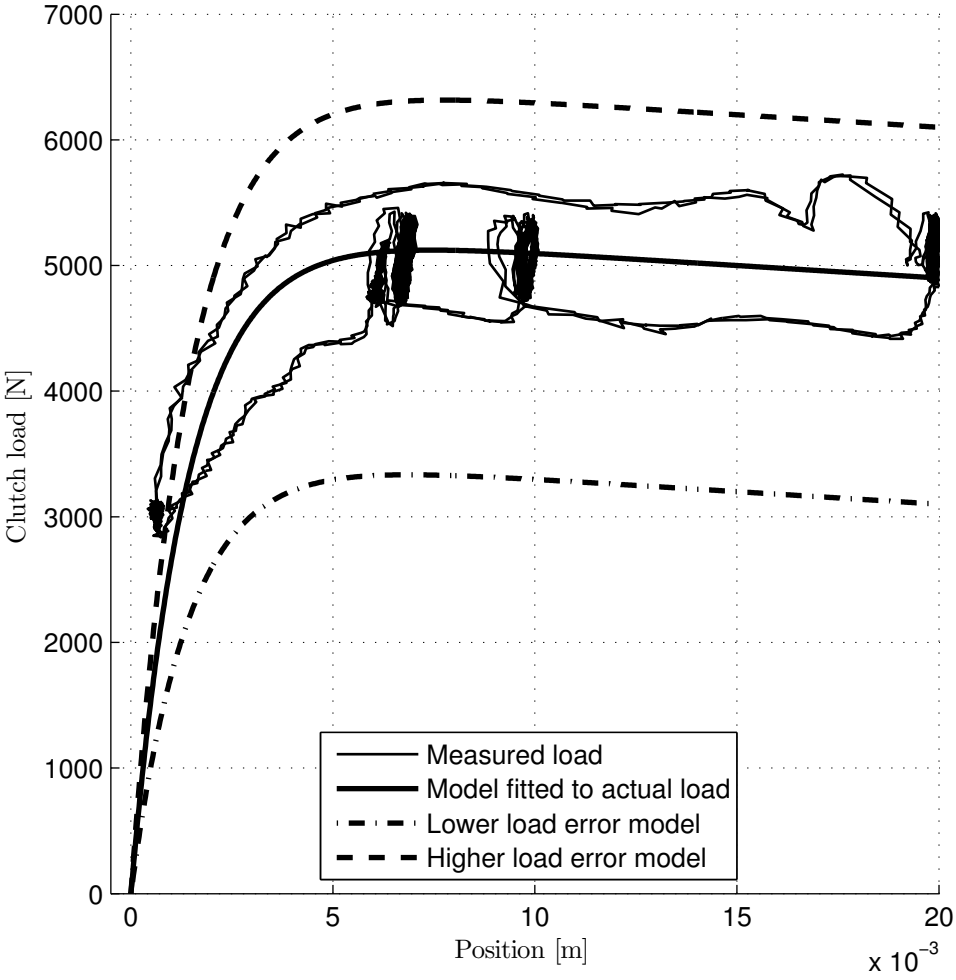

Figure 4.5: Clutch load characteristics. Actual clutch load "measured" through $A(p - P_0)$ (also including dynamic friction) is shown together with three configurations of the clutch load characteristic model given by equation (4.2).

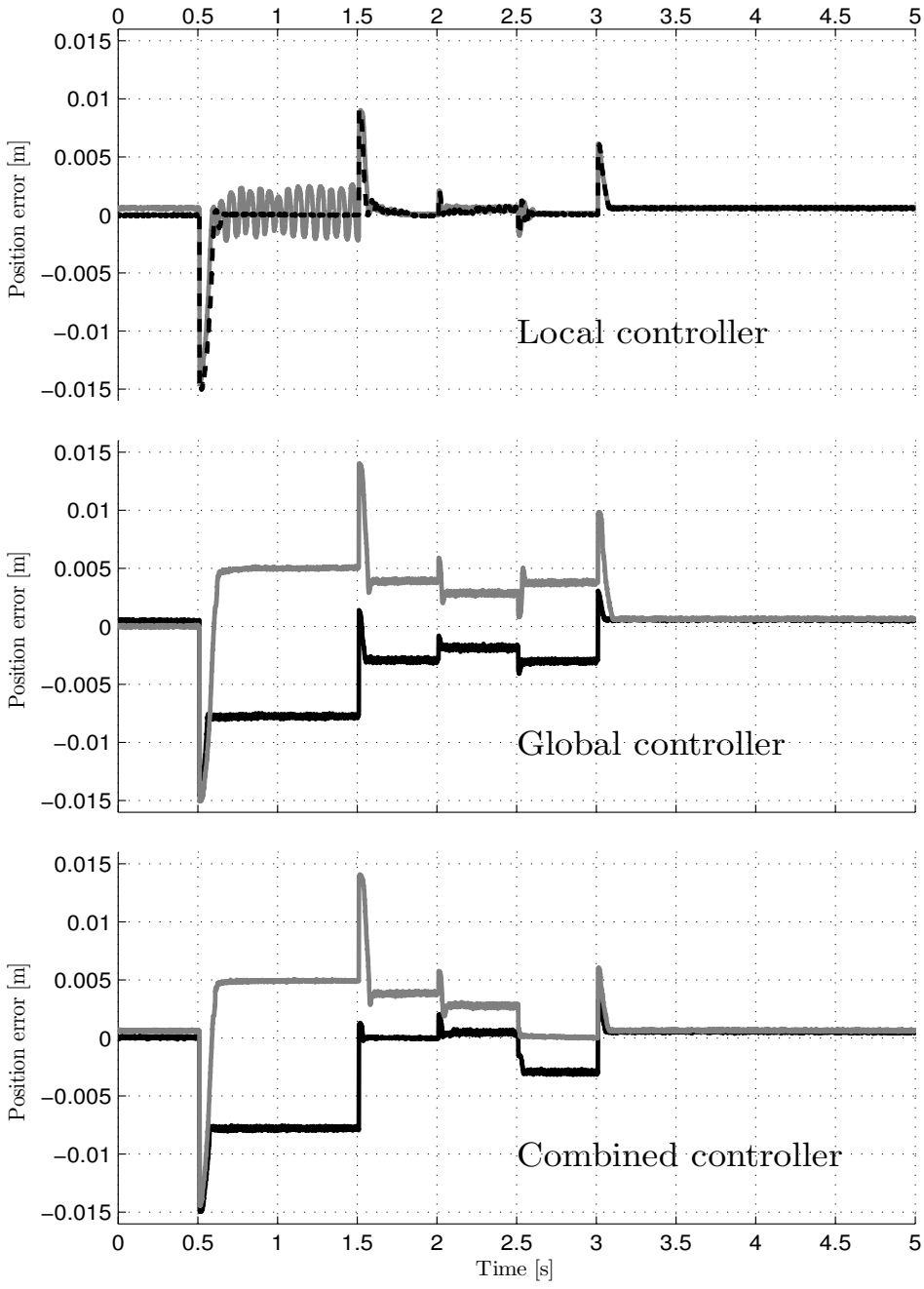

Figure 4.6: The position errors of experiments with local, global and dual-mode controller with error in the modeled clutch load characteristic, with higher load model in gray and lower load model in black.

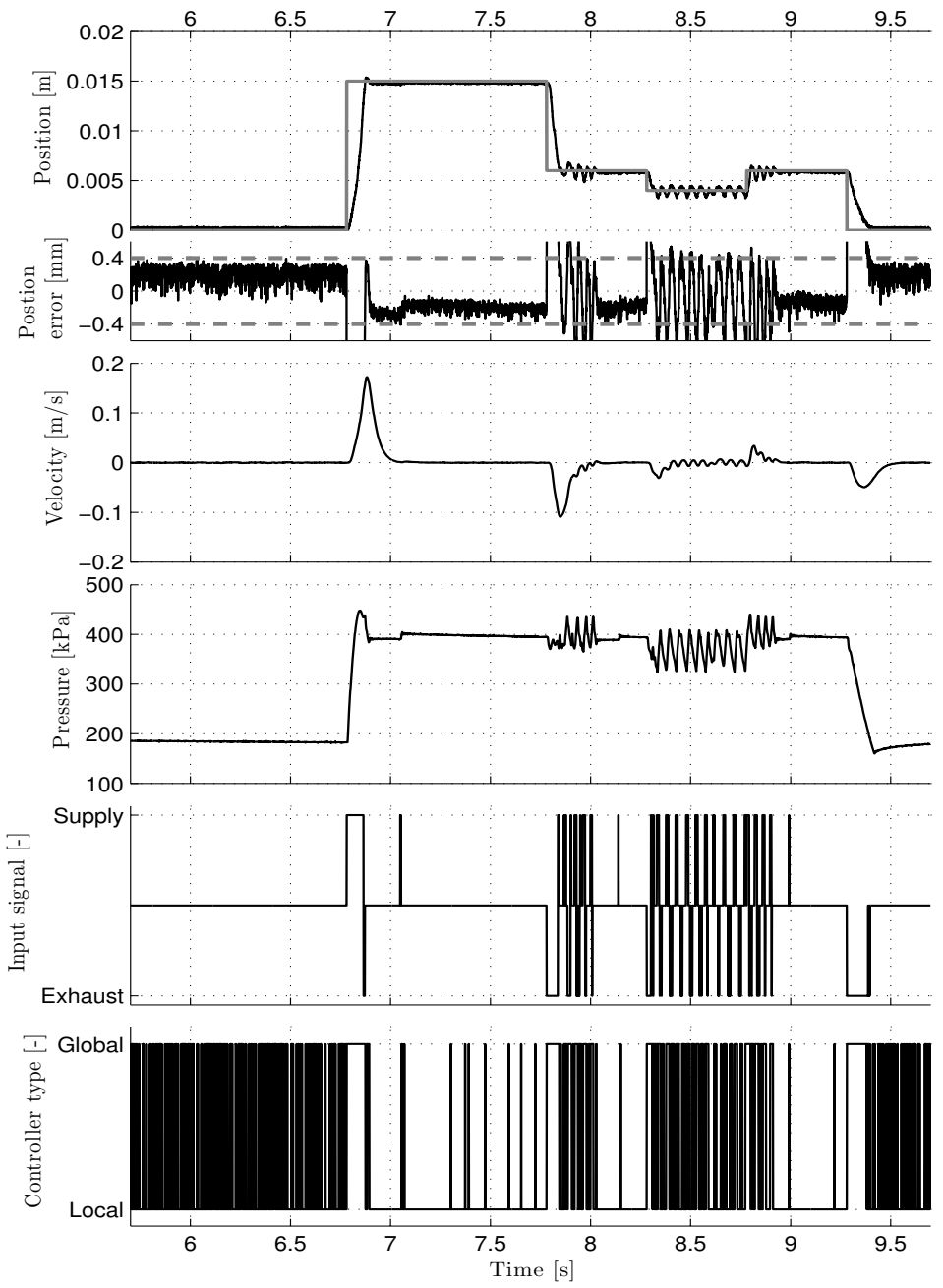

Figure 4.7: Results of experimental testing showing dual-mode controller performance with the pre-prototype valveset present in the truck. The gray curve for position is the reference position, while the dashed gray lines for position error are the requirement limits.

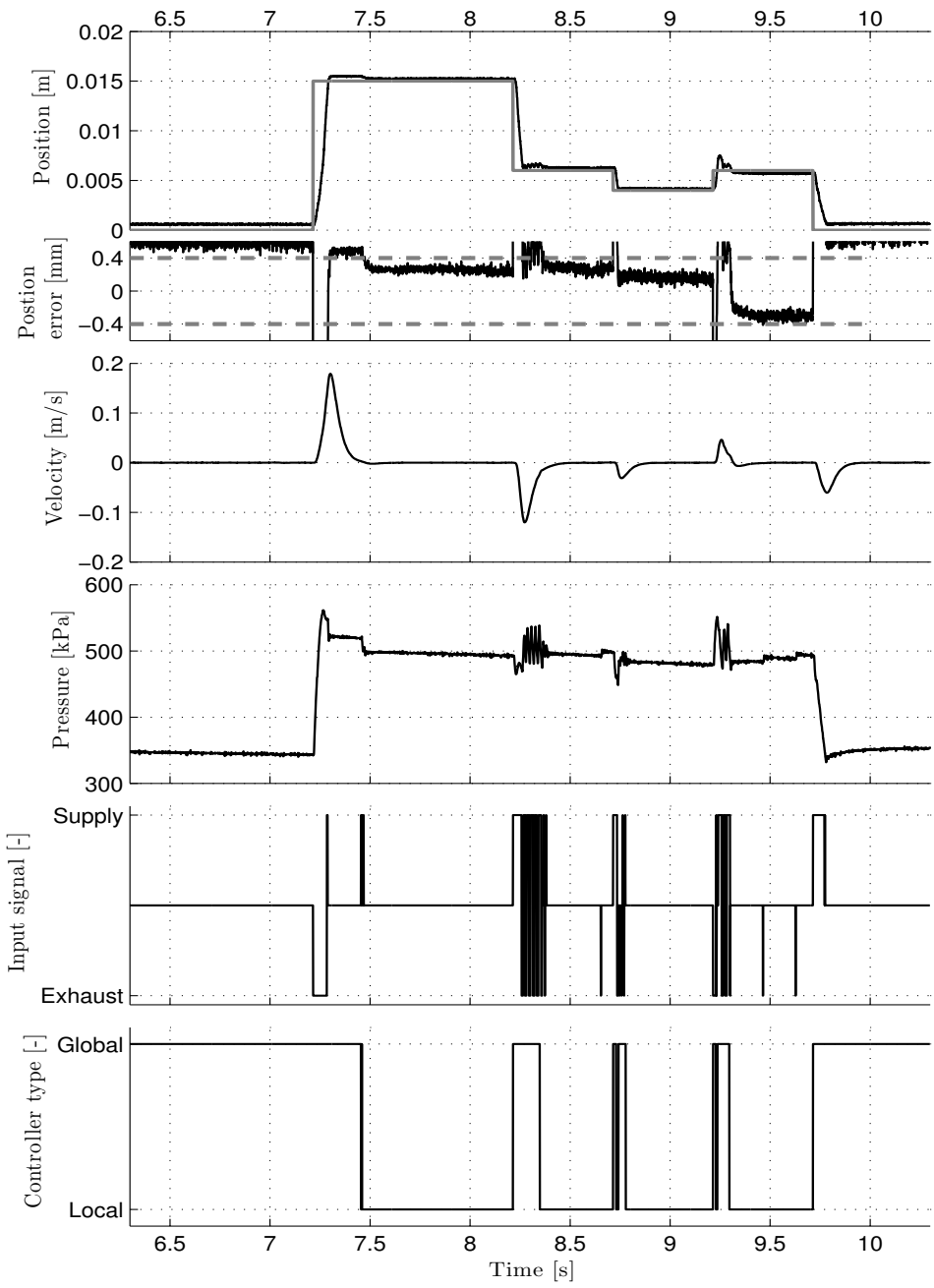

Figure 4.8: Results of experimental testing showing dual-mode controller performance with the prototype valveset present in the truck. The gray curve for position is the reference position, while the dashed gray lines for position error are the requirement limits.

due to the fact that the controller is shut down whenever $|\tilde{x}_1| < 0.4$ mm something which is chosen for comparison as experiments with the pre-prototype valveset were conducted using this limit. The tuning of the controller has been improved between the experiments with the pre-prototype and the prototype valvesets, and the effect of this is clear comparing the performances. One improvement is that the chattering experienced in the first tests is not present anymore in the second test results. Also the switching between the local and the global controller, decided by the value of ϵ, has been better tuned for the tests with the prototype valveset in the truck, resulting in fewer input switches, see Table 4.6. For the dual-mode controller also the number of switches between the controllers is reduced from 1210 for the pre-prototype experiment to 706 in the prototype experiment. These results show how important proper tuning of the controllers is.

It also seems like the prototype valves have larger capacities than the pre-prototype valves in these experiments, even though their maximum volumetric flow rates are the same. This come from the fact that the capacities in general will vary with pressure and temperature.

Controller	*Valvetype*	*Position error*	*Input switches*	*Reach time*	*Settle time*[3]
Local	Pre-proto	1.7 mm	366	63.0 ms	-
	Proto	1.1 mm	231	42.1 ms	96.8 ms
Global	Pre-proto	0.83 mm	375	63.5 ms	-
	Proto	0.813 mm	245	43.2 ms	69.8 ms
Combined	Pre-proto	0.749 mm	269	49.9 ms	138.0 ms
	Proto	0.669 mm	115	61.1 ms	156.8 ms

Table 4.6: Performance parameters of the local, global and dual-mode controllers employing pre-prototype and prototype valvesets.

4.6 Discussions

Switched controllers for an electropneumatic clutch actuator have been presented. The controllers are designed to switch between available inputs in a way that ensures that at each switching time the most negative Lyapunov time-derivative is obtained. The best results are obtained by the dual-mode switching controller. This controller is a combination of the two other switched controllers, and preserves the best individual properties of these controllers. Experimental results conducted in the test vehicle verify the stability properties of the controller, and show that it is well suited for the system.

The unmodeled delay of the on/off solenoid valve dynamics may lead to oscillations around the reference point, as experienced in the results from testing with the local controller. This happens as the dynamic response of the last command

[3]There are oscillations in some cases, such that the response has not always settled, and an average settle time cannot be calculated.

input signal is not finished before the next is commanded. Taking these delays into consideration, the chattering appearing in some of the experiments could be reduced. It is also evident from the robustness evaluations that the controller will benefit from online adaptation of the clutch load, as this is the main uncertainty in the system model. A practical implementation in a production system must therefore consider adaptation of the load characteristics and possibly other model parameters. All analyses are made under the assumption of full state feedback. In the experiments both a position and a pressure sensor have been used, with velocity calculated by numerical differentiation and filtering, described in Section 4.1.1. Adaptive observers that estimate velocity and pressure are treated in the next chapter.

Chapter 5

Nonlinear adaptive observer design

In this chapter we present adaptive nonlinear observers for the electropneumatic clutch actuation system, making full-state feedback for the controller design in Chapter 4 possible. This chapter is mainly based on Langjord et al. (2011a) and Langjord et al. (2010).

5.1 Introduction

Only position measurement will be available in the finalized production clutch actuator system, and to be able to employ the controllers described in the previous chapter, a nonlinear observer must be designed to be able to provide estimates of the unmeasured states. The robustness study in Section 4.5.2 also shows that the control design will suffer in case of model errors, which also motivates for including adaptation in the observer design.

Extended Kalman filters (EKF) are the most widely used algorithm for nonlinear state estimations. This because they are easy to construct, and often produces good results even though analytical stability of the estimates is not necessarily guaranteed. EKFs suffer from high computational complexity, due to the recursive solution of the Riccati equation, and are therefore not convenient for application in the clutch actuator system. As previous discussed, general designs for nonlinear observers have been developed for particular classes of nonlinear systems. Wu et al. (2004) consider nonlinear observability analyses for a pneumatic actuator systems, and conclude that in general it is not feasible to guarantee a convergent pressure estimate from measurement of position only. Therefore, observers presented for pneumatic actuator systems are designed and analysed specifically. Bigras and Khayati (2002) present a nonlinear observer for estimation of the pressure in a pneumatic cylinder, ensuring exponential stability of the estimation error. Pandian et al. (2002) propose a Luenberger-type observer and a sliding mode observer to estimate pressure in a cylinder actuator, and Gulati and Barth (2005) present

two Lyapunov-based pressure observers for a pneumatic actuator system. In our clutch actuator system, the clutch load is a position dependent and time-varying load while observers in the above references threat electropneumatic actuators with constant loads. Some load independent and varying load observers can be found, Taghizadeh et al. (2010) design a Kalman filter to estimate velocity for a pneumatic actuator with varying load, while Gulati and Barth (2009) present an energy-based observer which is load-independent. But as Taghizadeh et al. (2010) only consider a velocity observer, while Gulati and Barth (2009) use both position and velocity measurements and focus only on pressure estimation, these observers are not applicable to our system. In addition all the above references use a simpler friction model than required in our system, and have no adaptation to capture a time-varying clutch load. The theses by Kaasa (2006) and Vallevik (2006) consider observer designs for the same clutch actuator system as ours, but without rigorously deriving sufficient conditions for the convergence of estimation errors and considering adaptation. These authors also consider a three-way proportional valve as the control valve while we consider on/off solenoid valves. Szabo et al. (2010) propose a feedback linearization-based observer for an electropneumatic clutch system actuated by on/off solenoid valves, but do not consider adaptation. The presented observers in this chapter are deterministic observers with linear output-injections.

5.1.1 Model for observer design

We make some modification of the LuGre friction model (3.7-3.8) presented in Section 3.2, to obtain a model suited for observer design while still give a adequate description of the friction in the clutch actuator system. To get a simple static friction characteristic, the dry friction characteristic is chosen as the constant Coloumb friction, $f_d = F$. In addition we remove the deflection damping term, $D_{\dot{z}}\dot{z}$, from the resulting friction force. To be more convenient for observer design we also rewrite the model by setting $z = \frac{K_z}{F}z$, where the new z state can be defined as the normalized pre-sliding deflection. This gives the friction force and the dynamics as

$$\frac{F}{K_z}\dot{z} = v - |v|z \tag{5.1}$$

$$f_f = Fz + Dv. \tag{5.2}$$

For observer design it is also convenient to express the system dynamics with the masses of air, m_A and m_B rather than the pressures p_A and p_B. The pressure in each chamber is then given as a function of the corresponding chamber volume and mass according to

$$p_A\left(p_A, y\right) = \frac{RT_0}{V_A\left(y\right)}m_A \tag{5.3}$$

$$p_B\left(p_B, y\right) = \frac{RT_0}{V_B\left(y\right)}m_B. \tag{5.4}$$

where the volume of each chamber is given as a function of position according to

$$V_A(y) = V_{A,0} + A_A y$$
$$V_B(y) = V_{B,0} - A_B y$$

where $V_{A,0}$ and $V_{B,0}$ describe the volumes in the chambers for $y = 0$.

Considering these assumptions, we present a 5th order model for observer design

$$\dot{y} = v \tag{5.5a}$$
$$M\dot{v} = -f_l(y) - f_f(v,z) + \frac{A_A RT}{V_A(y)} m_A - \frac{A_B RT}{V_B(y)} m_B - A_0 P_0 \tag{5.5b}$$
$$\frac{F}{K_Z}\dot{z} = v - |v| z \tag{5.5c}$$
$$\dot{m}_A = w_v(p_A, u) \tag{5.5d}$$
$$\dot{m}_B = w_r(p_B) \tag{5.5e}$$

where the flows $w_v(p_A, u)$ and $w_r(p_B)$ are described by (3.18) and (3.21), respectively. The clutch load force $f_l(y)$ is described by (3.24) with the splines described in Section 3.5, and the friction force $f_f(v, z)$ is described by (5.2). Parameter values are given in Table 5.1 where nominal values for the parameters are indicated.

Experimental data from the test truck provides position and pressure measurements, and the employed position reference is shown in Figure 5.1. The input signal, which in these experiments is constructed by PWM, is also available. The observer uses the input signal and the position measurement, while pressure measurement and a velocity signal filtered from the position measurement are used for validation of the observer performance. The observer is implemented in Simulink by using explicit Euler discretization with step size 0.1 ms. The position and pressure sensors are production quality sensors, providing data with a sampling interval of 1 ms, and are influenced by both noise and motor vibrations as discussed in Section 2.2.4.

5.2 Reduced-order observer design

Assuming all model parameters are known, we first propose a reduced-order observer by not estimating position

$$M\dot{\hat{v}} = -\phi^T(y)\theta - D\hat{v} - F\hat{z} + \frac{A_A RT_0}{V_A(y)}\hat{m}_A \tag{5.6a}$$
$$- \frac{A_B RT_0}{V_B(y)}\hat{m}_B - A_0 P_0 + l_v(\dot{y} - \hat{v}) \tag{5.6b}$$
$$\frac{F}{K_z}\dot{\hat{z}} = \hat{v} - |\dot{y}|\hat{z} \tag{5.6c}$$
$$\dot{\hat{m}}_A = w_v(\hat{p}_A, u) + \frac{l_m}{V_A(y)}(\dot{y} - \hat{v}) \tag{5.6d}$$
$$\dot{\hat{m}}_B = w_r(\hat{p}_B), \tag{5.6e}$$

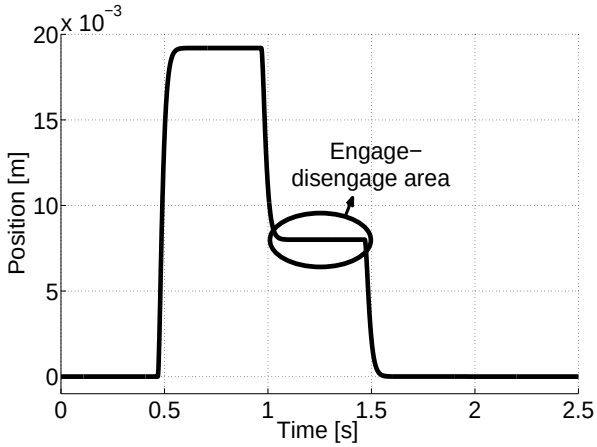

Figure 5.1: Reference clutch sequence used in the experiments in this chapter.

Parameter	*Notation*	*Value*	*Unit*
Clutch actuator parameters			
Mass	M	10	kg
Area of chamber A	A_A	$12.3 \cdot 10^{-3}$	m^2
Area of chamber B	A_B	$11.848 \cdot 10^{-3}$	m^2
Area of piston rod	A_0	$4.52 \cdot 10^{-4}$	m^2
Ambient pressure	P_0	$1 \cdot 10^5$	Pa
Supply pressure	P_S	$9.5 \cdot 10^5$	Pa
Temperature	T_0	293	K
Gas constant of air	R	288	J/kgK
Volume in chamber A at y=0	$V_{A,0}$	$0.148 \cdot 10^{-3}$	m^3
Volume in chamber B at y=0	$V_{B,0}$	0.012	m^3
Viscous damping	D	2500	Ns/m
Asperity stiffness	K_z	$1 \cdot 10^6$	N/m
Coulomb friction	F	400	N
Density	ρ_0	1.185	$\mathrm{kg/m}^3$
Conductance of outlet restriction	C_r	$5 \cdot 10^{-8}$	$\mathrm{m}^4\mathrm{s/kg}$
Weighting parameter vector for clutch load ch.	θ	$[4, 5]$	–
On/off valve parameters			
Duty cycle for valveopening of supply valve	$R_{0,s}$	0.07	–
Duty cycle for valveopening of exhaust valve	$R_{0,e}$	0.07	–
Duty cycle for fully opened supply valve	$R_{1,s}$	0.93	–
Duty cycle for fully opened exhaust valve	$R_{1,e}$	0.93	–
Conductance for supply valve	C_s	$17 \cdot 10^{-9}$	$\mathrm{m}^4\mathrm{s/kg}$
Conductance for exhaust valve	C_e	$23 \cdot 10^{-9}$	$\mathrm{m}^4\mathrm{s/kg}$

Table 5.1: Model parameters used in the testing of the observer performance.

where $l_v, l_m \geq 0$ are observer injection gains.

Remark 5.2.1. *Introducing $\dot{y}$ in observer design requires careful attention, as differentiation of the measured signal will amplify any measurement noise. Note that the injection terms $l(\dot{y} - \hat{v})$ are implementable with only y measured,* i.e. *without using $\dot{y}$ explicitly. Considering the velocity dynamics to demonstrate the principle*

$$M\dot{\hat{v}} = u_v + l_v(\dot{y} - \hat{v}),$$

where u_v contains the remaining terms from (5.6a). Integration gives

$$\begin{aligned} M\hat{v} &= \int_0^t \left(u_v + l_v\left(\frac{dy}{d\tau} - \hat{v}\right)\right) d\tau \\ &= \int_0^t (u_v - l_v\hat{v})\, d\tau + l_v \int_{y(0)}^{y(t)} dy \\ &= \int_0^t (u_v - l_v\hat{v})\, d\tau + l_v(y(t) - y(0)). \end{aligned}$$

and the estimate $\hat{v}$ can be implemented without differentiation as

$$\begin{aligned} \dot{x_v} &= u_v - l_v\hat{v} \\ M\hat{v} &= x_v + l_v(y - y(0)). \end{aligned}$$

Using the same approach, the estimate for $\hat{m}_A$ can be implemented as

$$\begin{aligned} \dot{x}_m &= w_v(\hat{p}_A, u) - \frac{l_m}{V_A(y)}\hat{v} \\ \hat{m}_A &= x_m + \frac{l_m}{A_A} ln\left(\frac{V_A(y)}{V_{A0}}\right). \end{aligned}$$

This approach fails for avoiding $|\dot{y}|$ in the implementation the estimate $\hat{z}$. But implementation in discrete-time of the $\hat{z}$ estimate in the case of using zero-order hold on the measurements and Euler integration, simply becomes

$$\hat{z}_{k+1} = \hat{z}_k + \frac{K_z \Delta t}{F}\hat{v}_k - \frac{K_z}{F}\hat{z}_k\,|y_{k+1} - y_k|,$$

where Δt is the sampling period. The effects of measurement noise will be discussed later when considering experimental results, and in Section 5.4 when considering a full-order estimator.

The error dynamics are

$$M\dot{\tilde{v}} = -(D + l_v)\,\tilde{v} - F\tilde{z} + \frac{A_A R T_0}{V_A(y)} - \frac{A_B R T_0}{V_B(y)}\tilde{m}_B\tilde{m}_A \tag{5.7a}$$

$$\frac{F}{K_z}\dot{\tilde{z}} = \tilde{v} - |v|\,\tilde{z} \tag{5.7b}$$

$$\dot{\tilde{m}}_A = -a(t)\,\tilde{m}_A - \frac{l_m}{V_A(y)}\tilde{v} \tag{5.7c}$$

$$\dot{\tilde{m}}_B = -b(t)\,\tilde{m}_B. \tag{5.7d}$$

where $\inf V_B(y) = V_{B\min}$ and we get from (3.22), (3.23) and the Mean Value Theorem that

$$a(t) = -\frac{\partial w_v(\bar{m}_A, u)}{\partial p_A} \geq 0 \tag{5.8}$$

$$b(t) = -\frac{\partial w_r(\bar{m}_B)}{\partial p_B} \geq b_0 > 0 \tag{5.9}$$

and

$$\bar{m}_A \in [\min(m_A, \hat{m}_A), \max(m_A, \hat{m}_A)] \subseteq \left[\frac{V_{A,\min}}{RT_0}P_0, \frac{V_{A,\max}}{RT_0}P_S\right]$$
$$\bar{m}_B \in [\min(m_B, \hat{m}_B), \max(m_B, \hat{m}_B)] \subseteq [0, \infty\rangle$$

where $V_{A,\min} = V_A(0)$ and $V_{A,\max} = \inf_y V_A(y)$.

Definition 5.2.2 (Persistently exciting (PE) signal)**.** *A signal ω is persistently exciting if there exist $T > 0$ and $\epsilon > 0$ such that $\int_t^{t+T} \omega^2(\tau)d\tau \geq \epsilon$ for all $t > t_0$.*

Proposition 5.2.3. *The observer presented in (5.6), where $l_v, l_m \geq 0$, ensures that for any physically meaningful initial conditions and system trajectories*

1. *the error dynamics are stable and all estimates are bounded*
2. *$\tilde{v}$ and $\tilde{m}_B$ converge to zero*
3. *if v is PE then also $\tilde{m}_A$ and $\tilde{z}$ converge to zero*

Proof. Stability of the error dynamics can be established using the Lyapunov function candidate

$$U(\tilde{v}, \tilde{z}, \tilde{m}_A, \tilde{m}_B) = \frac{M}{2}\tilde{v}^2 + \frac{F^2}{2K_z}\tilde{z}^2 + \frac{A_A RT_0}{2l_m}\tilde{m}_A^2 + \frac{1}{2Db_0}\left(\frac{A_B RT_0}{V_{B\min}}\right)^2 \tilde{m}_B^2, \tag{5.10}$$

The time-derivative of U along the trajectories of the error dynamics are

$$\begin{aligned}
\dot{U} =& -(D + l_v)\tilde{v}^2 - F\tilde{v}\tilde{z} + \frac{A_A RT_0}{V_A(y)}\tilde{v}\tilde{m}_A - \frac{A_B RT_0}{V_B(y)}\tilde{v}\tilde{m}_B + F\tilde{v}\tilde{z} \\
& - F|v|\tilde{z}^2 - \frac{A_A RT_0}{l_m}a(t)\tilde{m}_A^2 - \frac{A_A RT_0}{V_A(y)}\tilde{v}\tilde{m}_A - \frac{b(t)}{Db_0}\left(\frac{A_B RT_0}{V_{B\min}}\right)^2 \tilde{m}_B^2 \\
=& -(D + l_v)\tilde{v}^2 - F|v|\tilde{z}^2 - \frac{A_A RT_0}{l_m}a(t)\tilde{m}_A^2 - \frac{A_B RT_0}{V_B(y)}\tilde{v}\tilde{m}_B \\
& - \frac{b(t)}{Db_0}\left(\frac{A_B RT_0}{V_{B\min}}\right)^2 \tilde{m}_B^2
\end{aligned}$$

which lead to

$$\dot{U} \leq -(D + l_v)\tilde{v}^2 - F|v|\tilde{z}^2 + \frac{A_B RT_0}{V_{B\min}}|\tilde{v}\tilde{m}_B| - \frac{1}{D}\left(\frac{A_B RT_0}{V_{B\min}}\right)^2 \tilde{m}_B^2.$$

Using Young's inequality

$$xy \leq \frac{x^2}{2\varepsilon} + \frac{\varepsilon y^2}{2}$$

with

$$\varepsilon = \frac{A_B R T_0}{D V_{B\,\min}},$$

we obtain

$$\frac{A_B R T_0}{V_{B\,\min}} \left|\tilde{v}\tilde{m}_B\right| \leq \frac{D}{2}\tilde{v}^2 + \frac{1}{2D}\left(\frac{A_B R T_0}{V_{B\,\min}}\right)^2 \tilde{m}_B^2.$$

This gives

$$\begin{aligned}
\dot{U} \leq & -\left(D + l_v\right)\tilde{v}^2 - F\left|v\right|\tilde{z}^2 - \frac{1}{D}\left(\frac{A_B R T_0}{V_{B\,\min}}\right)^2 \tilde{m}_B^2 \\
& + \frac{D}{2}\tilde{v}^2 + \frac{1}{2D}\left(\frac{A_B R T_0}{V_{B\,\min}}\right)^2 \tilde{m}_B^2 \\
= & -\left(\frac{D}{2} + l_v\right)\tilde{v}^2 - F\left|v\right|\tilde{z}^2 - \frac{1}{2D}\left(\frac{A_B R T_0}{V_{B\,\min}}\right)^2 \tilde{m}_B^2,
\end{aligned}$$

and proves stability of the error dynamics. From Barbalat's lemma (Khalil (2000)) we have that $\tilde{v}$ and $\tilde{m}_B$ converge to zero. Since the solution of the error dynamics are continuous and Lipschitz, this also implies that $\dot{\tilde{v}}$ converges to zero, thus in the limit

$$-F\tilde{z} + \frac{A_A R T_0}{V_A\left(y\right)}\tilde{m}_A = 0. \tag{5.11}$$

With PE of v, $\dot{U}$ will be negative definite also in $\tilde{z}$, which by Barbalat's lemma implies that $\tilde{z}$ also converges to zero, thus from (5.11) $\tilde{m}_A$ must converge too.

Remark 5.2.4. *For the special case $v = 0$, with $\tilde{v} = \tilde{m}_B = 0$, the $(\tilde{z}, \tilde{m}_A)$–dynamics are governed by*

$$\dot{\tilde{z}} = 0 \tag{5.12}$$

$$\dot{\tilde{m}}_A = -a\left(t\right)\tilde{m}_A. \tag{5.13}$$

Hence if $\int_t^{t+T} a\left(\tau\right) d\tau > 0$, which is achieved with PE of u, $\tilde{m}_A$ must converge to zero, hence also $\tilde{z}$. In the case that u is not PE, leading to $a\left(t\right) = 0$, the observer may get stuck at $\tilde{m}_A \neq 0$, $\tilde{z} \neq 0$, with persistent errors in the estimates of pressure $\hat{p}_A$ and the dynamic friction $\hat{z}$. Since $z, \hat{z} \in [-\frac{F}{K_z}, \frac{F}{K_z}]$[1] we have the following bound on the error

$$\left|\tilde{m}_A\right| \leq \frac{F V_A(y_{max})}{A_A R T_0}\frac{F}{K_z}.$$

□

[1]The limit is a property of the LuGre friction model.

5.2.1 Experimental results

Figure 5.2 shows results with of the open-loop observer, i.e. with zero gain. Nominal values of the friction and the clutch load parameter are used. We see that there are some errors in the estimated pressure in chamber A, especially in the engage/disengage area. The noise on the estimations of v and z are mostly due to sensor noise on y entering through $f_l(y)$. Figure 5.3 shows results with the injection gains tuned to $l_v = 2000$ and $l_m = 10^{-5}$, and these gains have been used throughout the rest of the thesis whenever adaptation is introduced. We get a more accurate steady-state estimates for the pressure in chamber A, especially in the engage/disengage area. However, the injection gains also add some extra noise to the estimated velocity and the low pressure areas of the estimate of the pressure in chamber A. This is due to the use of the derivative of the position measurement, $\dot{y}$, in the observer design.

5.3 Adaptive nonlinear reduced-order observer

Due to temperature changes and wear, the friction and clutch load characteristic change during the operation and lifetime of the clutch. Therefore, adaptation of the load and friction characteristics are desired in order to achieve sufficient accuracy of the observer, and we propose adaptation laws for the clutch load parameter, θ, and the viscous damping, D.

Remark 5.3.1. *Adaptation of the Coulomb friction, F, has been considered too, but has been left out as it enters nonlinearly into the friction dynamics and an adaptive law is more diffucult to design. It is also found that sufficient accuracy can be obtained without estimating F and no significant improvement would be achieved by estimating F, see Section 5.3.3.*

Remark 5.3.2. *To account for the clutch load curve moving significantly to the left/right due to wear and temperature, a Multiple Model Scheme can be used as discussed in Section 3.5.*

5.3.1 Adaptation of the clutch load characteristic

Since there are uncertain parameters in the clutch load characteristic, the observer (5.6) is implemented with the estimated parameter vector $\hat{\theta}$ instead of θ. This results in the parametric uncertainty

$$\tilde{f}_l(y) = \phi^T(y)\left(\theta - \hat{\theta}\right),$$

which appear in the resulting $\tilde{v}$–dynamics as

$$M\dot{\tilde{v}} = -\phi^T(y)\,\tilde{\theta} - (D + l_v)\,\tilde{v} - F\tilde{z} + \frac{A_A R T_0}{V_A(y)}\tilde{m}_A - \frac{A_B R T_0}{V_B(y)}\tilde{m}_B.$$

We propose an adaptation law

$$\dot{\hat{\theta}} = -\Gamma\phi(y)\,(\dot{y} - \hat{v}) \tag{5.14}$$

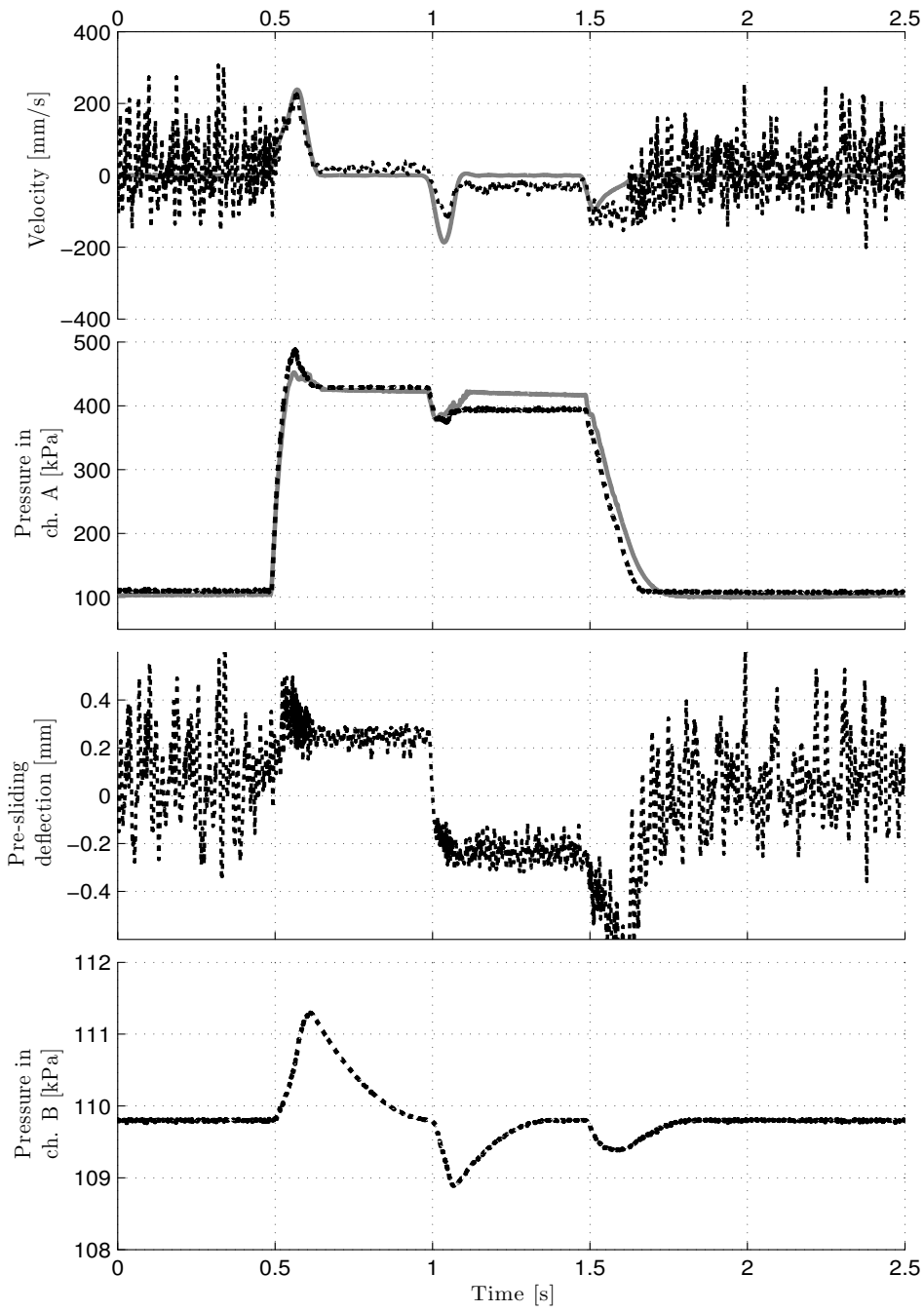

Figure 5.2: Performance of the open loop observer. Observer states are dashed, and measurement from the truck are shown in solid gray. For velocity, the measurement curve is filtered from position measurement.

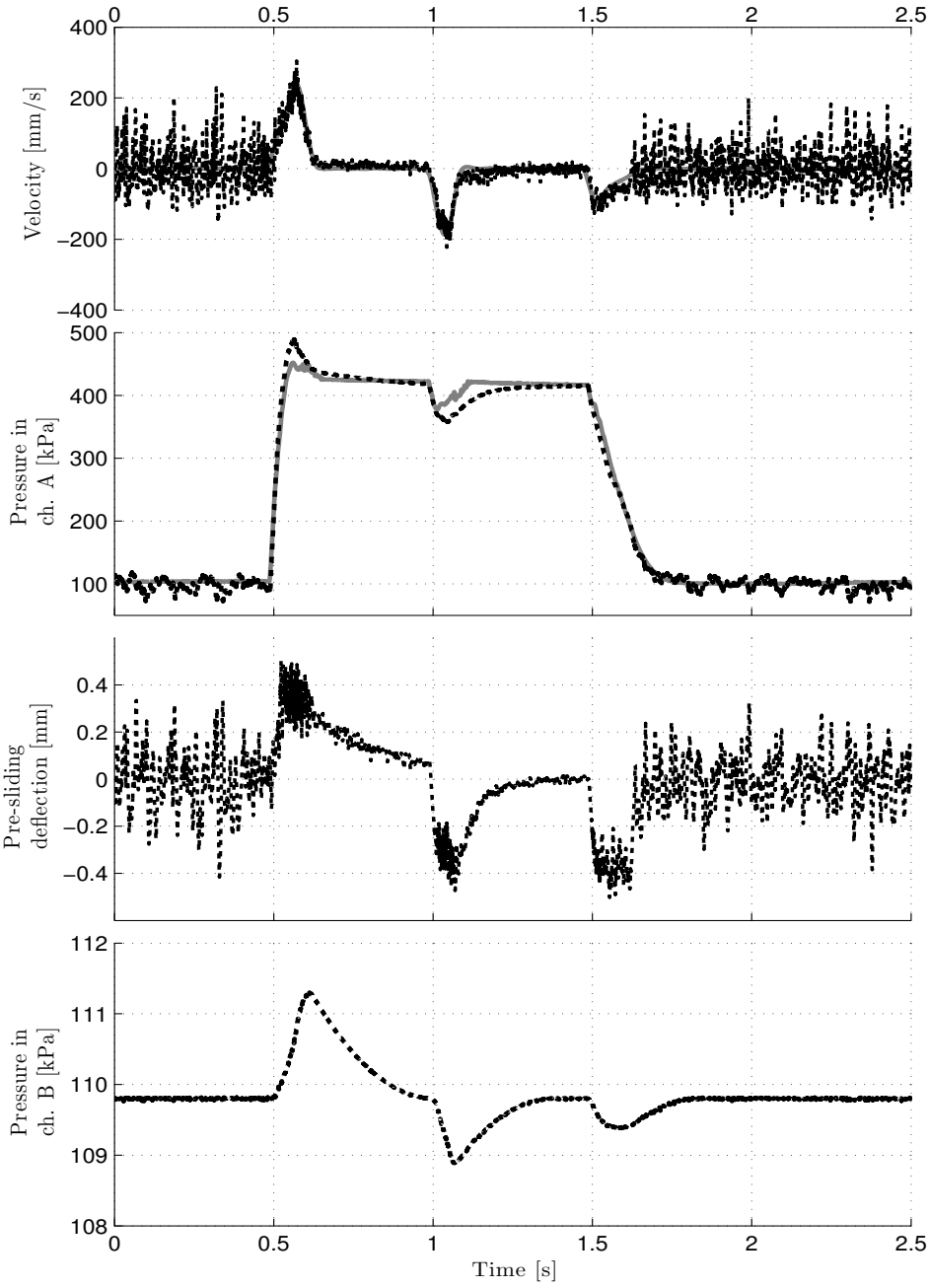

Figure 5.3: Performance of the observer with input injections $l_v = 2000$ and $l_m = 10^{-5}$. Observer states are dashed, and measurement from the truck are shown in solid gray. For velocity, the measurement curve is filtered from position measurement.

with some gain matrix $\Gamma = \Gamma^T > 0$.

Proposition 5.3.3. *The observer presented in (5.6) implemented with $\hat{\theta}$ and the adaption law (5.14), where $l_v, l_m \geq 0$ and $\Gamma = \Gamma^T > 0$, ensures that for any physically meaningful initial conditions and system trajectories*

1. *the error dynamics are stable and all estimates are bounded*
2. *$\tilde{v}$ and $\tilde{m}_B$ converge to zero*
3. *if u and v are PE, then also $\tilde{m}_A$, $\tilde{z}$ and $\tilde{\theta}$ converge to zero*

Proof. Using the Lyapunov function candidate

$$V\left(\tilde{v}, \tilde{z}, \tilde{m}_A, \tilde{m}_B, \tilde{\theta}\right) = U\left(\tilde{v}, \tilde{z}, \tilde{m}_A, \tilde{m}_B\right) + \frac{1}{2}\Gamma^{-1}\tilde{\theta}^T\tilde{\theta}, \tag{5.15}$$

the time-derivative along the trajectories of the error dynamics satisfies

$$\begin{aligned}\dot{V} \leq & -\left(\frac{D}{2} + l_v\right)\tilde{v}^2 - F\left|v\right|\tilde{z}^2 \\ & - \frac{1}{2D}\left(\frac{A_B R T_0}{V_{B\,\min}}\right)^2 \tilde{m}_B^2 - \tilde{\theta}^T\phi\left(y\right)\tilde{v} + \Gamma^{-1}\tilde{\theta}^T\dot{\tilde{\theta}}.\end{aligned}$$

With the adaptation law (5.14) the $\tilde{\theta}$–dynamics satisfies

$$\dot{\tilde{\theta}} = \Gamma\phi\left(y\right)\tilde{v},$$

which makes $\dot{V}$ negative semi-definite;

$$\dot{V} \leq -\left(\frac{D}{2} + l_v\right)\tilde{v}^2 - F\left|v\right|\tilde{z}^2 - \frac{1}{2D}\left(\frac{A_B R T_0}{V_{B\,\min}}\right)^2 \tilde{m}_B^2$$

and proves stability of the error dynamics. Barbalat's lemma gives that $\tilde{v}$ and $\tilde{m}_B$ converges to zero. Since the solution of the error dynamics are continuous and Lipschitz, this also implies that $\dot{\tilde{v}}$ converges to zero, thus in the limit

$$-\phi^T(y)\tilde{\theta} - F\tilde{z} + \frac{A_A R T}{V_A\left(y\right)}\tilde{m}_A = 0. \tag{5.16}$$

With PE of v, $\dot{V}$ will be negative definite also in $\tilde{z}$, which implies that $\tilde{z}$ also converges to zero. Considering (5.13) which with PE of u implies that also $\tilde{m}_A$ converges to zero. It then follows from (5.16) that $\tilde{\theta}$ must converge to zero too. □

Remark 5.3.4. *Intuitively, PE of u will result in PE of v as motion of the pistion is a direct consequence of changes in the input signal u.*

5.3.2 Adaptation of the viscous damping coefficient

With uncertainties in the viscous friction, the adaptive observer is implemented with estimated coefficient $\hat{D}$ instead of D. Denoting $\tilde{D} = D - \hat{D}$ the resulting error becomes

$$Dv - \hat{D}\hat{v} = D(v - \hat{v}) + \tilde{D}\hat{v}$$

which appears in the resulting $\tilde{v}$–dynamics as

$$M\dot{\tilde{v}} = -\phi^T(y)\,\tilde{\theta} - (D + l_v)\,\tilde{v} - \tilde{D}\hat{v} - F\tilde{z} + \frac{A_A R T_0}{V_A(y)}\tilde{m}_A - \frac{A_B R T_0}{V_B(y)}\tilde{m}_B.$$

We propose the adaptation law

$$\dot{\hat{D}} = -\gamma_D \hat{v}(\dot{y} - \hat{v}). \tag{5.17}$$

with $\gamma_D > 0$.

Proposition 5.3.5. *The observer presented in (5.6) implemented with $\hat{\theta}$, $\hat{D}$ and the adaptation laws (5.14) and (5.17), where $l_v, l_m \geq 0$ and $\Gamma = \Gamma^T > 0, \gamma_D > 0$, ensures that for any physically meaningful initial conditions and system trajectories*

1. *the error dynamics are stable and all estimates are bounded*
2. *$\tilde{v}$ and $\tilde{m}_B$ converge to zero*
3. *if v and u are PE then also $\tilde{m}_A$ and $\tilde{z}$ converge to zero*

Proof. Using the Lyapunov function candidate

$$Z(\tilde{v}, \tilde{z}, \tilde{m}_A, \tilde{m}_B, \tilde{\theta}, \tilde{D}) = V(\tilde{v}, \tilde{z}, \tilde{m}_A, \tilde{m}_B, \tilde{\theta}) + \frac{1}{2\gamma_D}\tilde{D}^2, \tag{5.18}$$

the time-derivative along the trajectories of the error dynamics satisfies

$$\begin{aligned}\dot{Z} \leq &-\left(\frac{D}{2} + l_v\right)\tilde{v}^2 - F\,|v|\,\tilde{z}^2 \\ &- \frac{1}{2D}\left(\frac{A_B R T_0}{V_{B\,\min}}\right)^2 \tilde{m}_B^2 - \tilde{D}\hat{v}\tilde{v} + \gamma_D^{-1}\tilde{D}\dot{\tilde{D}}.\end{aligned}$$

With the adaptation law (5.17) the $\tilde{D}$–dynamics satisfies

$$\dot{\tilde{D}} = \gamma_D \hat{v}\tilde{v},$$

which would make $\dot{Z}$ negative semi-definite,

$$\dot{Z} \leq -\left(\frac{D}{2} + l_v\right)\tilde{v}^2 - F\,|v|\,\tilde{z}^2 - \frac{1}{2D}\left(\frac{A_B R T_0}{V_{B\,\min}}\right)^2 \tilde{m}_B^2$$

and proves stability of the error dynamics. Barbalat's lemma gives that $\tilde{v}$ and $\tilde{m}_B$ converges to zero. With PE of v, $\dot{Z}$ will be negative definite also in $\tilde{z}$, which implies that $\tilde{z}$ also converges to zero, and (5.13) implies that with PE of u also $\tilde{m}_A$ converges to zero.

Remark 5.3.6. *Asymptotically we have* $-\phi^T(y)\tilde{\theta} - \tilde{D}\hat{v} = 0$ *and with PE of* $\phi^T(y)$ *and* $\hat{v}$ *it seems intuitive that* $\tilde{\theta}$ *and* $\tilde{D}$ *will converge to zero. Intuitively, PE of* u *will lead to motion of the actuator piston and PE of* y, v *and* $\hat{v}$.

□

5.3.3 Experimental results

Figure 5.4 shows the state estimate results for the reduced-order adaptive observer. Values of the tuning parameters are given in Table 5.2. The initial values of the parameter estimates have been set far from the expected values to test the performance of the adaptation laws. Results from the two initial conditions 1) $\theta_0 = [10, 10]$, $D_0 = 50$ and 2) $\theta_0 = [1, 1]$, $D_0 = 5000$ are included in Figures 5.5, which shows the estimated parameter values, and in Figure 5.6, which shows the clutch load characteristic, to demonstrate the convergence of the estimated parameters. Note that such large changes in friction and clutch load characteristics as used for testing here will normally not occur during the normal operation of the clutch actuator system. We have used slow adaptation of the clutch load, as this is expected to improve the robustness of the approach and the uncertain parameters are expected to change slowly. The gain Γ is set 30 times higher in the region $3 - 6$ mm as the clutch load characteristic is especially important in this area due to the steep curve, and since this region is visited only for short transient periods with a typical clutch sequence. The adaptation is shut down whenever the position is not changing, due to lack of PE that might lead to drift or divergence of the estimates due to noise. The estimate of the pressure in chamber A improves over time and we have a good estimate after approximately 150 s corresponding to adaptation in about 60 clutch sequences as seen in Figure 5.4. The estimates of the velocity and the pre-sliding deflection state suffer, as the observer without adaptation, from some noise. From Figure 5.6 it is clear that the adaptation of θ gives an accurate estimate of the clutch load characteristic. This indicates that the clutch sequence in Figure 5.1 provides sufficient excitation to estimate both load and friction parameters simultaneously.

Parameter	*Value*
l_y	10
l_v	2000
l_m	10^{-5}
Γ	$I \cdot 0.1$
γ_D	$1 \cdot 10^6$

Table 5.2: Observer and adaptation gains.

Comparison with the gradient method

As an alternative, we also adapt θ, F and D through slow adaptation not designed jointly with the observer, only updating estimates when the position changes. This

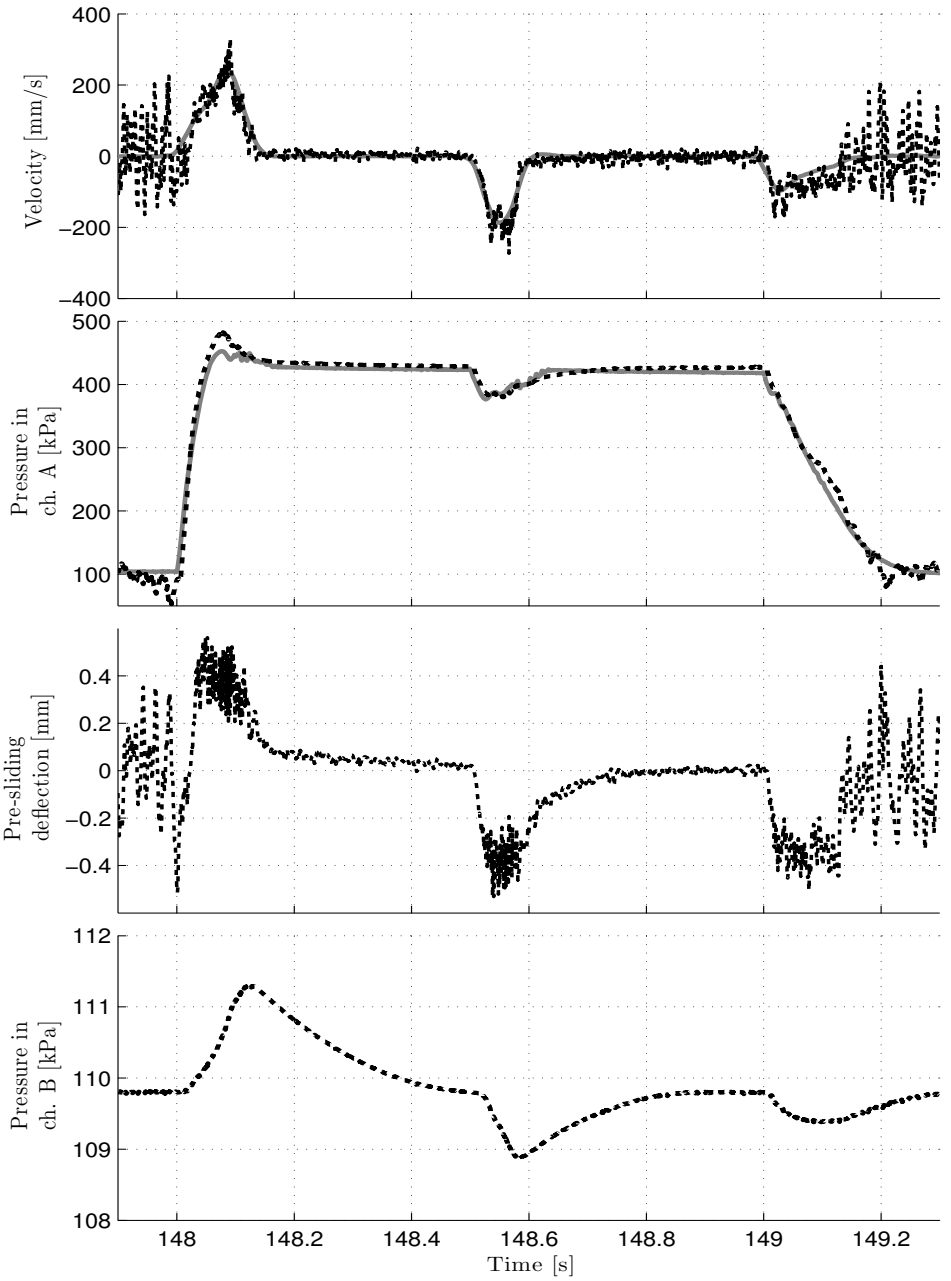

Figure 5.4: Experiments with reduced-order adaptive observer. The curves show estimates after $t = 148$ where the parameter adaptation has already converged, after about 60 clutch sequences. Observer states are dashed, and measurement from the truck are shown in solid gray. For velocity, the measurement curve is filtered from position measurement.

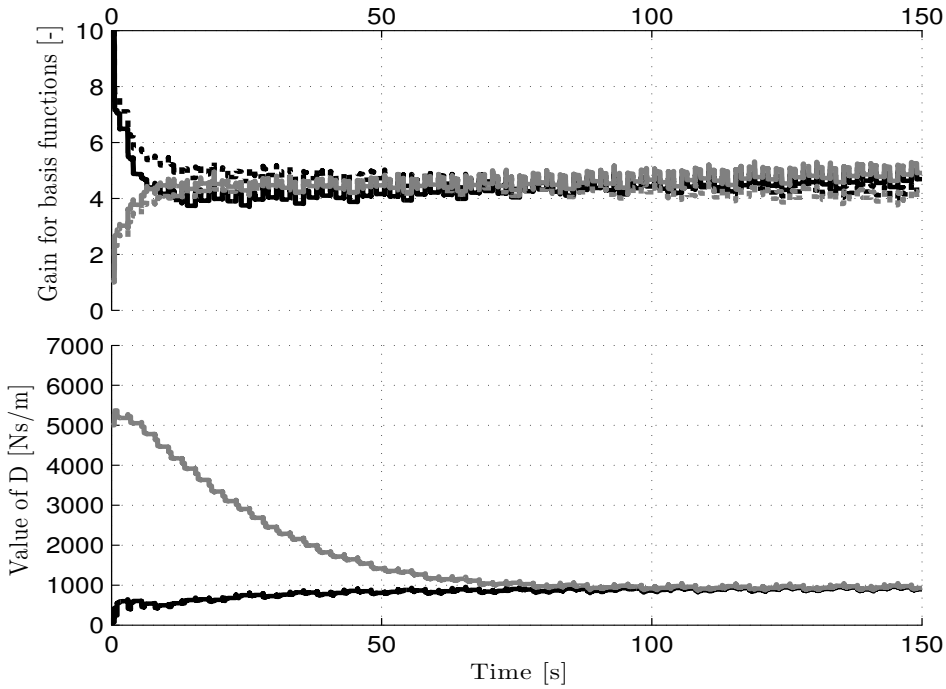

Figure 5.5: Estimated parameters with the reduced-order adaptive observer during 150 s where 60 clutch sequences are executed. Results for $\theta_0 = [10, 10]$, $D_0 = 50$ are shown in black and for $\theta_0 = [1, 1]$, $D_0 = 5000$ in gray. θ_1 are shown dotted and θ_2 are shown solid in the upper plot.

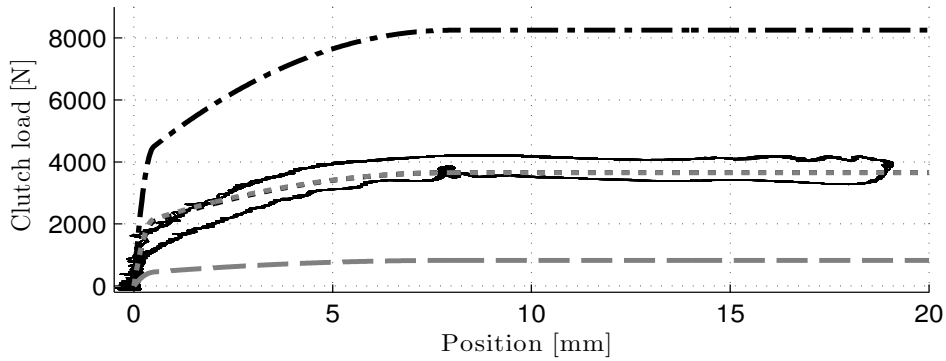

Figure 5.6: Clutch load characteristics, estimated through $A_A(p_A - P_0)$ in solid, dot dashed in black for $\theta_0 = [10, 10]$, $D_0 = 50$ and dashed in gray for $\theta_0 = [1, 1]$, $D_0 = 5000$.The curves with the estimated $\hat{\theta}$ from the reduced-order adaptive observer at $t = 150$ (overlapping) are dotted in black and gray, respectively.

is done to evaluate the performance of the adaptation laws. The standard gradient method (Ioannou and Sun (1996)) is used,

$$\dot{\vartheta} = -\gamma \frac{\partial J}{\partial \theta}(\vartheta(t))$$

where $\vartheta = [\theta, D, F]$ and the cost function J can be the least squares error

$$J(\vartheta) = \frac{1}{2}\epsilon^2 = \frac{1}{2}(y - \hat{y})^2.$$

$\hat{y}$ is a position prediction

$$\hat{y} = \frac{1}{M}(-\phi_f(y)^T\hat{\theta} + \hat{D}\dot{y}_f + \hat{F}z_f + r_f) \tag{5.19}$$

where

$$\begin{aligned}
\phi_f(y) &= \frac{1}{(1+t_d s)^2}\phi(y) \\
\dot{y}_f &= -\frac{1}{(1+t_d s)^2}\dot{y} \\
z_f &= -\frac{1}{(1+t_d s)^2}z \\
r_f &= \frac{1}{(1+t_d s)^2}r \\
r &= \frac{A_A R T_0}{V_A(y)}m_A - \frac{A_B R T_0}{V_B(y)}m_B - A_0 P_0
\end{aligned}$$

and t_d is a low pass filter time constant and the signals z, v and r are given by the observer, see Figure 5.7. This results in the adaptive laws

$$\dot{\hat{\theta}} = -\frac{\lambda_1}{M}\epsilon\phi_f(y)^T \tag{5.20}$$

$$\dot{\hat{D}} = \frac{\lambda_2}{M}\epsilon\dot{y}_f \tag{5.21}$$

$$\dot{\hat{F}} = \frac{\lambda_3}{M}\epsilon z_f \tag{5.22}$$

with gains $\lambda_1, \lambda_2, \lambda_3 > 0$.

Figures 5.8, 5.9 and 5.10 show estimated states and parameters, and resulting clutch load characteristics from tests of the reduced order observer with this adaptation method. We see similar behavior for the estimates of all states, except the normalized pre-sliding deflection. This is due to the fact that also F is estimated and the normalized deflection depends on this. The comparison shows that the adaptation integrated in the observer provides better result than the alternative adaptation, even with one parameter less being estimated.

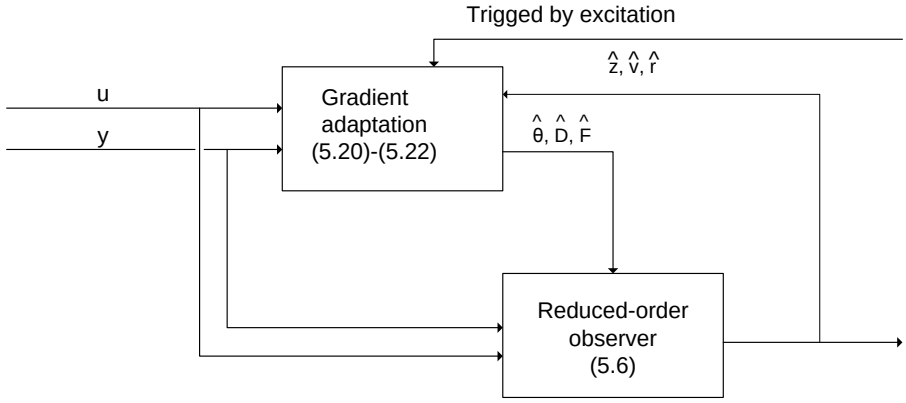

Figure 5.7: Alternative estimation scheme

5.4 Full-order adaptive observer

To reduce noise, we also propose a full-order adaptive observer where position is filtered

$$\dot{\hat{y}} = \hat{v} + l_y(y - \hat{y}) \tag{5.23a}$$

$$M\dot{\hat{v}} = -\phi^T(\hat{y})\hat{\theta} - \hat{D}\hat{v} - F\hat{z} + \frac{A_A R T_0}{V_A(y)}\hat{m}_A \tag{5.23b}$$

$$- \frac{A_B R T_0}{V_B(y)}\hat{m}_B - A_0 P_0 + l_v(\dot{y} - \hat{v}) \tag{5.23c}$$

$$\frac{F}{K_z}\dot{\hat{z}} = \hat{v} - |\dot{y}|\,\hat{z} \tag{5.23d}$$

$$\dot{\hat{m}}_A = w_v(\hat{p}_A, u) + \frac{l_m}{V_A(y)}(\dot{y} - \hat{v}) \tag{5.23e}$$

$$\dot{\hat{m}}_B = w_r(\hat{p}_B), \tag{5.23f}$$

where $l_y, l_v, l_m \geq 0$ are observer injection gains and the adaptation laws for $\hat{\theta}$ and $\hat{D}$ are given in (5.14) and (5.17).

Proposition 5.4.1. *The observer presented in (5.23) with the adaptation laws (5.14) and (5.17), where* $l_v, l_m \geq 0$, $l_y > \frac{(\alpha + K\theta_{\max})^2}{2\alpha l_v}$, $\alpha > 0$ *and* $\Gamma = \Gamma^T > 0, \gamma_D > 0$, *ensures that for any physically meaningful initial conditions and system trajectories*

1. *the error dynamics are stable and all estimates are bounded*
2. $\tilde{v}$, $\tilde{m}_B$ *and* $\tilde{y}$ *converge to zero*

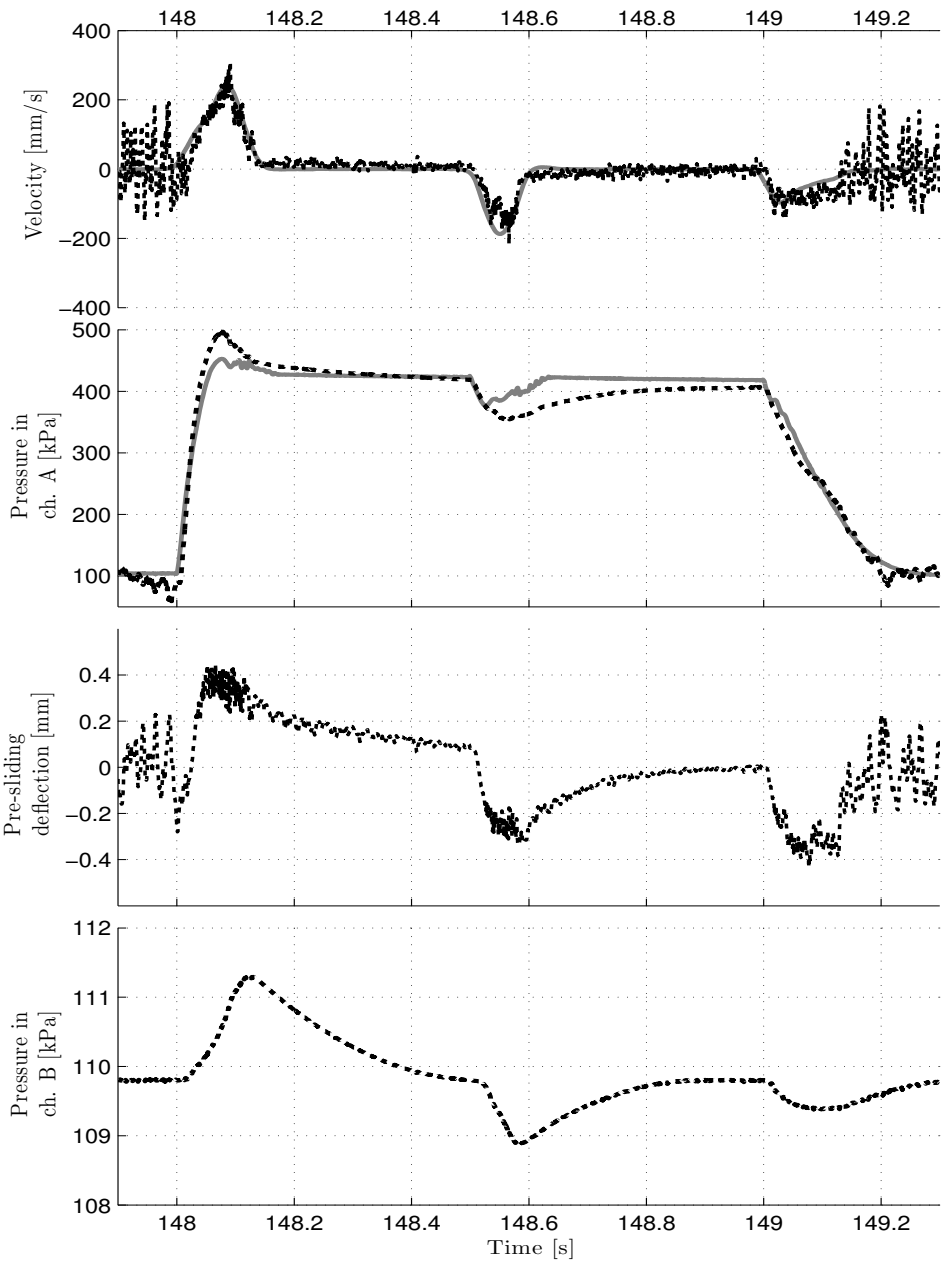

Figure 5.8: Experiments with the reduced-order observer with alternative parameter adaptation. The curves show estimates after $t = 148$ where the parameter adaptation has already converged, after about 60 clutch sequences. Observer states are dashed, and measurement from the truck are shown in solid gray. For velocity, the measurement curve is filtered from position measurement.

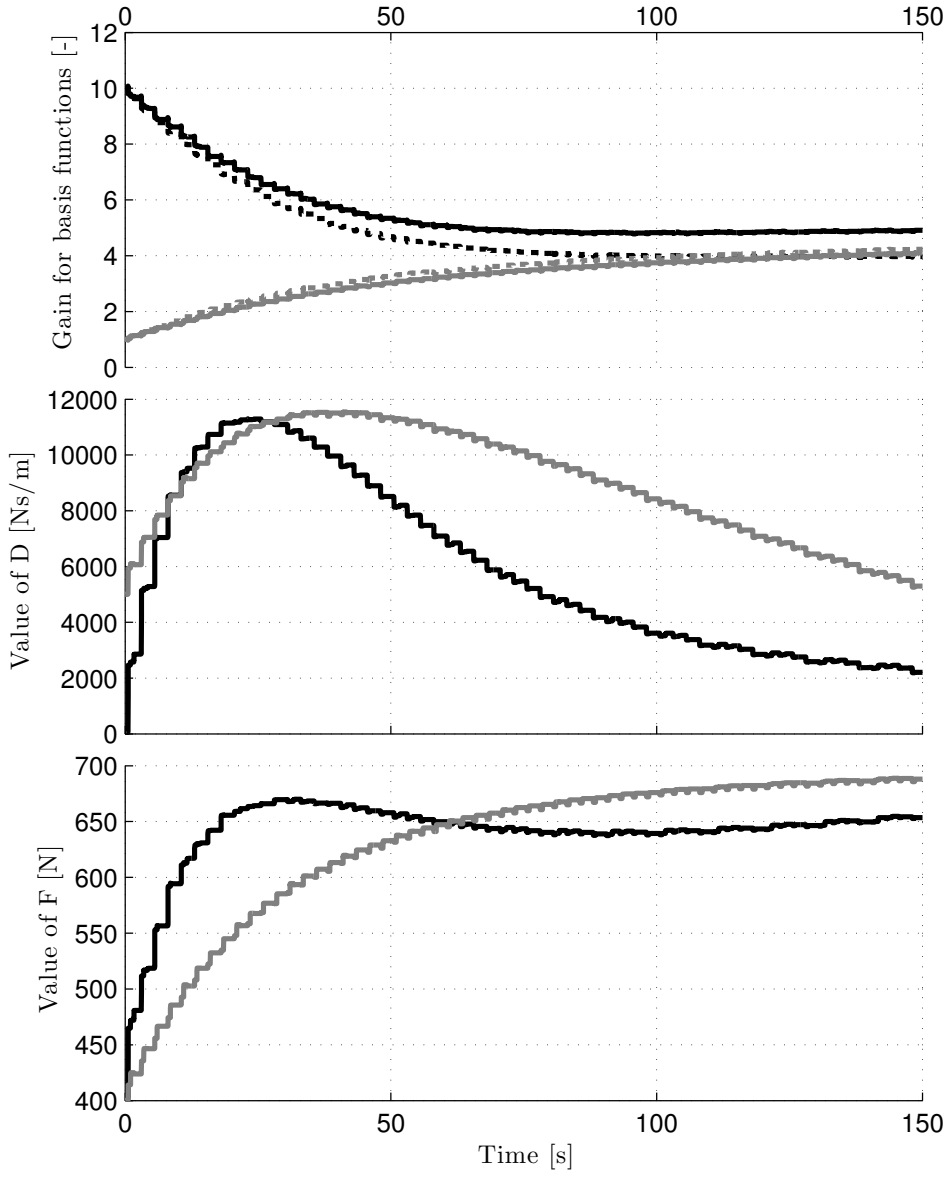

Figure 5.9: Estimated parameters with the reduced-order observer with alternative parameter adaptation during 150 s where 60 clutch sequences are executed. Results for $\theta_0 = [10, 10]$, $D_0 = 50$ are shown in black and for $\theta_0 = [1, 1]$, $D_0 = 5000$ in gray. θ_1 are shown dotted and θ_2 are shown solid in the upper plot.

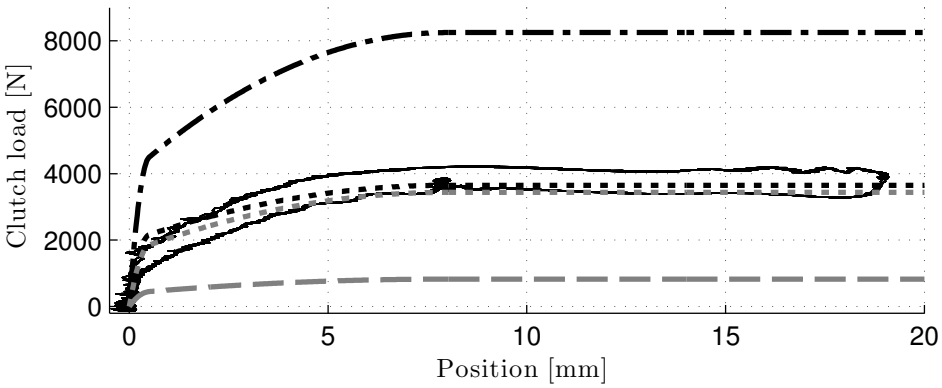

Figure 5.10: Clutch load characteristics, estimated through $A_A(p_A - P_0)$ in solid, dot dashed in black for $\theta_0 = [10, 10]$, $D_0 = 50$ and dashed in gray for $\theta_0 = [1, 1]$, $D_0 = 5000$. The curves with the estimated $\hat{\theta}$ from the reduced-order observer with alternative parameter adaptation at $t = 150$ are dotted in black and gray, respectively.

3. if v and u are persistently exciting (PE) then also $\tilde{m}_A$ and $\tilde{z}$ converge to zero

Proof. The error dynamics are given by

$$\begin{aligned}
\dot{\tilde{y}} =& \tilde{v} - l_y \tilde{y} \\
M\dot{\tilde{v}} =& -\phi^T(y)\theta + \phi^T(\hat{y})\hat{\theta} - (D + l_v)\,\tilde{v} \\
& - \tilde{D}\hat{v} - F\tilde{z} + \frac{A_A R T_0}{V_A(y)}\tilde{m}_A - \frac{A_B R T_0}{V_B(y)}\tilde{m}_B \\
\frac{F}{K_z}\dot{\tilde{z}} =& \tilde{v} - |v|\,\tilde{z} \\
\dot{\tilde{m}}_A =& -a(t)\,\tilde{m}_A - \frac{l_m}{V_A(y)}\tilde{v} \\
\dot{\tilde{m}}_B =& -b(t)\,\tilde{m}_B \\
\dot{\tilde{\theta}} =& \Gamma\phi^T(\hat{y})\tilde{v} \\
\dot{\tilde{D}} =& \gamma_D \hat{v}\tilde{v}
\end{aligned}$$

Stability of the error dynamics can be established using the Lyapunov function candidate

$$\begin{aligned}
W =& \frac{\alpha}{2}\tilde{y}^2 + \frac{M}{2}\tilde{v}^2 + \frac{F^2}{2K_z}\tilde{z}^2 + \frac{1}{2}\Gamma^{-1}\tilde{\theta}^T\tilde{\theta} + \frac{1}{2\gamma_D}\tilde{D}^2 \\
& + \frac{A_A R T_0}{2l_m}\tilde{m}_A^2 + \frac{1}{2Db_0}\left(\frac{A_B R T_0}{V_{B\min}}\right)^2 \tilde{m}_B^2,
\end{aligned} \tag{5.24}$$

where $\inf_y V_B(y) = V_{B\min}$. The time-derivative of W along the trajectories of the error dynamics is

$$\begin{aligned}\dot{W} =&\alpha\tilde{y}\tilde{v} - \alpha l_y\tilde{y}^2 - \phi^T(y)\theta\tilde{v} + \phi^T(\hat{y})\theta\tilde{v} - (D + l_v)\,\tilde{v}^2 \\ &- F\,|v|\,\tilde{z}^2 - \frac{A_A RT_0}{l_m}a(t)\,\tilde{m}_A^2 - \frac{A_B RT_0}{V_B(y)}\tilde{v}\tilde{m}_B - \frac{b(t)}{Db_0}\left(\frac{A_B RT_0}{V_{B\min}}\right)^2\tilde{m}_B^2.\end{aligned}$$

The Mean Value Theorem gives

$$|\phi^T(y) - \phi^T(\hat{y})| \le K|\tilde{y}| \tag{5.25}$$

where $K = \max_{\bar{y}}\left\|\frac{\partial\phi(\bar{y})}{\partial y}\right\|$. Using the bound (5.25), $\theta_{max} \ge \|\theta\|$ and (5.9), we see that $\dot{W}$ satisfies

$$\begin{aligned}\dot{W} \le&\alpha\tilde{y}\tilde{v} - \alpha l_y\tilde{y}^2 + \theta_{max}K|\tilde{y}\tilde{v}| - (D + l_v)\,\tilde{v}^2 - F\,|v|\,\tilde{z}^2 \\ &+ \frac{A_B RT_0}{V_{B\min}}\,|\tilde{v}\tilde{m}_B| - \frac{1}{D}\left(\frac{A_B RT_0}{V_{B\min}}\right)^2\tilde{m}_B^2 - \frac{A_A RT_0}{l_m}a(t)\,\tilde{m}_A^2.\end{aligned}$$

Using Young's inequality

$$xy \le \frac{x^2}{2\varepsilon} + \frac{\varepsilon y^2}{2}$$

with

$$\varepsilon_1 = \frac{A_B RT_0}{DV_{B\min}},$$

and

$$\varepsilon_2 = \frac{K\theta_{max} + \alpha}{l_v},$$

we obtain

$$\frac{A_B RT_0}{V_{B\min}}\,|\tilde{v}\tilde{m}_B| \le \frac{D}{2}\tilde{v}^2 + \frac{1}{2D}\left(\frac{A_B RT_0}{V_{B\min}}\right)^2\tilde{m}_B^2$$

and

$$(K\theta_{max} + \alpha)|\tilde{y}\tilde{v}| \le \frac{l_v}{2}\tilde{v}^2 + \frac{(K\theta_{max} + \alpha)^2}{2l_v}\tilde{y}^2.$$

This gives

$$\begin{aligned}\dot{W} \le&-\frac{D + l_v}{2}\tilde{v}^2 - F|v|\tilde{z}^2 - \frac{1}{2D}\left(\frac{A_B RT_0}{V_{Bmin}}\right)\tilde{m}_B^2 \\ &- \frac{A_A RT_0}{l_m}a(t)\,\tilde{m}_A^2 - \left(-\frac{(K\theta_{max} + \alpha)^2}{2l_v} + \alpha l_y\right)\tilde{y}^2\end{aligned}$$

Since

$$l_y > \frac{(\alpha + K\theta_{max})^2}{2\alpha l_v}$$

this proves stability of the error dynamics. Barbalat's lemma, Khalil (2000), gives that $\tilde{y}$, $\tilde{v}$ and $\tilde{m}_B$ converge to zero. With PE of v it follows by standard arguments that $\dot{W}$ will be negative definite also in $\tilde{z}$, which implies that $\tilde{z}$ converges to zero. PE of u implies that also $\tilde{m}_A$ converges to zero. □

5.4.1 Experimental results

State estimates from the full-order adaptive observer are shown Figure 5.11 with parameter estimates shown in Figure 5.12 and clutch load characteristics in Figure 5.13. The initial condition and the tuning are set just as for the testing of the reduced-order adaptive observer. Significant improvements in velocity and friction, which suffered from noise in the reduced order observer, are shown. As a result of this, also the estimate of the pressure in chamber A is improved, see Table 5.3 for average pressure errors.

Adaptive observer	*Maximum pressure error*	*Average pressure error*
Full-order	45.01 kPa	6.01 kPa
Reduced-order	75.86 kPa	8.44 kPa

Table 5.3: Maximum and average errors for pressure of chamber A for full- and reduced-order adaptive observers, calculated in the time interval $140 \leq t \leq 150$.

5.5 Discussions

Adaptive observer designs for estimation of unmeasured states of the electropneumatic clutch actuator are presented, with adaptation laws for parameter estimations of the clutch load characteristics and the viscous friction force. The state estimation errors are shown to be convergent under PE conditions, and from the experimental results these conditions seem to be fulfilled by a standard clutch position reference sequence. In some cases, such as a cold start of the truck, faster adaptation may be needed due to large temperature gradients. Certainly, this is possible if the clutch is used sufficiently and the piston position reference is changed often enough, i.e. PE of u and v are provided, something which usually will be done when starting to drive. The adaptation gains can also be increased for the first $10 - 20$ gear shifts after a cold start, but care must be taken as testing show that the parameter estimates start to divergence if the gains are set too high.

The full-order adaptive observer which extends the reduced order adaptive observer with a filtered position estimate, shows improvement with respect to noise aspects. The estimated friction dynamic state and pressure in chamber B are in themselves not important, but good estimates of these states are important to obtain accurate estimates of the pressure in chamber A.

The experimental tests validate the adaptive observer designs, and good performances are shown. This may make the adaptive observer designs suitable for state feedback for the switched controllers developed in Chapter 4, and validation of such an adaptive observer-based switched control design is the topic of the next chapter.

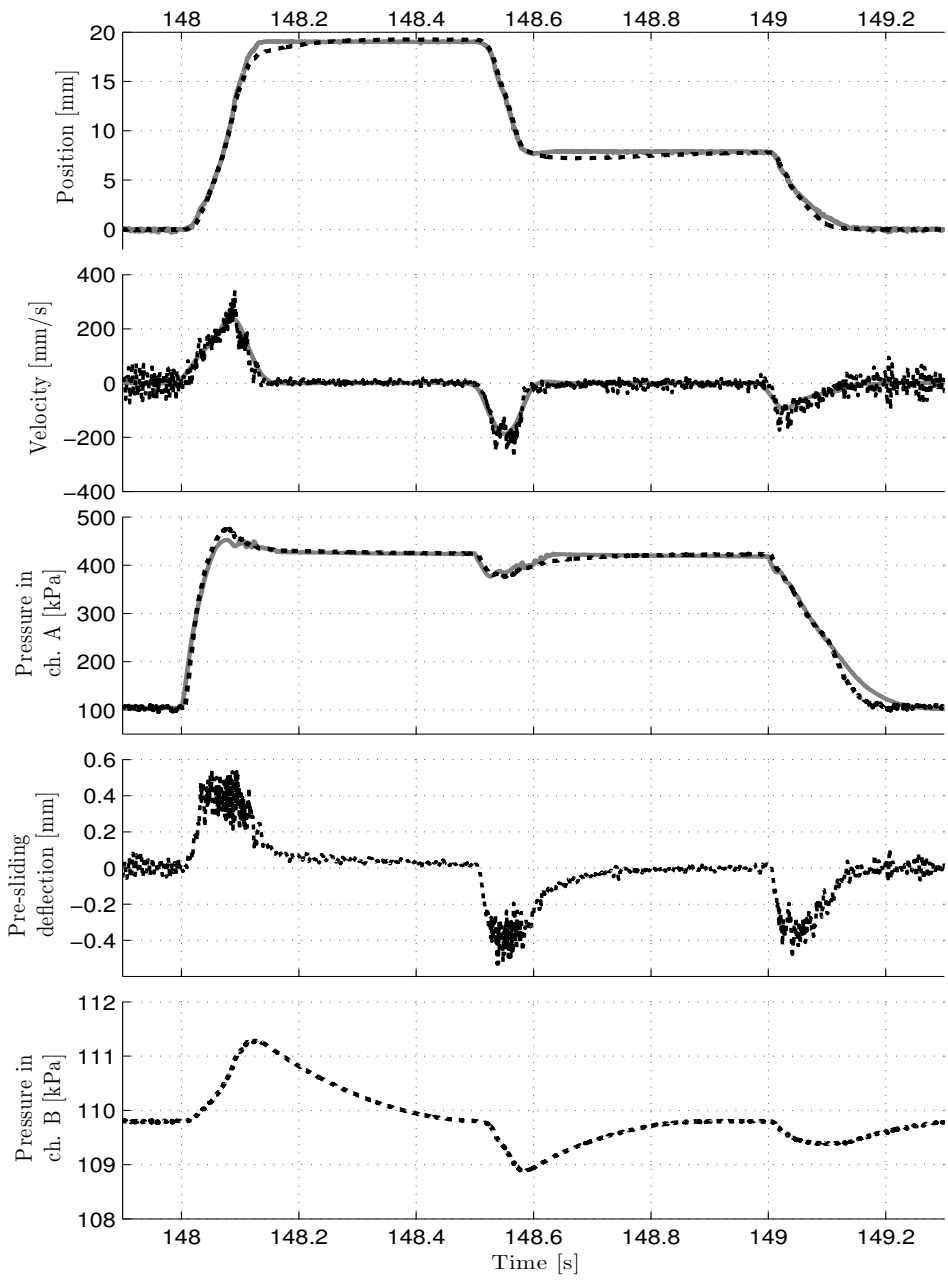

Figure 5.11: Experiments with full-order adaptive observer. The curves show estimates after $t = 148$ where the parameter adaptation has already converged, after about 60 clutch sequences. Observer states are dashed, and measurement from the truck are shown in solid gray. For velocity, the measurement curve is filtered from position measurement.

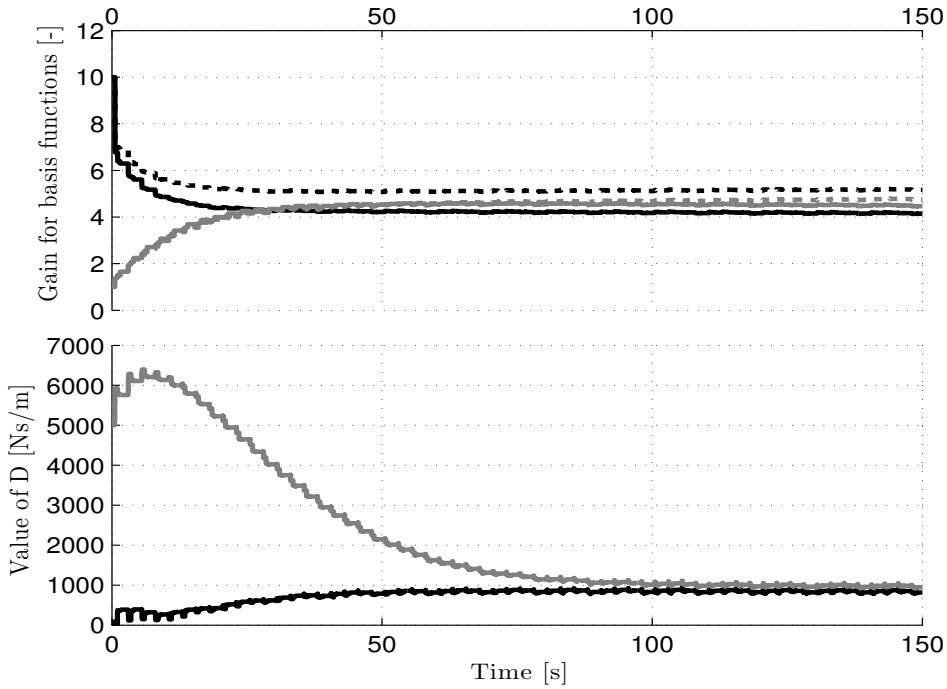

Figure 5.12: Estimated parameters with the full-order adaptive observer during 150 s where 60 clutch sequences are executed. Results for $\theta_0 = [10, 10]$, $D_0 = 50$ are shown in black and for $\theta_0 = [1, 1]$, $D_0 = 5000$ in gray. θ_1 are shown dotted and θ_2 are shown solid in the upper plot.

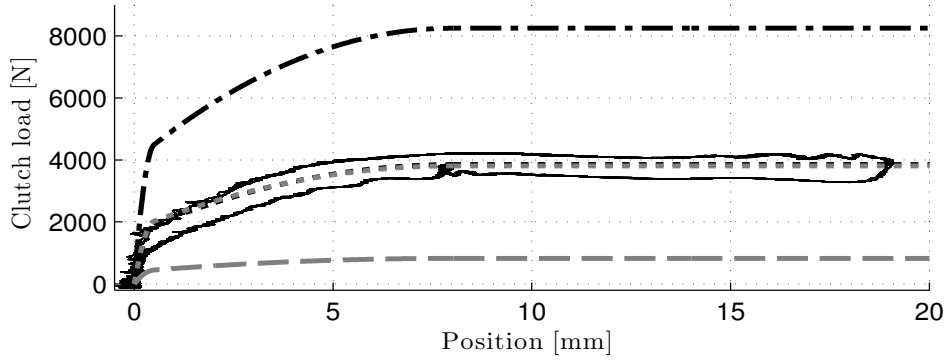

Figure 5.13: Clutch load characteristics, estimated through $A_A(p_A - P_0)$ in solid, dot dashed in black for $\theta_0 = [10, 10]$, $D_0 = 50$ and dashed in gray for $\theta_0 = [1, 1]$, $D_0 = 5000$. The curves with the estimated $\hat{\theta}$ from the full-order adaptive observer at $t = 150$ (overlapping) are dotted in black and gray, respectively.

Chapter 6

Adaptive observer-based switched control

In this chapter we propose a combined design of the dual-mode switched controller from Section 4.4 and the full-order adaptive nonlinear observer design presented in Section 5.4. The focus is on validation of the output feedback with only position sensor, and this is done by simulation.[1] This chapter is mainly based on Langjord et al. (2011b).

6.1 Introduction

In recent years, much work have been done on position control for pneumatic systems with on/off solenoid actuation, but not much is done on observers for such systems, Szabo et al. (2010), even though most proposed controllers require full state feedback. The main objective of the adaptive observer designs in the former chapter was to provide state feedback for control purposes, and particularly for the switched controller designs presented in Chapter 4. In this chapter we combine the previous designs into an adaptive observer-based switched controller validated with simulations, and discuss practical aspects for application to the electropneumatic clutch actuator system.

[1] At the time the adaptive observer design was finalized, experimental testing in the test truck at KA was unfortunately no longer possible. Hence, evaluation of the adaptive observer-based switched control has to be done by constructing and considering realistic simulations.

6.1.1 Simulation model and assumptions for application

The 5th order observer design model (5.5) is also used as a basis for simulation, expressed with chamber pressures instead of masses of air,

$$\dot{y} = v \tag{6.1a}$$

$$\dot{v} = \frac{1}{M}(A_A p_A - A_B p_B - A_0 P_0 - f_l(y) - f_f(v,z)) \tag{6.1b}$$

$$\dot{p}_A = -\frac{A_A v}{V_A(y)} p_A + \frac{RT_0}{V_A(y)} w_v(p_A, u) \tag{6.1c}$$

$$\dot{p}_B = \frac{A_B v}{V_B(y)} p_B + \frac{RT_0}{V_B(y)} w_r(p_B) \tag{6.1d}$$

$$\frac{F}{K_z}\dot{z} = v - |v|z \tag{6.1e}$$

where $f_l = \phi^T(y)\theta$, $f_f = Fz + Dv$ and the flows are given by (3.18) and (3.21). In

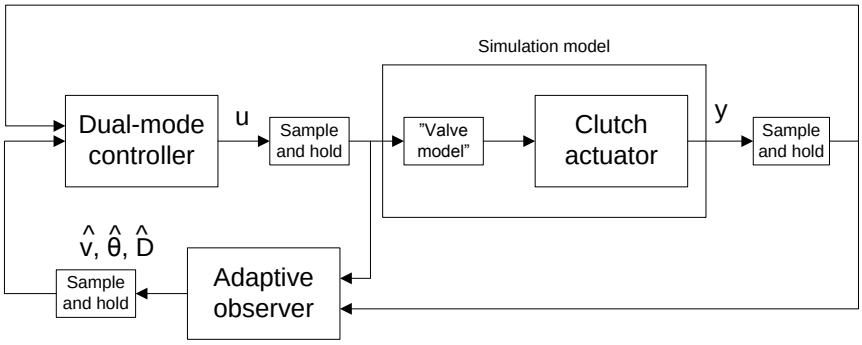

Figure 6.1: Connection of the switched controller and the adaptive observer.

addition a "valve model" is included, which delays the input signals by 2 ms and 3.5 ms which correspond to the average response time of the on/off supply and exhaust solenoid valves, respectively, in the truck set up. This valve model is also added to the observer model. Figure 6.1 gives an overview of how the controller, the clutch actuator and the adaptive observer are connected for simulation. White noise corresponding to that measured in the system, see Figure 2.7 in Section 2.2.4, is added to the position output of the clutch actuator model, to capture the sensor noise present in measurements obtained in the test truck. The sampling rate of the position measurement in the actual truck and in the simulations is 1 ms, and the control signals to the on/off solenoid valves are set at the same rate. The position

from the clutch actuator model, the calculated input signal and the estimated states are therefore generated by a sample-and-hold, to imitate this.

The clutch actuator model and the adaptive nonlinear observer are implemented using explicit Euler discretization,

$$\begin{aligned}
y_k =& y_{k-1} + \Delta t v_{k-1} \\
v_k =& v_{k-1} + \Delta t(-\phi^T(y_{k-1})\theta - Dv_{k-1} \\
& - Fz_{k-1} + A_A p_{A,k-1} - A_B p_{B,k-1} - A_0 P_0) \\
z_k =& z_{k-1} + \Delta t \frac{K_z}{F}(v_{k-1} - |v_{k-1}|z_{k-1}) \\
p_{A,k} =& p_{A,k-1} + \Delta t \left(-\frac{A_A v_{k-1}}{V_A(y_{k-1})} p_{A,k-1} + \frac{RT_0}{V_A(y_{k-1})} w_v(p_{A,k-1}, u_{k-1}) \right) \\
p_{B,k} =& p_{B,k-1} + \Delta t \left(\frac{A_B v_{k-1}}{V_B(y_{k-1})} p_{B,k-1} + \frac{RT_0}{V_B(y_{k-1})} w_r(p_{B,k-1}) \right)
\end{aligned}$$

and

$$\begin{aligned}
\hat{y}_k =& \hat{y}_{k-1} + \Delta t \hat{v} + l_y(y_{k-1} - \hat{y}_{k-1}) \\
\hat{v}_k =& \hat{v}_{k-1} + \frac{\Delta t}{M}\Big(- \phi^T(\hat{y}_{k-1})\hat{\theta}_{k-1} - \hat{D}_{k-1}\hat{v}_{k-1} - F\hat{z}_{k-1} + \frac{A_A RT_0}{V_A(y_{k-1})}\hat{m}_{A,k-1} \\
& - \frac{A_B RT_0}{V_B(y_{k-1})}\hat{m}_{B,k-1} - A_0 P_0 - l_v \hat{v}_{k-1}\Big) + \frac{l_v}{M}(y_k - y_{k-1}) \\
\hat{z}_k =& \hat{z}_{k-1} + \frac{K_z}{F}(\Delta t \hat{v}_{k-1} - \hat{z}_{k-1}|y_k - y_{k-1}|) \\
\hat{m}_{A,k} =& \hat{m}_{A,k-1} + \Delta t\Big(w_v(\hat{p}_{A,k-1}, u_{k-1}) \\
& - \frac{l_m}{V_A(y_{k-1})}\hat{v}_{k-1}\Big) + \frac{l_m}{V_A(y_{k-1})}(y_k - y_{k-1}) \\
\hat{m}_{B,k} =& \hat{m}_{B,k-1} + \Delta t w_r(\hat{p}_{B,k-1}) \\
\hat{\theta}_k =& \hat{\theta}_{k-1} + \Delta t \Gamma \phi(y_{k-1})\hat{v}_{k-1} - \Gamma\phi(y_{k-1})(y_k - y_{k-1}) \\
\hat{D}_k =& \hat{D}_{k-1} + \Delta t \gamma_D \hat{v}_{k-1}^2 - \gamma_D \hat{v}_{k-1}(y_k - y_{k-1})
\end{aligned}$$

where the Euler integration step, Δt, is set to 0.1 ms. Parameters are given in Table 6.1. The simulation model, including the valve delay, is validated against experimental data from the test truck, see Figure 6.2, and is shown to capture the main behavior of the clutch actuator. The performance of the combined system is tested against the same clutch reference, see Figure 2.5, as the experimental tests, and the controller is switched off whenever the steady state requirement is fulfilled. The observer and adaptation gains have been set based on the tuning in Chapter 5, see Table 5.2. The gain Γ is set 30 times higher in the region $3 - 6$ mm as the clutch load characteristic is especially important in this area due to its steep curve, and since this region is visited only for short transient periods with a typical clutch sequence. The adaptation is switched off whenever the position is not changing, due to lack of PE which might lead to drift or divergence of the estimates.

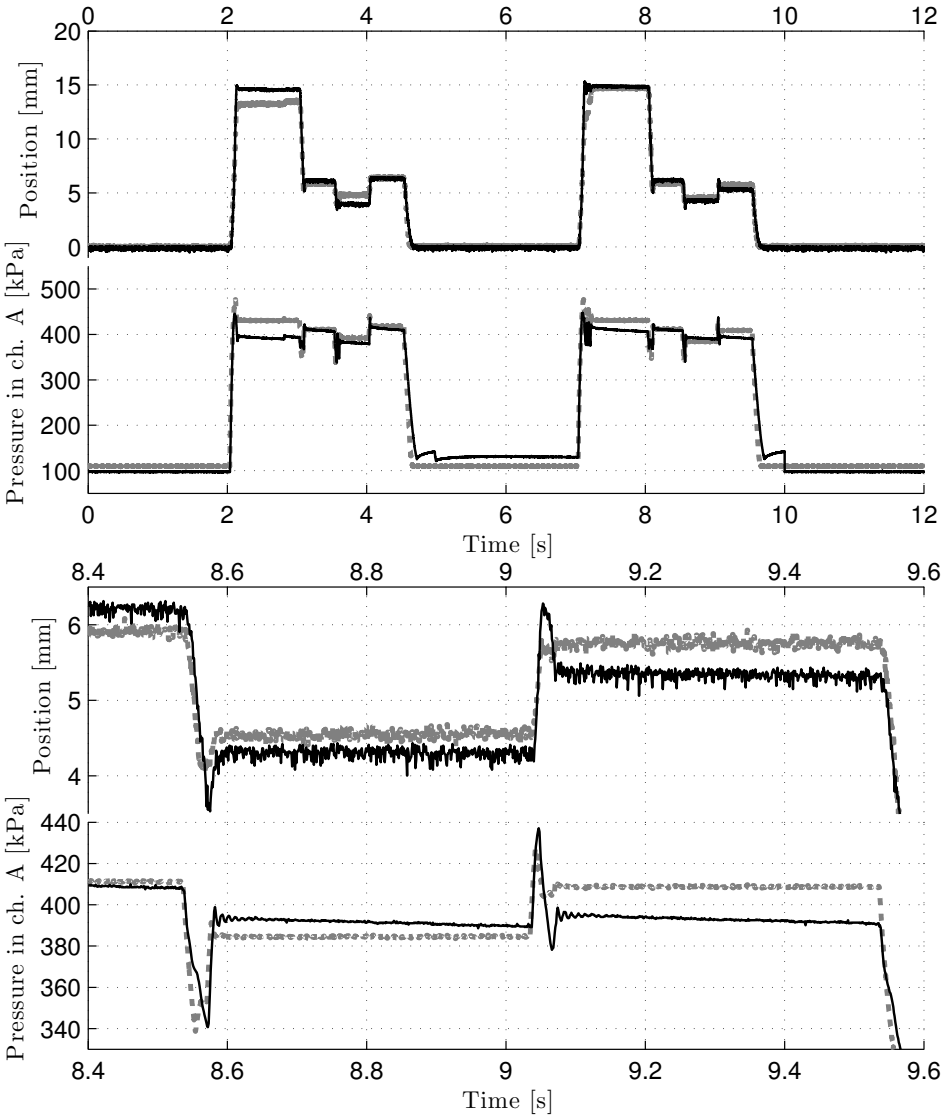

Figure 6.2: Experimental measurements from truck (solid) and results from the simulation model (dashed in gray).

Parameter	*Notation*	*Value*	*Unit*
Mass	M	10	kg
Area of chamber A	A_A	$12.3 \cdot 10^{-3}$	m^2
Area of chamber B	A_B	$11.848 \cdot 10^{-3}$	m^2
Area of piston rod	A_0	$4.52 \cdot 10^{-4}$	m^2
Ambient pressure	P_0	$1 \cdot 10^5$	Pa
Supply pressure	P_S	$9.5 \cdot 10^5$	Pa
Temperature	T_0	293	K
Gas constant of air	R	288	J/kgK
Volume in chamber A at y=0	$V_{A,0}$	$0.148 \cdot 10^{-3}$	m^3
Volume in chamber B at y=0	$V_{B,0}$	0.012	m^3
Viscous damping	D_v	2500	Ns/m
Asperity stiffness	K_z	$1 \cdot 10^6$	N/m
Coulomb friction	F	200	N
Density	ρ_0	1.185	$\mathrm{kg/m}^3$
Conductance of outlet restriction	C_r	$5 \cdot 10^{-8}$	$\mathrm{m}^4\mathrm{s/kg}$
Weighting parameter vector for clutch load ch.	θ	$[3, 6]$	–
Conductance for supply valve	C_s	$17 \cdot 10^{-9}$	$\mathrm{m}^4\mathrm{s/kg}$
Conductance for exhaust vavle	C_e	$32.5 \cdot 10^{-9}$	$\mathrm{m}^4\mathrm{s/kg}$

Table 6.1: Model parameters used in the simulations in this chapter.

Remark 6.1.1. *The controller is implemented with the estimated states $\hat{v}$ and $\hat{p_A}$, and with $\hat{\theta}$ and $\hat{D}$, as illustrated in Figure 6.1. The stability result of the switched controllers holds if the true states and parameters are used for feedback, while we are actually violating this assumption by using estimated states and parameters. Since no general nonlinear system separation principle holds, the stability and the performance are evaluated using simulations.*

6.2 Simulation results

In this section we consider both simulation of the observer-based switched controller, and simulation where the pressure is obtained from the simulation model representing the actual system. This is done for comparison of the performance of the pressure estimate obtained from the observer against the estimate of the actual pressure measurement.

6.2.1 Performance of observer-based switched controller

Figure 6.3 shows simulation results for the dual-mode switched controller combined with full-order adaptive observer with nominal values of the clutch load characteristics and the viscous friction, $\theta_0 = [3, 6]$ and $D_0 = 2500$. The controller makes the piston position meet the requirements, without too much unnecessary switching which could induce chattering, see Figure 6.4. Noise leads to a bias in the estimated value of D, shown in Figure 6.5, while the clutch load characteristic

parameters stay at their nominal values. In Figure 6.6 simulation results with $\theta_0 = [5, 9]$ and $D_0 = 4500$ are shown. It is clear that the controller combined with the observer still manages to meet the requirements. Figure 6.8 shows that the estimated parameters converge, but not exactly to their nominal values. The total force of the clutch load and the friction force, on the other hand, converges to the same value for both simulations with parameter adaptation. This is in agreement with the analyses in the previous chapter which proves that PE may be needed for parameters and certain states to converge, (in particular p_A). These simulation results show that the dual-mode switched controller has good robustness properties, performing well with measurement noise affecting the state feedback signal.

6.2.2 Performance of switched controller with pressure measurement

Simulations with the dual-mode switched controller and

- position from the simulation model including noise
- velocity filtrated from position
- pressure from the simulation model including noise

have been conducted for comparison and results are shown in Figure 6.9. The performance is similar to that shown in Figure 6.3, see Figure 6.10 and Table 6.2 which compares position results in more detail. Given that the simulation model captures the real system well enough, we can state that exchanging the pressure sensor with an observer does not result in any loss of performance.

Simulations with exactly the same state feedback sensors, filtering, and controller configuration, as the experimental tests shown in Section 4.5, have also been conducted. Comparing these results we get that they are quite similar, with a bit less chattering in the simulated results. This was expected as additional noise and disturbances are expected be present in the truck due to motor vibration etc., and there may also be other unmodeled phenomena. The similarity in performance confirms that the simulation model captures the main behavior of the actual system.

Pressure from	*Position error*	*Pressure error*	*Input switches*	*Controller switches*
Observer	0.963 mm	14.03 kPa	247	2163
Measurement	0.976 mm	95.86 kPa	242	2164

Table 6.2: Performance parameters for simulations with pressure obtained from observer and measurement estimates. The position and pressure errors are average absolute values.

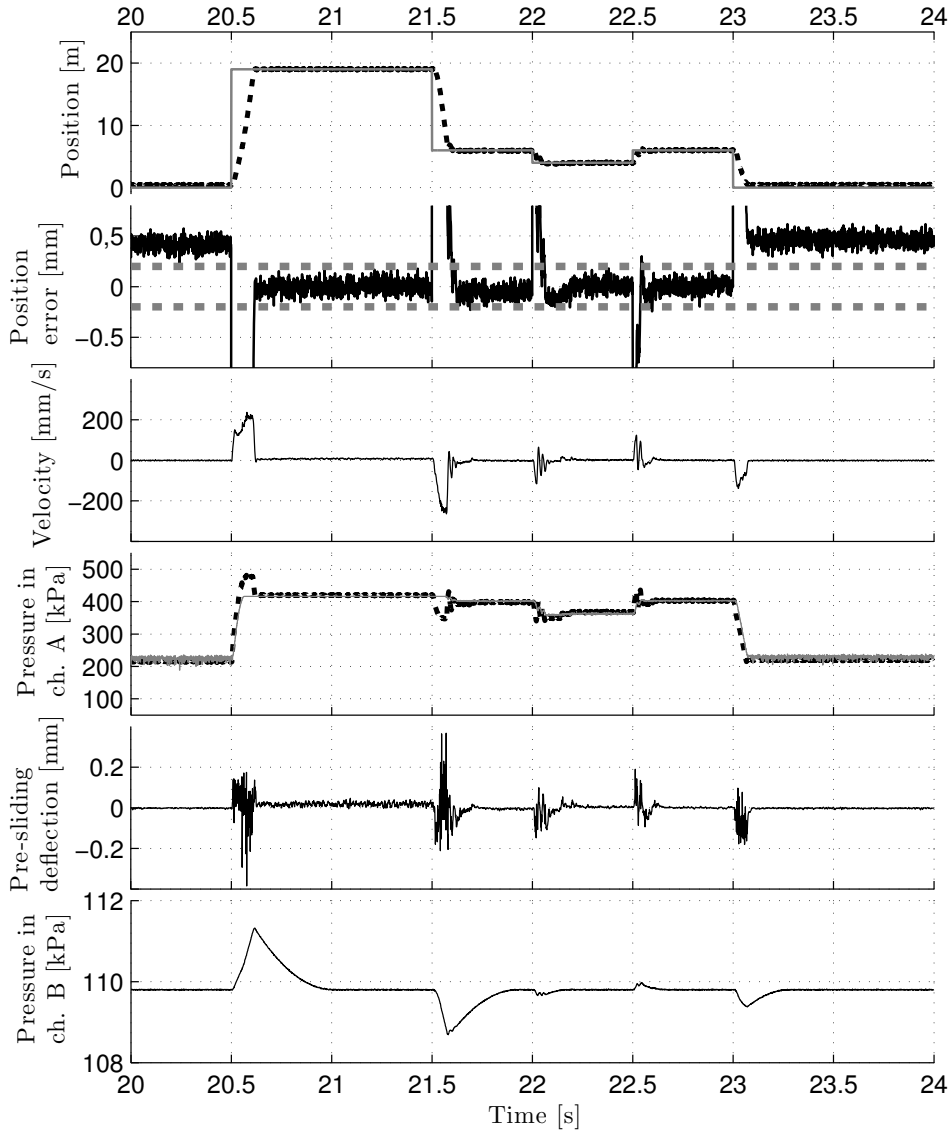

Figure 6.3: Simulations of dual-mode controller and full-order adaptive observer with nominal values $\theta_0 = [3, 6]$ and $D_0 = 2500$. For position, the simulated state (dashed) and the reference (solid) are shown, and for pressure in chamber A, the estimated reference (solid) and the observer state (dashed) are shown.

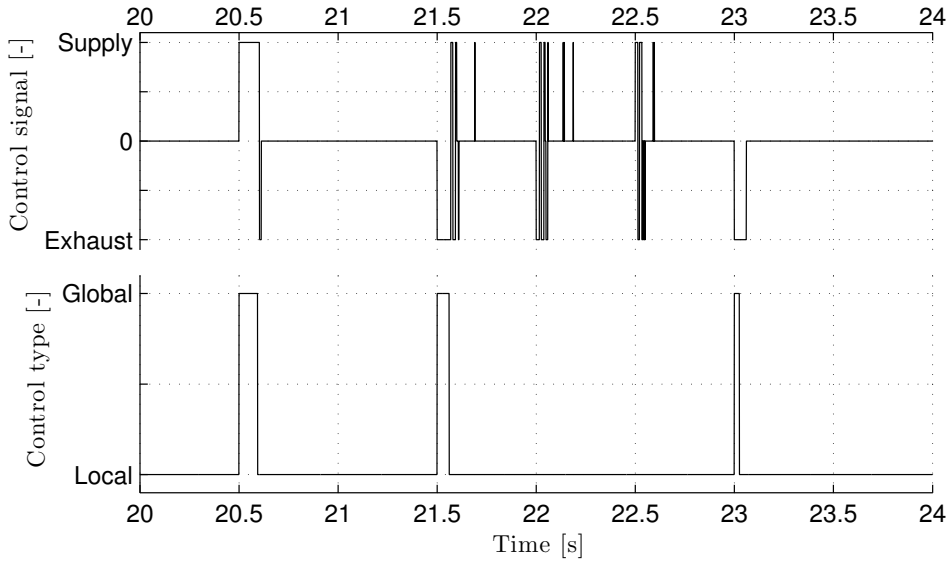

Figure 6.4: Controller signal and controller used in the simulations of dual-mode controller and full-order adaptive observer with nominal values $\theta_0 = [3, 6]$ and $D_0 = 2500$.

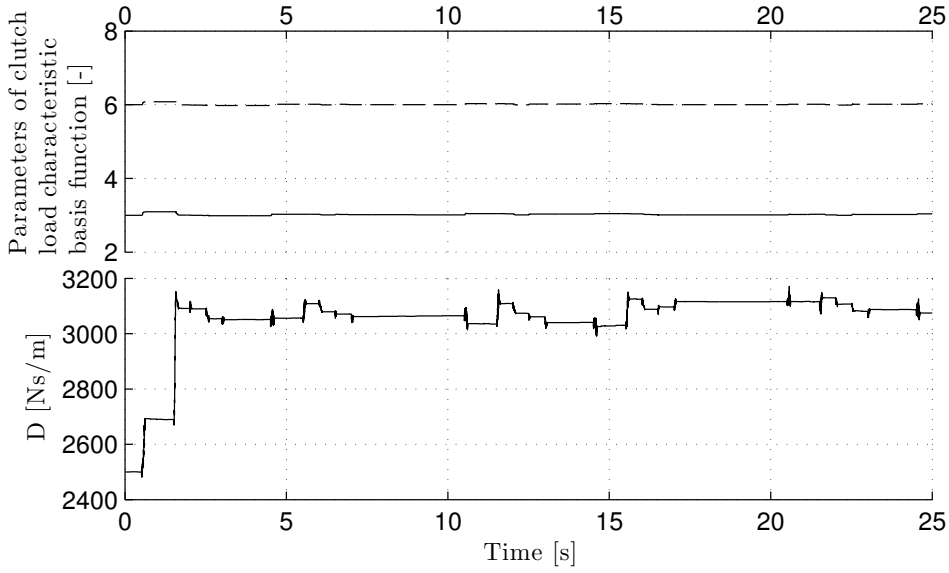

Figure 6.5: Estimated parameters of the simulations of dual-mode controller and full-order adaptive observer with nominal values $\theta_0 = [3, 6]$ and $D_0 = 2500$.

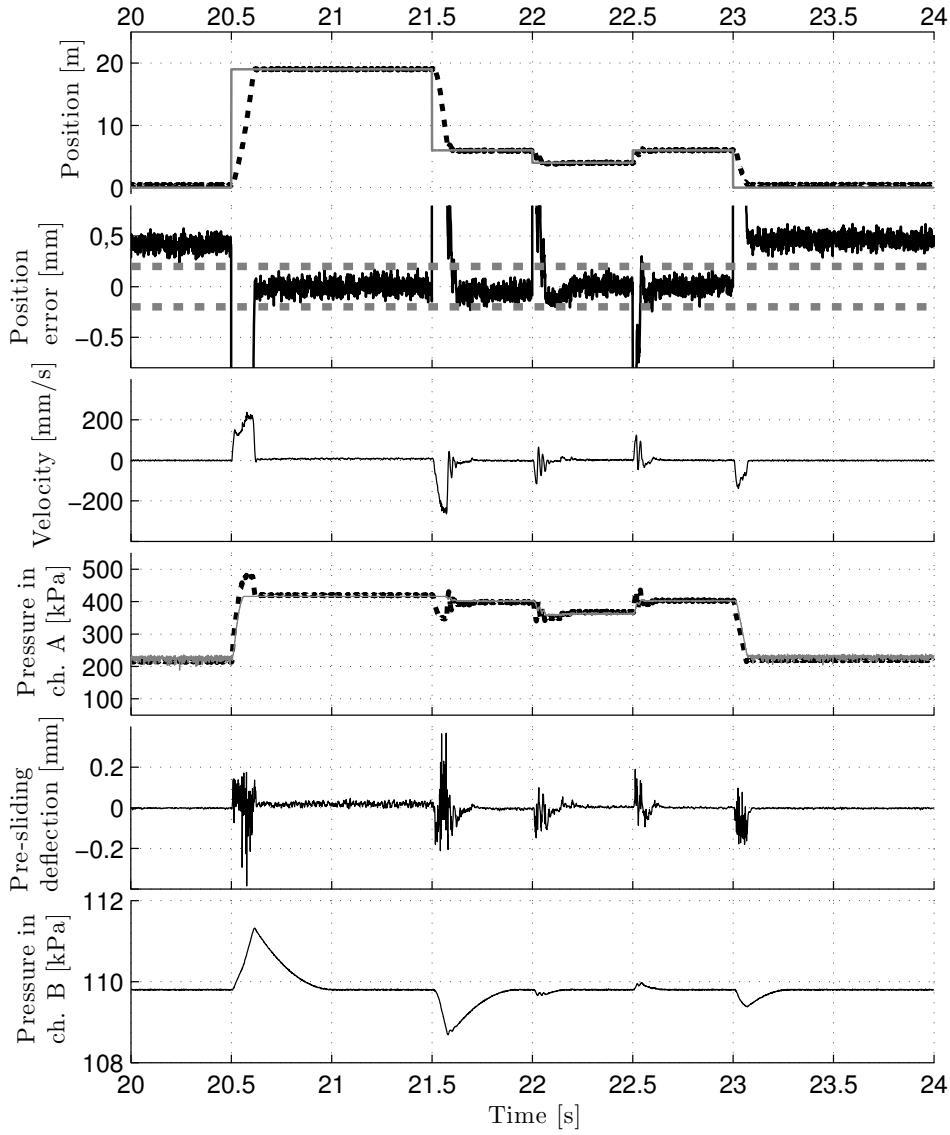

Figure 6.6: Simulations of dual-mode controller and full-order observer with $\theta_0 = [5, 9]$ and $D_0 = 4500$. For position, the simulated state (dashed) and the reference (solid) are shown, and for pressure in ch. A, the estimated reference (solid) and the observer state (dashed) are shown.

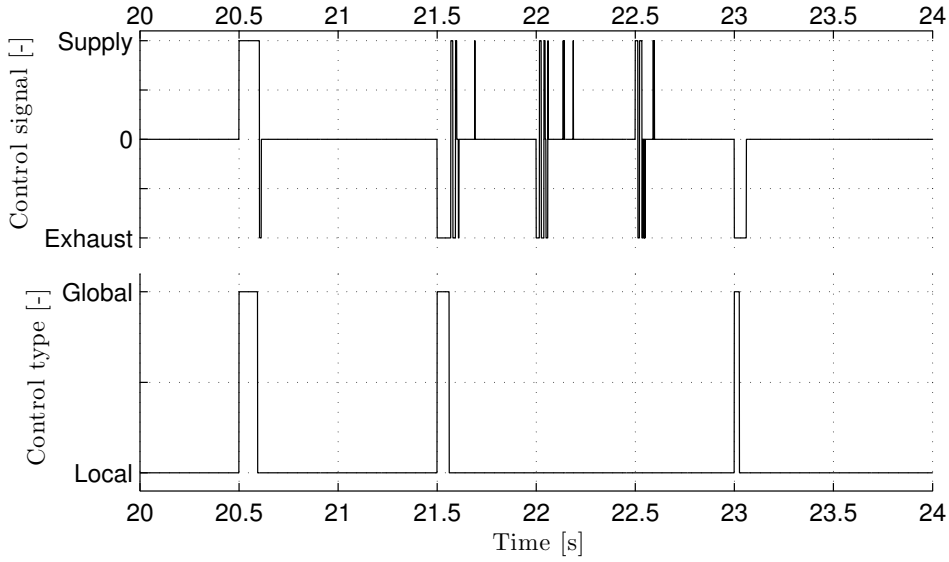

Figure 6.7: Controller signal and controller used in the simulations of dual-mode controller and full-order adaptive observer with nominal values $\theta_0 = [5, 9]$ and $D_0 = 4500$.

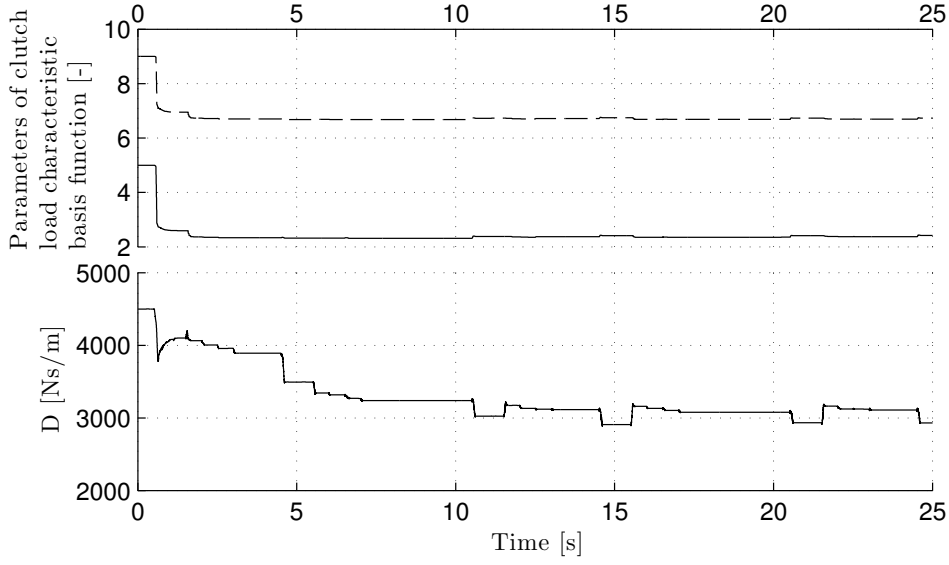

Figure 6.8: Estimated parameters of the simulations of dual-mode controller and full-order adaptive observer with nominal values $\theta_0 = [5, 9]$ and $D_0 = 4500$.

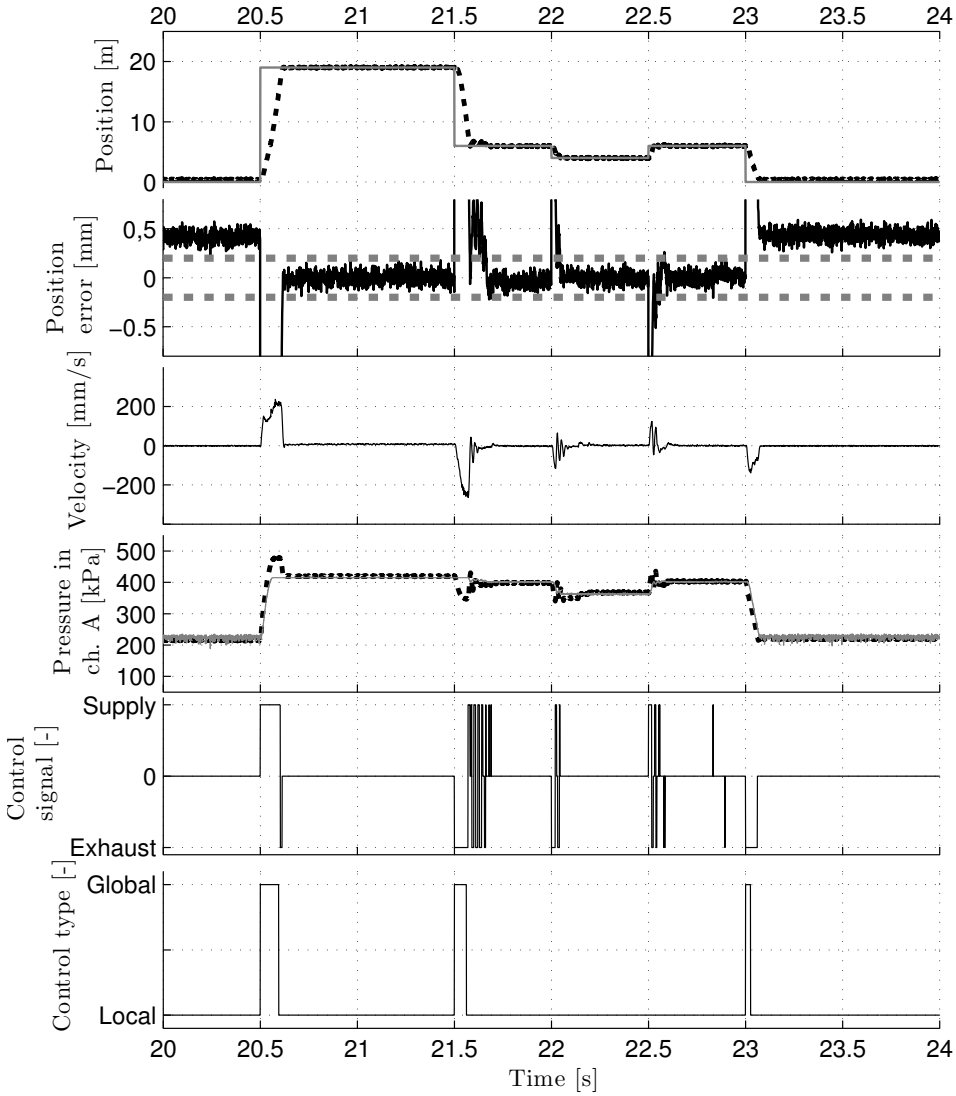

Figure 6.9: Simulations of controller with feedback from pressure measurement. For position simulated state (dashed) and reference (solid) are shown, and for pressure in ch. A solid estimated reference (solid) and observer state (dashed).

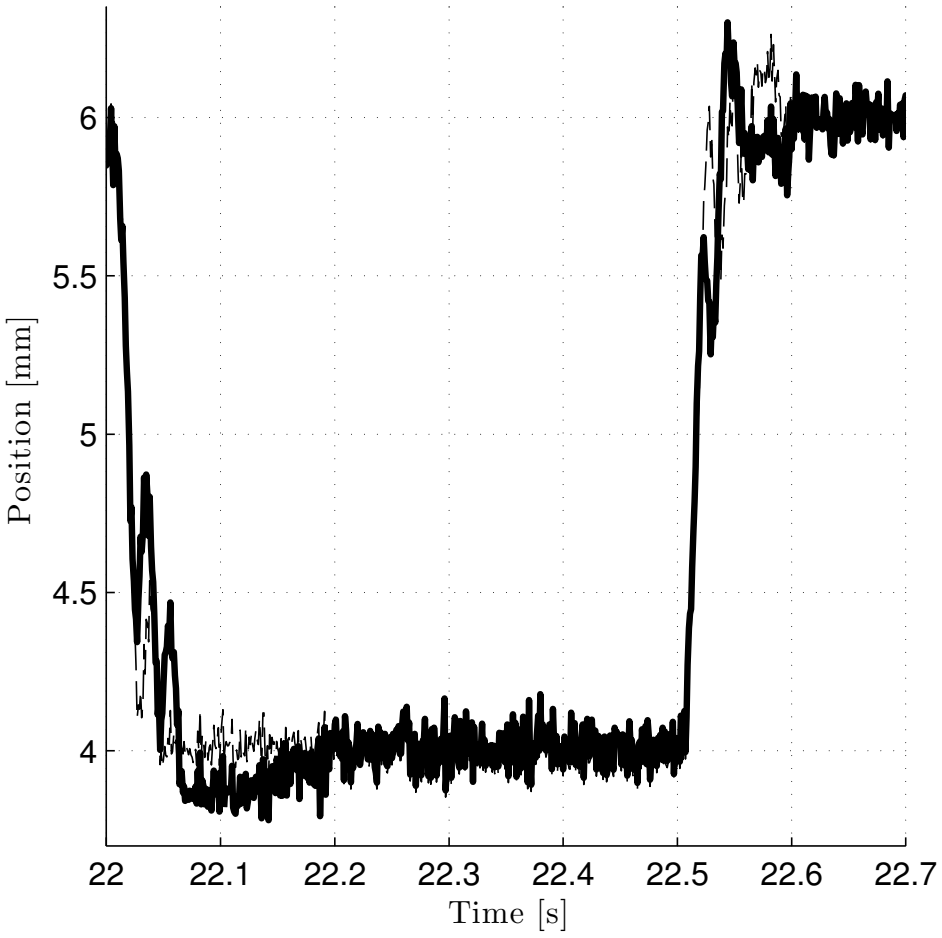

Figure 6.10: Segment of the resulting position for simulations of the controller with pressure feedback from measurement in dashed and from observer in solid.

6.3 Discussions

It is well know that combining individually designed observers and controllers are not straightforward from a theoretical point of view. The stability proofs of the controllers are no longer valid, as estimates from the observer are employed rather than true measurement which was assumed in the controller analysis. Still, no theoretical stability analysis of the combined system is included in this chapter. The focus was set on validation by simulations, as the developed observer-based switched controller is intended for use in physical systems and the performance in the actual system may be more interesting than the theoretical performance analysis.

Position control for an electropneumatic clutch actuator is considered, using the dual-mode switched controller design and utilizing the full-order adaptive nonlinear observer. Tests using the validated simulation model show that the combined design makes the piston position follow the position reference with sufficient precision, even when starting with large offsets in friction and clutch load characteristics in the observer model. The simulations indicate that the pressure sensor can be eliminated by an adaptive nonlinear observer used as a basis for a nonlinear state feedback control design, and that similar accuracy as in the experimental results in Section 4.5 might be possible to achieve also without a pressure sensor.

Chapter 7

Conclusions

7.1 Conclusions

The thesis focus on position control of an electropneumatic clutch actuator for heavy duty trucks. This has been achieved by developing appropriate switched controllers and adaptive nonlinear observers for applications to the clutch actuator system.

The mechanical configuration of the clutch actuator system greatly influences how the control task is approached. Some design choices, such as the reduction of the dead volume, hence reducing the effect of hysteresis in the actuator, are taken to simplify the control task. But most design choices are motivated primarily by cost, such as the choice of on/off solenoid valves and the choice to only provide a position sensor in the finalized production system. The decision on on/off solenoid valves makes switched controllers an appealing control strategy.

The main contribution in Chapter 4 is the dual-mode switched controller, combining the two switched controllers designed based on appropriate Control Lyapunov functions. Experimental testing shows that the controllers are well suited for application to the electropneumatic clutch actuator system. A strength of these switched controllers is that they are robust to noise. The feedback signals, which may be corrupted by noise, are for the switched controllers only used to decide on one of the inputs available for the system. Another quality of the switched controllers are their simple designs. Combined with an adaptive observer, the controllers can be applied to clutch actuator system without knowledge on the detailed response and capacity of the on/off solenoid valves, and the degree of wear for the clutch compression springs.

The full-order adaptive observer presented in Chapter 5 produces estimates of the unmeasured states and calculates parameters for clutch load characteristics and viscous friction. Stability and boundness of the state estimates are proved under PE conditions of the input and the velocity signals. The experimental testing indicates that the PE conditions are met under typical clutch sequences, and convergence of the state estimates are shown. The pressure in chamber B seems to have little effect on the dynamics of the rest of the system, and could have been

neglected to simplify the design. It was shown in robustness tests of the switched controllers, considering errors in the clutch load characteristics, that performance of the controllers diminish rapidly with the presence of such model errors. The parameter estimation provided by the proposed adaptive observer will therefore be an essential contribution for robust performance of the clutch actuator system to account for wear and variations in temperature.

The combination of the two main contributions into an adaptive observer-based switched controller for position control of the actuator piston is treated in Chapter 6. Simulation results indicate that the measurement from a pressure sensor can be replaced by the estimate from the nonlinear adaptive observer without loss of accuracy. A simple valve dynamic have been included in the simulation model used in this chapter to represent the clutch actuator system. By comparison of the position and the pressure estimates obtained from this simulation model and actual truck measurements, it is shown that the simulation model captures the main behavior of the clutch actuator system.

7.2 Recommendations for future work

The proposed adaptive observer-based switched controller shows promising performance from simulations. Experimental tests with this controller employed in the eletropneumatic clutch actuator in a heavy duty truck is clearly the most important topic for future work.

The work in this thesis has focused on showing that the idea of using switched controllers, is appealing for the clutch actuator system with on/off valves. For application, future adjustment will have to be done. For instance, too much focus has been on response time, and too little on avoiding overshoots. Such aspects must be considered to obtain a robust design for use in a production system.

The parameterization of the clutch load used is very simple, and improvement to this parameterization should be considered. Including method to account for the curve shifting left/right, such as a Multiple Model Scheme, will make the design more adaptable to different clutches with different degree of wear.

To make the control design more independent of the mechanical structure of the clutch actuator system, the valve dynamics could be taken into account in a rigorous way. This would make it easier to tune the controller when valvesets are changed.

The observer design can be further improved by using $\hat{v}$ instead of $\dot{y}$. This is likely to improve the observer performance as noise is no longer amplified through the differentiation of the position measurement.

Bibliography

Ahn, K., Yokota, S., 2005. Intelligent switching control of pneumatic actuator using on/off solenoid valves. Mechatronics 15, 683–702.

Ali, H. I., Noor, S. B. B. M., Bashi, S. M., Marhaban, H., 2009. A review of pneumatic actuators (modeling and control). Australian Journal of Basic and Applied Science 3, 440–454.

Andersson, S., Söderberg, A., Björklund, S., 2007. Friction models for sliding dry, boundary and mixed lubricated contacts. Tribology International 40, 580–587.

Bakkeheim, J., Johansen, T. A., 2006. Transient performance, estimatior resetting and filtering innonlinear multiple model adaptive backstepping control. IEE Proceedings - Control Theory & Applications 153, 536–545.

Bastin, G., Gevers, M. R., 1988. Stable adaptive observers for nonlinear time-varying systems. IEEE Transactions on Automatic Control 33, 650–658.

Bemporad, A., Borelli, F., Glielmo, L., Vasca, F., 2001. Hybrid control of dry clutch engagement. In: Proceedings of the European Control Conference, Porto, Portugal.

Besancon, G., 2000. Remarks on nonlinear adaptive observer design. Systems & Control Letters 41, 271–280.

Besancon, G. (Ed.), 2007. Nonlinear Observers and Applications. Lecture Notes in Control and Information Science 363. Springer-Verlag.

Bigras, P., Khayati, K., 2002. Nonlinear observer for pneumatic system with non negligble connection port restriction. In: Proceedings of the 21th American Control Conference. Anchorage, AK.

Bobrow, J. E., McDonell, B. W., 1998. Modeling, identification, and control of a pneumatically actuated, force controllable robot. IEEE Transaction on Robotics and Automation 14, 732–742.

Canudas de Wit, C., Olsson, H., ström, K., Lischinsky, P., 1995. A new model for control of systems with friction. IEEE Transactions on Automatic Control 40, 419–425.

Carducci, G., Foglia, M., Gentile, A., Giannoccaro, N. I., Messina, A., 2004. Pneumatic robotic arm controlled by on-off valves for automatic harvesting based on vision localisation. In: IEEE International Conference on Industrial Technology. Vol. 2. pp. 1017–1022.

Cho, Y. M., Rajamani, R., 1997. A systematic approach to adaptive observer synthesis for nonlinear systems. IEEE Transaction on Automatic Control 4, 534–537.

Egeland, O., Gravdahl, J. T., 2002. Modeling and Simulation for Automatic Control. Marine Cybernetics.

Filippov, A. F., 1960. Differential equations with discontinuous rigth-hand sides. Am. Math. Soc. Transl. 42, 199–231.

Filippov, A. F., 1979. Differential equations with second member discontinuous on intersection surface. Diff. Eq. 15, 1292–1299.

Gentile, A., Giannoccaro, N. I., Reina, G., 2002. Experimental tests on position control of a pneumatic actuator using on/off solenoid valves. In: IEEE ICIT'02. Bangkok, Thailand.

Girin, A., Plestana, F., Brun, X., Glumineau, A., 2009. High-order sliding-mode controllers of an electropneumatic actuator: Application to a aeronautic benchmark. IEEE Transactions on Control System Technology 17 (3), 663–645.

Gjone, K., 2007. Robustness tests and analysis of control strategies on an electropneumatic actuator. Master's thesis, Norwegian Univeristy of Science and Technology.

Glielmo, L., Iannelli, L., Vacca, V., Vasca, F., 2006. Gearshift control for automated manual transmissions. IEEE/ASME Transactions on Mechatronics 11, 17–26.

Grancharova, A., Johansen, T., 2009a. Explicit approximate model predictive control of constrained nonlinear systems with quantized inputs. In: Mangi, L., Raimondo, D., Allgower, F. (Eds.), Assessment and Future Directions of Nonlinear Model Predictive Control. Springer Lecture Notes in Control and Information Science. Springer Verlag.

Grancharova, A., Johansen, T. A., 2009b. Explicit model predictive control of an electropneumtaic clutch actuator using on/off valves and pulse-width modulation. In: Proceedings of the European Control Conference. Budapest, Hungary.

Grancharova, A., Johansen, T. A., 2010. Design and comparison of explicit model predictive controllers for an electropneumatic clutch actuator using on/off valves. IEEE/ASME Transactions on Mechatronics.

Gulati, N., Barth, E. J., 2005. Non-linear pressure observer design for pneumatic actuators. In: Proceedings of the 2005 IEEE/ASME International Conference on Advanced Intelligent Mechatronics. Monterey, CA.

Gulati, N., Barth, E. J., 2009. A globally stable load-independent pressure observer for the servo control of pneumatic actuators. IEEE/ASME Transactions on Mechatronics 14, 295–306.

Håkansson, K., Johansson, M., 2007. Modeling and control of an electro-pneumatic actuator system using on/off valves. Master's thesis, Linkping university.

Helgeland, E., 2008. Sliding mode control of an electro-pneumatic clutch actuator. Master's thesis, Norwegian Univeristy of Science and Technology.

Horn, J., Bamberger, J., Michau, P., Pindl, S., 2003. Flatness-based clutch control for automated manual transmissions. Control Engineering Practice 11, 1353–1359,

Ioannou, P., Sun, J., 1996. Robust Adaptive Control. Prentice Hall, Inc.

ISO, 1989. ISO 6358 - Pneumatic Fluid Power - Components Using Compressible Fluids - Determination of Flow-Rate Characterictics. ISO-International Organization for Standardization, 1st Edition.

Kaasa, G. O., 2006. Nonlinear output-feedback control applied to electro-pneumatic clutch actuation in heavy-duty trucks. Ph.D. thesis, Norwegian Univeristy of Science and Technology.

Khalil, H. K., 2000. Nonlinear Systems. Prentice Hall, Upper Saddle River, New Jersey.

Kimoto, M., Iti, H., 2003. Nonlinear robust compensation for control of a pneumatic actuator. In: SICE Annual Conference in Fukui.

Knudsen, K. A., 2005. Nonlinear obseerver design for electropneumatic clutch actuators. Master's thesis, Norwegian Univeristy of Science and Technology.

Kristic, M., Kanellakopoulos, I., Kokotovic, P., 1995. Nonlinear and Adaptive Control Design. Wiley Interscience.

Kuroiwa, H., Ozaki, N., Okada, T., Yamasaki, M., 2004. Next-generation fuel-efficient automated manual transmission. Hitachi Review 53, 205–209.

Langjord, H., Johansen, T. A., 2010. Dual-mode switched control of an electropneumatic clutch actuator. IEEE/ASME Transaction on Mechatronics 15, 969–981.

Langjord, H., Johansen, T. A., Bratli, C., 2009. Dual-mode switched control of an electropneumatic clutch actuator with input restrictions. In: Proceedings of the European Control Conference. Budapest, Hungary.

Langjord, H., Johansen, T. A., Hespanha, J. P., 2008a. Switched control of an electropneumatic clutch actuator using on/off valves. In: Proceedings of the 27th American Control Conference. Seattle, WA.

Langjord, H., Johansen, T. A., Snare, S. R., Bratli, C., 2008b. Estimation of electropneumatic clutch actuator load characteristics. In: Proceedings of the 17th IFAC World Congress. Seoul, Korea.

Langjord, H., Kaasa, G. O., Johansen, T. A., 2010. Nonlinear observer and parameter estimation for electropneumatic clutch actuator. In: Proceedings of the 8th IFAC Symposium on Nonlinear Control Systems. Bologna, Italy.

Langjord, H., Kaasa, G. O., Johansen, T. A., 2011a. Adaptive nonlinear observer for electropneumatic clutch actuator with position sensor. To appear, as a brief paper, in IEEE Transaction on Control Systems Technology.

Langjord, H., Kaasa, G. O., Johansen, T. A., 2011b. Adaptive observer-based switched controller for electropneumatic clutch actuator with position sensor. In: Submitted to: IFAC World Congress. Milan, Italy.

Lee, D. S., Kim, M. G., Kim, H. K., Youn, M. J., 1991. Controller design of multivariable variable structure systems with nonlinear switching surfaces. Control Theory and Applications, IEEE Proceedings D 138, 493–499.

Li, Z. G., Wen, C. Y., Soh, Y. C., 2001. Switched controllers and their applications in bilinear systems. Automatica 37, 447–481.

Løkken, K., 2006. Adaptive backstepping with application with electro-pneumatic clutch actuators. Master's thesis, Norwegian Univeristy of Science and Technology.

Lucente, G., Montanari, M., Rossi, C., 2007. Modelling of an automated manual transmission system. Mechatronics 17, 73–91,

Lyshevski, S. E., 2000. Sliding mode and soft switching control in dynamic systems. In: Proceedings of the 19th American Control Conference. Chicago, IL.

Marino, R., 1990. Adaptive observers for single output nonlinear systems. IEEE Transactions on Automatic Control 35, 1054–1058.

Marino, R., Tomei, P., 1992. Global adaptive observers for nonlinear systems via filtered transformations. IEEE Transactions on Automatic Control 37, 1239–1245.

Marino, R., Tomei, P., 1995. Adaptive observers with arbitrary exponential rate of convergence for nonlinear systems. IEEE Transactions on Automatic Control 40, 1300–1304.

Messina, A., Giannoccaro, N. I., Gentile, A., 2005. Experimenting and modelling the dynamics of pneumatic actuators controlled by the pulse width modulation (pwm) technique. Mechatronics 15, 859–881.

Montanari, M., Ronchi, F., Rossi, C., Tilli, A., Tonielli, A., 2004. Control and performance evaluation of a clutch servo system with hydraulic actuation. Control Engineering Practice 12, 1369–1379,

Narendra, K. S., George, K., 2002. Adaptive control of simple nonlinear systems using multiple models. In: Proceedings of the 21th American Control Conference. Anchorage, AK, pp. 1779–1784.

Nguyen, T., Leavitt, J., Jabbari, F., Bobrow, J. E., 2007. Accurate sliding-mode control of pneumatic systems using low-cost solenoid valves. IEEE/ASME Transactions on Mechatronics 12, 216–219.

Pandian, S. R., Takemura, F., Hayakawa, Y., Kawamura, S., 2002. Pressure observer-controller design for pneumatic cylinder actuators. IEEE/ASME Transaction on Mechatronics 7, 490–499.

Paul, A. K., Mishra, J. K., Radke, M. G., 1994. Reduced order sliding mode control for pneumatic actuator. IEEE Transactions on Control Systems Technology 2, 271–276.

Rajamani, R., Hedrick, K., 1995. Adaptive observer for active automotive suspensions: Theory and experiment. IEEE Transactions on Control Systems Technology 3, 86–93.

Rao, Z., Bone, G. M., 2008. Nonlinear modelling and control of servo pneumatic actuators. IEEE Transaction on Control System Technology 16, 562–569.

Sande, H., Johansen, T. A., Kaasa, G. O., Snare, S. R., Bratli, C., 2007. Switched backstepping control of an electropneumatic clutch actuator using on/off valves. In: Proceedings of the 26th American Control Conference. New York, pp. 76–81.

Sekhavat, P., Wu, Q., Sepehri, N., 2005. Impact control in hydraulic actuators. Journal of Dynamic Systems, Measurement and Control 127, 197–205.

Shen, X., Zhang, J., Barth, E. J., Goldfarb, M., 2004. Nonlinear averaging applied to the control of pulse width modulated (pwm) pneumatic systems. In: Proceedings of the 23th American Control Conference. Boston, MA.

Shimazu, T., Yanagihara, S., Tanaka, H., 1986. Directly control pneumatic clutch for heavy duty vehicle. In: Proceedings of the American Control Conference. Seattle.

Smaoui, M., Brun, X., Thomasset, D., 2005. A combined first and second order sliding mode approach for position and pressure control of an electropneumatic system. In: Proceedings of the American Control Conference. Portland.

Smaoui, M., Brun, X., Thomasset, D., 2006. A study on tracking position control of an electropneumtaic system using backstepping design. Control Engineering Practice 14, 923–933.

Szabo, T., Buckholz, M., Dietmayer, K., 2010. A feedback linearization based observer for an electropneumatic clutch actuated by on/off solenoid valves. In: Proceedings of the 2010 IEEE Multi-conference on Systems and Control. Yokahama, Japan.

Taghizadeh, M., Ghaffari, A., Najafi, F., 2009. Modeling and identification of a solenoid valve for pwm control applications. Comptes Rendus Mcanique 337, 131–141.

Taghizadeh, M., Najafi, F., Ghaffari, A., 2010. Multimodel pd-control of a pneumatic actuator under variable loads. International Journal of Advanced Manufacturing Technology 48, 665–662.

Tanaka, H., Wada, H., 1995. Fuzzy control of clutch engagement for automated manuel transmission. Vehicle System Dynamics 24, 365–376.

Topcu, E. E., Yksel, I., Kamis, Z., 2006. Development of electro-pneumatic fast switching valve and investigation of its characteristics. Mechatronics 16, 365–378.

Vallevik, G., 2006. Adaptive nonlinear observer for electropneumatic clutch actuation. Master's thesis, Norwegian Univeristy of Science and Technology.

Varseveld, R. B. V., Bone, G. M., 1997. Accurate position control of a pneumatic actuator using on/off solenoid valves. IEEE/ASME Transactions on Mechatronics 2, 195–204,

Vasca, F., Iannelli, L., Reale, A. S. G., 2010. Torque transmissibility assessment for automotive dry-clutch engagement. IEEE/ASME Transactions on Mechatronics,.

Wu, J., Goldfarb, M., Barth, E., 2004. On the observability of pressure in a pneumatic servo actuator. Journal of Dynamic Systems, Measurement, and Control 126, 921–924.

Xiang, F., 2001. Block-orintated nonlinear control of pneumatic actuator system. Ph.D. thesis, Royal institute of technology, KTH.

Xiang, F., Wikander, J., 1997. Modeling and control of the volvo pneuamtic actuated truck clutch system. Tech. rep., DAMEK Research group, Royal institute of technology.

Appendix A

Estimation of electropneumatic clutch actuator load characteristics

This chapter includes the paper Langjord et al. (2008b).

Estimation of electropneumatic clutch actuator load characteristics

Hege Langjord, Tor Arne Johansen *
Sten Roar Snare, Christian Bratli **

* *Department of Engineering Cybernetics, NTNU, Trondheim, Norway, e-mail: {hegesan,torj}@itk.ntnu.no*
** *Kongsberg Automotive ASA, Kongsberg, Norway, e-mail: {sten.roar.snare,christian.bratli}@ka-group.com*

Abstract:
This paper propose a dynamic model of an electropneumatic clutch actuator system for heavy duty trucks. The focus is set on modeling of the clutch load characteristic which should be parameter affine, and the main purpose of the modeling task in this paper is to prepare for on-line adaption of this load characteristics. The knowledge of the clutch load characteristic is important for being able to estimate the pressure in the system online, when this is not measurable. In this paper off-line estimation is used to find parameters such that the model is a good representation of the system. The resulting 5^{th} order model is verified by comparison to actual truck measurements.

1. INTRODUCTION

Automated clutch actuation makes it easier for the driver, particularly in stop and go- traffic, and have especially seen a recent growth in the European automotive industry. This have raised the interest for automated manual transmission (AMT) systems. An AMT system consist of a manual transmission through the clutch disc, and an automated actuated clutch during gear shifts, and one of the AMT's largest advantages is low cost, high efficiency, reduced clutch wear and improved fuel consumption.

Most attention in this trend has been given to hydraulic clutch system for cars. Lucente et al. [2007] provides a nonlinear model for dry clutches with electrohydraulic actuator, in addition to models of the gear system, while Montanari et al. [2004] and Horn et al. [2003] concentrate on control and trajectory position tracking of similar electrohydraulic systems. In the paper by Zhang et al. [2002] we find a dynamic model for clutch engagement using hydraulic actuators, and Moon et al. [2004] presents a dynamic model for an electromechanical clutch system in his paper on clutch-by-wire system.

In this paper we will deal with the modeling of an electropneumatic clutch actuator for AMTs and clutch-by-wire systems for heavy duty trucks. There is a significant difference between the clutches designed for cars and ones designed for heavy duty trucks. In a truck, a much higher level of torque is required to be transmitted from the motor through the clutch disc, and hence are these discs needed to be of much larger radius than the ones for cars. Another difference is that in trucks pressurized air is available. This is the reason why it will be preferred to use pneumatics to actuate the clutch system, even though this complicates the modeling task due to the compressibility of air.

⋆ This work has been sponsored by the Norwegian Research Council and Kongsberg Automotive ASA.

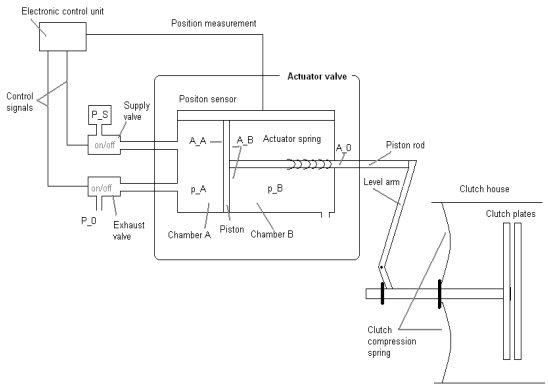

Fig. 1. Drawing of the electropneumatic clutch system

The considered clutch system is the same as the one treated by Kaasa in his Ph.D. thesis, Kaasa [2006]. The allocation of air to the clutch actuator, which were controlled by a three-way proportional valve, is in this paper assumed to be controlled by a set of on/off-valves. These have a dynamic response that is harder to model accurately, but they are desired because of space, cost and robustness advantages.

Figure 1 show a drawing of the main components of the clutch system, which is a pull-type clutch. In addition to the on/off valves, the system consist of an electronic control unit, a position sensor and an actuator valve. The state of the clutch plates (engaged/disengaged/slipping) is decided by the position of the clutch actuator piston, which is a result of the forces acting on the piston. These

forces are mainly pressure, friction and clutch load. The clutch load characteristic is a lumped force of the clutch compression spring and a counteracting, much weaker, actuator spring. The compression spring is a stiff and highly nonlinear diaphragm spring, while the actuator spring on the other hand is a linear coil spring.

It is desired to be able to estimate the clutch load characteristic during the lifetime of the clutch, as the characteristic changes as the clutch wears. These changes have a large influence on the system, and will introduce large errors if not recalculated during the clutch's lifetime. We will therefore find a model for the clutch load characteristics which is suitable for parameter estimation, and estimate these parameters off-line. It is also desired that position is the only measured state of the system. This is another reason why we are so interested in the clutch load. If this is know, it is possible to calculate the pressure in the system from a dynamic model, as velocity can be derived from the position measurement.

This paper is organized as follows. In Section 2 we give a description of the system and present the proposed model for the system. Section 3 contains the results from the parameter estimations as well as the simulations that verifies our model. Concluding remarks are given in Section 4.

2. CLUTCH ACTUATOR MODEL

2.1 Motion dynamics

The motion of the clutch actuator piston can be described by

$$M\frac{d^2y}{dt^2} = A_A p_A - A_B p_B - A_0 P_0 - f_l - f_f \tag{1}$$

where y is the position, f_f is the friction force, f_l is the clutch load force and P_0, p_A and p_B are the atmospheric pressure and the pressures in chamber A and B. The areas A_A, A_B and $A_0 = A_A - A_B$ are the areas in chamber A and B, and the difference in area of the piston in chamber A and B, and M is the mass of the piston.

2.2 Friction between piston and cylinder

The friction between the piston and the cylinder is modeled by a dynamical friction model, a LuGre model,

$$f_f = D_v v + K_z z + D_{\dot{z}}\dot{z} \tag{2}$$

where z describes a pre-sliding seal deflection, D_v is the viscous effect, K_z is the deflection stiffness and $D_{\dot{z}}$ is the deflection damping coefficient. The dynamic pre-sliding can be given by

$$\dot{z} = v - \frac{K_z}{F_C}|v|\, z \tag{3}$$

where F_C is the Coulomb friction. The parameter values are found from the work of Kaasa [2006].

2.3 Pressure

We use a simple model of the pressure dynamics

$$\dot{p}_A = -\frac{A_A v}{V_A(y)}p_A + \frac{RT_0}{V_A(y)}w_v \tag{4}$$

$$\dot{p}_B = \frac{A_B v}{V_B(y)}p_B + \frac{RT_0}{V_B(y)}w_r \tag{5}$$

where w_v and w_r are the resulting flow to/from the two chambers A and B. This model is based on 6 assumptions

- constant chamber temperature, i.e isothermal conditions
- constant supply pressure and that the exhaust pressure is equal to the atmospheric pressure
- air behaves as an ideal gas obeying the ideal gas equation of state
- the energy change in the fluid due to elevation is negligible
- the thermodynamic properties are uniformly distributed in the volume
- frictionless flow is assumed, i.e. isentropic flow

2.4 Valve dynamics

From Kaasa [2006] we have that flow through an orifice can be described by

$$\psi(r, B) = \Omega_0(r) + B\Omega_1(r, sgn(B)) \tag{6}$$

where

$$\Omega_0 = \begin{cases} \sqrt{1-r^2}, & r \in [0,1] \\ 0, & r > 1 \end{cases} \tag{7}$$

$$\Omega_1(r,+1) = -\Omega_0 + \begin{cases} 1, & r \in [0, B_0] \\ \sqrt{1-(\frac{r-B_0}{1-B_0})^2}, & r \in \langle B_0, 1] \\ 0, & r > 1 \end{cases} \tag{8}$$

$$\Omega_1(r,-1) = \Omega_0 - \begin{cases} 1-r, & r \in [0,1] \\ 0, & r > 1 \end{cases} \tag{9}$$

and where $r = \frac{p_l}{p_h}$ is the relation between the low and the high pressure at the sides of the orifice. The basis functions in (8) and (9) can be characterized as approximately isentropic or incompressible laminar flow, and the value of B decides which of these should be used.

The air flow to/from chamber A is $w_v = w_{vs} - w_{ve}$, where w_{vs} is the flow through the on/off valve controlling the supply and w_{ve} is the flow through the valve controlling exhaust. These flows can be described by

$$w_{vx} = g_{vx}(p_h, p_l, C_{vx}, B_{vx})y_{vx}(u_{vx}, R_{0,vx}, R_{1,vx})$$

where

$$g_{vx} = \rho_0 C_{vx}\psi(\frac{p_{l,vx}}{p_{h,vx}}, B_{vx})p_{h,vx} \tag{10}$$

and the valve opening degree is described

$$y_{vx} = sat_{[0,1]}(\frac{1}{R_{1,vx} - R_{0,vx}}(u_{vx} - R_{0,vx})), u_{vx} \in [0,1] \tag{11}$$

The subscript vx stands for vs and vem, $R_{0,vx}$ and $R_{1,vx}$ are valve opening constants and the parameter u_{vx} is the duty cycle of the valve's PWM (Pulse Width Modulation) input. The pressures is $p_{l,vs} = p_A$, $p_{l,ve} = P_0$, $p_{h,vs} = P_S$, $p_{h,ve} = P_B$ where P_S is the supply pressure.

The flow to/from chamber B, $w_r = w_{in} - w_{out}$ can be modeled as a fixed orifice,

$$w_{in} = \rho_0 C_r \psi(\frac{p_B}{P_0}, B_{in}) \tag{12}$$

$$w_{out} = \rho_0 C_r \psi(\frac{p_B}{P_0}, B_{out}) \tag{13}$$

2.5 Clutch load

To prepare for easy adaption of the clutch load characteristics, the model should be parameter affine and the number of parameters should be small. We propose a simple model for the load characteristic

$$f_l(y) = \Theta^T \phi(y) \tag{14}$$

where $\Theta^T = [\theta_1, \theta_2, \theta_3]^T$ and ϕ are three B-splines curves defined by the following polynomials and slope conditions.

$$\phi_1(y) = \begin{cases} 0, & y < t_1 \\ y - t_1, & t_1 \le y < t_2 \\ a_1 y^2 + b_1 y + c_1, & t_2 \le y < t_3 \\ a_1 t_3^2 + b_1 t_3 + c_1, & y \ge t_3 \end{cases} \tag{15}$$

- Transition between linear and quadratic part shall be smooth: $a_1 t_2^2 + b_1 t_2 + c_1 = t_2 - t_1$
- Derivative in t_2 shall be equal to one: $2a_1 t_2 + b_1 = 1$
- Derivative in t_3 shall be equal to zero: $2a_1 t_3 + b_1 = 0$

$$\phi_2(y) = \begin{cases} 0, & y < t_2 \\ a_2 y^2 + b_2 y + c_2, & t_2 \le y < t_3 \\ y + d_2, & y \ge t_3 \end{cases} \tag{16}$$

- The quadratic part shall start at zero in t_2: $a_2 t_2^2 + b_2 t_2 + c_2 = 0$
- The quadratic part shall have a gradient equal to zero in t_2: $2a_2 t_2 + b_2 = 0$
- The spline shall be continuous in t_3: $a_2 t_3^2 + b_2 t_3 + c_2 = t_3 + d_2$
- The derivative in t_3 shall be equal to one: $2a_2 t_3 + b_2 = 1$

$$\phi_3(y) = \begin{cases} 0, & y < t_2 \\ a_3 y^3 + b_3 y^2 + c_3 y + d_3, & t_2 \le y < t_4 \\ e_3 y^3 + f_3 y^2 + g_3 y + h_3, & t_4 \le y < t_5 \\ 0, & y \ge t_5 \end{cases} \tag{17}$$

where $t_5 = 2t_4 - t_2$.

- The first cubic part shall start at zero in t_2: $a_3 t_2^3 + b_3 t_2^2 + c_3 t_2 + d_3 = 0$
- The first cubic part shall have a gradient equal to zero in t_2: $3a_3 t_2^2 + 2b_3 t_2 + c_3 = 0$
- The first cubic part shall have a value equal to one millimeter in t_4: $a_3 t_3^4 + b_3 t_4^2 + c_3 t_4 + d_3 = 0.001$
- The first cubic part shall have a gradient equal to zero in t_4: $3a_3 t_4^2 + 2b_3 t_4 + c_3 = 0$
- The second cubic part shall start at zero in $2t_4 - t_2$: $e_3(2t_4 - t2)^3 + f_3(2t_4 - t2)^2 + g_3(2t_4 - t2) + h_3 = 0$
- The second cubic part shall have a gradient equal to zero in $2t_4 - t_2$: $3e_3(2t_4 - t2)^2 + 2f_3(2t_4 - t2) + g_3 = 0$
- The second cubic part shall have a value equal to one millimeter in t_4: $e_3 t_4^3 + f_3 t_4^2 + g_3 t_4 + h_3 = 0.001$
- The second cubic part shall have a gradient equal to zero in t_4: $3e_3 t_4^2 + 2f_3 t_4 + g_3 = 0$

Rewritten we have

$$\xi_i = A_i^{-1} B_i \qquad i = 1, 2, 3 \tag{18}$$

where

$$A_1 = \begin{bmatrix} t_2^2 & t_2 & 1 \\ 2t_2 & 1 & 0 \\ 2t_3 & 1 & 0 \end{bmatrix}$$

$$A_2 = \begin{bmatrix} t_2^2 & t_2 & 1 & 0 \\ 2t_2 & 1 & 0 & 0 \\ t_3^2 & t_3 & 1 & -1 \\ 2t_3 & 1 & 0 & 0 \end{bmatrix}, \tag{19}$$

$$A_3 = \begin{bmatrix} t_2^3 & t_2^3 & t_2 & 1 & 0 & 0 & 0 & 0 \\ 3t_2^2 & 2t_2 & 1 & 0 & 0 & 0 & 0 & 0 \\ t_4^3 & t_4^2 & t_4 & 1 & 0 & 0 & 0 & 0 \\ 3t_4^2 & 2t_4 & 1 & 0 & 0 & 0 & 0 & 0 \\ 0 & 0 & 0 & 0 & (2t_4 - t_2)^3 & (2t_4 - t_2)^2 & (2t_4 - t_2) & 1 \\ 0 & 0 & 0 & 0 & 3(2t_4 - t_2)^2 & 2(2t_4 - t_2) & 1 & 0 \\ 0 & 0 & 0 & 0 & t_4^3 & t_4^2 & t_4 & 1 \\ 0 & 0 & 0 & 0 & 3t_4^2 & 2t_4 & 1 & 0 \end{bmatrix}$$

$$B_1 = \begin{bmatrix} t_2 - t_1 \\ 1 \\ 0 \end{bmatrix}, B_2 = \begin{bmatrix} 0 \\ 0 \\ t_3 \\ 1 \end{bmatrix}, B_3 = \begin{bmatrix} 0 \\ 0 \\ 0.001 \\ 0 \\ 0 \\ 0 \\ 0.001 \\ 0 \end{bmatrix} \tag{20}$$

and the ξ_i's are the collection of parameters a_i, b_i.... The knots are chosen, based on knowledge of the considered clutch, to be in the positions $t = [0\ 2\ 8.5\ 11.5]^T\ mm$, and we get the following parameters

$$\xi_1 = \begin{bmatrix} -76.92308 \\ 1.3077 \\ -3.0769 \cdot 10^{-4} \end{bmatrix}$$

$$\xi_2 = \begin{bmatrix} 7.6923 \cdot 10^{-2} \\ -3.0769 \cdot 10^{-4} \\ 3.0769 \cdot 10^{-7} \\ -8.4968 \cdot 10^{-3} \end{bmatrix} \tag{21}$$

$$\xi_3 = \begin{bmatrix} 47.2372 \\ -2.3327 \cdot 10^{3} \\ -0.1610 \\ 1.6900 \\ 1.5163 \cdot 10^{-4} \\ -6.9439 \cdot 10^{-3} \\ -113.7192 \\ 2.3327 \cdot 10^{3} \end{bmatrix}$$

The resulting B-spline curves are shown in Figure 2.

2.6 Model

Summarized we get the 5^{th} order model

$$\begin{aligned} \dot{y} &= v \\ \dot{v} &= \frac{1}{M}(A_A p_A - A_B p_B - A_0 P_0 - f_l - f_f) \\ \dot{p}_A &= -\frac{A_A v}{V_A(y)} p_A + \frac{RT_0}{V_A(y)} w_v \\ \dot{p}_B &= \frac{A_B v}{V_B(y)} p_B + \frac{RT_0}{V_B(y)} w_r \end{aligned} \tag{22}$$

$$\dot{z} = v - \frac{K_z}{F_C} |v| z \tag{23}$$

and all the parameter values can be found in the Appendix.

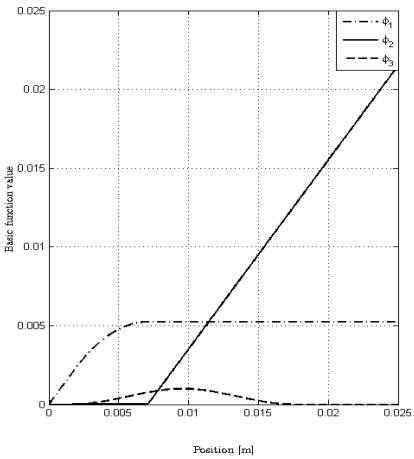

Fig. 2. The B-spline basis functions

3. EXPERIMENTAL RESULTS

3.1 Parameter estimation

The parameter estimation for the load characteristic is conducted by use of the *lsqnonlin* algorithm in MatLab, where the cost function is the sum of the position errors. The position error vector is found from either ballistic or partitioned ballistic simulations. In partitioned ballistic simulation, the simulation is initialized by the position measurement after each N^{th} simulation step. As we have no measurement of the other state variables, we initialize these by the values of the former simulation step. For the first simulation the initial values

$$\begin{aligned} y_0 &= y_{mes} \\ v_0 &= 0 \\ p_{A0} &= P_0 \\ p_{B0} &= P_0 \\ z_0 &= 0 \end{aligned} \tag{24}$$

are used. In ballistic simulation no new initialization is done during the simulation. All simulations are conducted with variable step length and *ode45* as the chosen solver.

The measurement used as reference is position and pressure measurement obtained from the truck Gamal at Kongsberg Automotive ASA. The operation range for the clutch is $y = [0, 25]$ mm, and the model is needed to be most precise in the region around engaging/disengaging of the clutch, in this case, the region $y = [5 - 8]$ mm.

The optimization routine for finding the parameters is conducted twice. The first one takes large steps and finds good initial values for further optimization. The second takes smaller optimization steps and finds the best parameters starting from these initial values.

Est. method	θ_1	θ_2	θ_3
Ballistic	$9.3850 \cdot 10^5$	$-0.5817 \cdot 10^5$	$0.3909 \cdot 10^5$
Part. ball., N=2	$8.4554 \cdot 10^5$	$-0.1678 \cdot 10^5$	$0.0971 \cdot 10^5$
Part. ball., N=4	$8.5581 \cdot 10^5$	$-0.2233 \cdot 10^5$	0
Part. ball., N=8	$9.8251 \cdot 10^5$	$-0.3468 \cdot 10^5$	$0.5386 \cdot 10^5$
Part. ball., N=16	$8.9178 \cdot 10^5$	$-0.3527 \cdot 10^5$	0
Part. ball., N=32	$8.8767 \cdot 10^5$	$-0.5476 \cdot 10^5$	0

Table 1. Estimated clutch load parameters

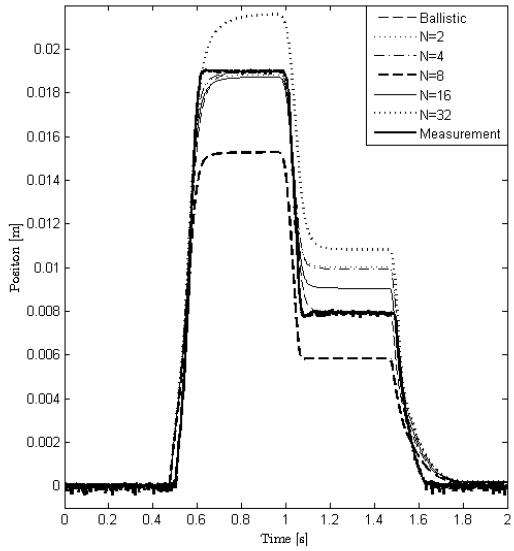

Fig. 3. Simulated positions

3.2 Results

Estimated parameters from ballistic and five partitioned ballistic simulations are presented in the Table 1 below. The number N stands for the number of partitions of the data set. Simulations results with these parameters are shown in Figure 3 and 4. Figure 5 show all the resulting clutch load characteristics. An estimation of the clutch load characteristic in the system is calculated from

$$f_l = A_A(p_A - p_0) \tag{25}$$

which is derived from motion dynamics equation (1) by assuming $v = 0$ and $p_B = P_0$.

The average position and pressure errors are presented in Table 2. From these and the simulation results we see that the parameters obtained from ballistic simulations gives the best results in position and the partitioned ballistic simulations with $N = 32$ gives the best results if considering the pressure of chamber A.

To verify that the estimated parameters gives a good model of the system, simulation with another data set from the truck have been done. Figure 6 and 7 show all the states, in addition to the measured position and pressure, from simulations with Θ obtained from ballistic simulations and from partitioned ballistic simulations with

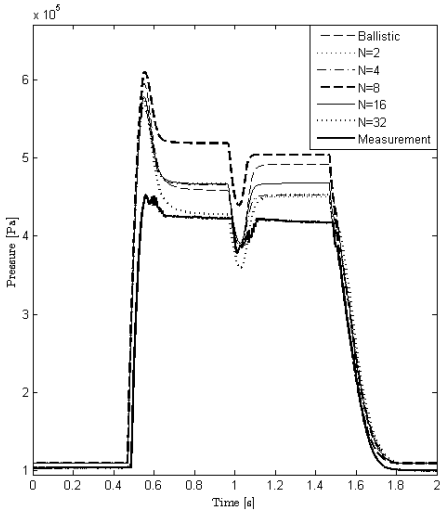

Fig. 4. Simulated pressure in chamber A

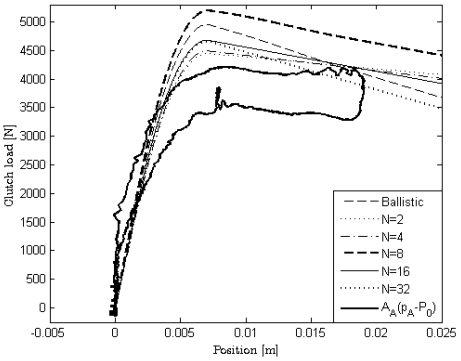

Fig. 5. Clutch load characteristic

Estimation method	Position error	Pressure error
Ballistic	$0.2678 \cdot 10^{-4}$	$2.7602 \cdot 10^{12}$
Part. ballistic, N=2	$8.8691 \cdot 10^{-4}$	$1.7203 \cdot 10^{12}$
Part. ballistic, N=4	$8.7327 \cdot 10^{-4}$	$1.7330 \cdot 10^{12}$
Part. ballistic, N=8	$3.3932 \cdot 10^{-4}$	$5.3149 \cdot 10^{12}$
Part. ballistic, N=16	$2.5684 \cdot 10^{-4}$	$2.1805 \cdot 10^{12}$
Part. ballistic, N=32	$4.1361 \cdot 10^{-3}$	$1.020 \cdot 10^{12}$

Table 2. Position and pressure errors

$N = 32$. The main goal of the clutch load estimation, is to be able to calculate the pressure of chamber A. By, as above, assuming that $V = 0$ and $p_B = P_0$ we can calculate this from

$$p_A = \frac{1}{A_A}(f_l + A_A * P_0). \tag{26}$$

Figure 8 show measured pressure together with pressures estimated this way, and, as expected, estimation from simulations with Θ from partitioned ballistic simulations with $N = 32$ give the best results.

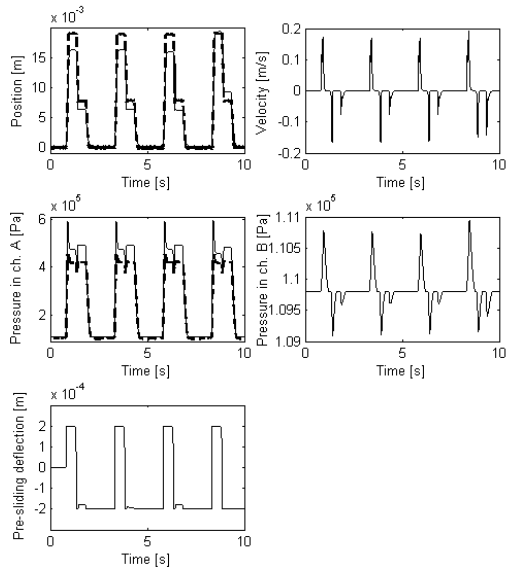

Fig. 6. All states from simulations with Θ from ballistic simulations

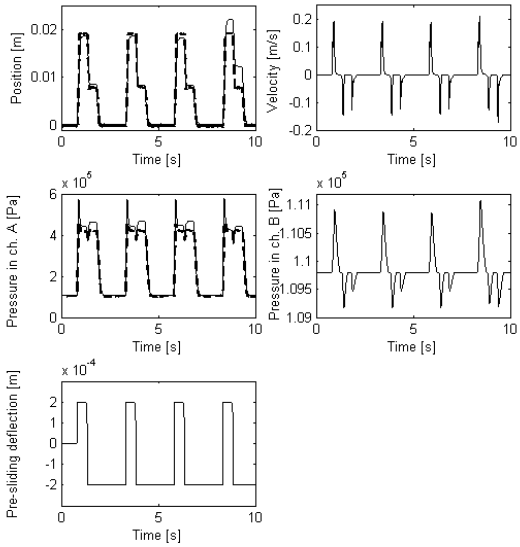

Fig. 7. All states from simulations with Θ from part. ballistic simulations with $N = 32$

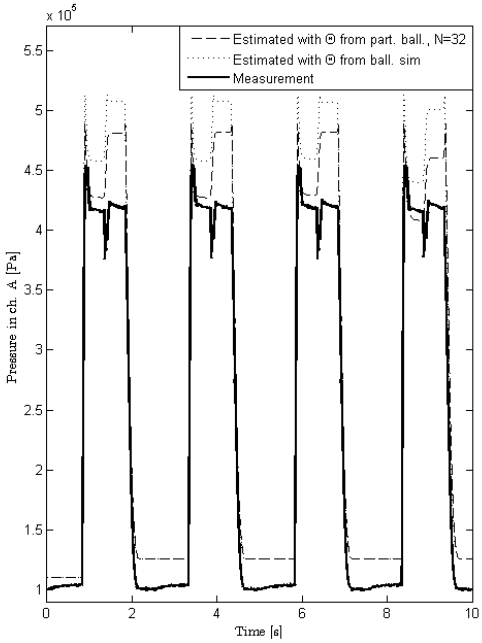

Fig. 8. Pressure in chamber A, estimated from $\frac{1}{A_A}(f_l + A_A P_0)$

Simulated position and the simulated pressure in chamber A deviate some from the measurement from the truck, which is not surprising as the proposed model is rather simple. From the clutch load characteristics in Figure 5, it is clear that the proposed model do not represent the system completely. There is also some uncertainty associate with the value of the supply pressure, which also may result in simulation deviations. The estimated pressure also suffer from these uncertainties. These results show the importance of an on-line adaption of the clutch load, especially since also wear of the clutch and temperature variations will change the truck's clutch load characteristics.

4. CONCLUDING REMARKS

The main purpose of this paper was to provide a rather simple model for the clutch actuator system, which is suited for on-line adaption of clutch load characteristic parameters. A 5^{th} order model of an electropneumatic clutch actuator have been presented, and parameters for clutch load characteristic are estimated off-line. The simulations verifies that the proposed model is a fair representation of the system, and that the model is a good basis for further development of the model, where emphasis should be placed on on-line adaption of clutch load characteristics and construction of a nonlinear observer.

REFERENCES

J. Horn, J. Bamberger, P. Michau, and S. Pindl. Flatness-based clutch control for automated manual transmissions. *Control Engineering Practice*, 11:1353–1359, 2003.

G. O. Kaasa. *Nonlinear output-feedback control applied to electro-pneumatic clutch actuation in heavy-duty trucks*. PhD thesis, NTNU, 2006.

G. Lucente, M. Mantanari, and C. Rossi. Modelling of an automated manual transmission system. *Mechatronics 17 (2007)*, pages 73–91, 2007.

M. Montanari, F. Ronchi, C. Rossi, A. Tilli, and A. Tonielli. Control and performance evaluation of a clutch servo system with hydraulic actuation. *Control Engineering Practice*, 12:1369–1379, 2004.

S. E. Moon, M. S. Kim, H. Yeo, H. S. Kim, S. H: Hwang, H. L. Song, and K. S. Han. Design and implementation of clutch-by-wire system for automated manual transmissions. *International Journal of Vehicle Design*, 36(1):83–100, 2004.

J. Zhang, L. Chen, and G. Xi. System dynamic modelling and adaptive optimal control for automatic clutch engagement of vehicles. *Proceedings of the Institution of Mechanical Engineers, Part D: Journal of Automobile Engineering*, 216:983–991, 2002.

Appendix A. PARAMETERS

Par.	Value	Unit	Description
A_A	$12.3 \cdot 10^{-3}$	m^2	Area of chamber A
A_B	$11.848 \cdot 10^{-3}$	m^2	Area of chamber B
$V_{0,A}$	$0.148 \cdot 10^{-3}$	m^3	Vol. of ch. A, $y = 0$
$V_{0,B}$	$1.2 \cdot 10^{-4}$	m^3	Vol. of ch. B, $y = 0$
P_0	$1.095 \cdot 10^5$	Pa	Ambient pressure
T_0	293	K	Temperature
R	288	$\frac{J}{kgK}$	Gas constant of air
M	10	kg	Mass of piston
P_S	$9 \cdot 10^5$	Pa	Supply pressure
D_v	5000	$[Ns/m]$	Viscous effect
K_z	$1 \cdot 10^6$	$[N/m]$	Deflect. stiffness
$D_{\dot{z}}$	5000	$[Ns/m]$	Deflect. damp. coeff.
F_C	200	$[N$	Coloumb friction
$R_{0,vs}$	0.07	-	Valveop. const.
$R_{0,ve}$	0.07	-	Valveop. const.
$R_{1,vs}$	0.93	-	Valveop. const.
$R_{1,ve}$	0.93	-	Valveop. const.
B_{vs}	0.1	-	Flow parameter
B_{ve}	-0.7	-	Flow parameter
C_{vs}	$19 \cdot 10^{-9}$	$[\frac{m^3}{Pa \cdot s}]$	Conductance
C_{ve}	$21.4 \cdot 10^{-9}$	$[\frac{m^3}{Pa \cdot s}]$	Conductance
C_r	$5 \cdot 10^{-8}$	$[\frac{m^3}{Pa \cdot s}]$	Conductance
B_0	0.582	-	Critical flow for air
B_{in}	0.5	-	Flow parameter
B_{out}	0.5	-	Flow parameter